

# Arbeitsbericht NAB 17-23

**Criticality safety assessment for  
geological disposal of spent fuel  
using PSI BUCSS-R methodology**

October 2017

J.J. Herrero, A. Vasiliev, M. Pecchia,  
D. Rochman, H. Ferroukhi, L. Johnson  
& S. Caruso

**National Cooperative  
for the Disposal of  
Radioactive Waste**

Hardstrasse 73  
P.O. Box 280  
5430 Wettingen  
Switzerland  
Tel. +41 56 437 11 11  
[www.nagra.ch](http://www.nagra.ch)



# Arbeitsbericht NAB 17-23

## Criticality safety assessment for geological disposal of spent fuel using PSI BUCSS-R methodology

October 2017

J.J. Herrero<sup>1</sup>, A. Vasiliev<sup>1</sup>, M. Pecchia<sup>1</sup>,  
D. Rochman<sup>1</sup>, H. Ferroukhi<sup>1</sup>, L. Johnson<sup>2</sup>  
& S. Caruso<sup>3</sup>

<sup>1</sup> Paul Scherrer Institut

<sup>2</sup> Independent consultant

<sup>3</sup> Nagra

### KEYWORDS

Spent fuel, criticality safety, burnup credit, fuel disposal,  
long term safety analysis, disposal canister

**National Cooperative  
for the Disposal of  
Radioactive Waste**

Hardstrasse 73  
P.O. Box 280  
5430 Wettingen  
Switzerland  
Tel. +41 56 437 11 11  
[www.nagra.ch](http://www.nagra.ch)

Nagra Arbeitsberichte ("Working Reports") present the results of work in progress that have not necessarily been subject to a comprehensive review. They are intended to provide rapid dissemination of current information.

"Copyright © 2017 by Nagra, Wettingen (Switzerland) / All rights reserved.

All parts of this work are protected by copyright. Any utilisation outwith the remit of the copyright law is unlawful and liable to prosecution. This applies in particular to translations, storage and processing in electronic systems and programs, microfilms, reproductions, etc."

## Abstract

In deep geological repositories for radioactive waste, a significant number of spent nuclear fuel assemblies are foreseen for disposal. The Swiss National Cooperative for the Disposal of Radioactive Waste (Nagra) plans to submit a general licence application for the site of a deep geological repository for the disposal of spent fuel, high-level and low- and intermediate-level wastes (for individual L/ILW and HLW repositories as well as for a combined repository) by around 2022. One of the requirements for the design of the repository is the safety of the installations (encapsulation facility and repository) from the point of view of a possible criticality excursion over a 1'000'000 year lifetime. Criticality, were it to occur, would produce elevated temperatures (several hundred degrees) in the near field, which could affect safety relevant properties and induce groundwater movement.

For the reasons above, the criticality safety issue for the disposal of canisters for spent fuel was investigated preliminarily by Nagra in 2002 in the context of the safety assessment for a repository for spent fuel and high-level waste in the Opalinus Clay. The methodology of this study were not considered sufficiently developed for the detailed design of canisters and for a systematic and comprehensive application of burnup credit to all Swiss spent fuel assemblies. However, the project came to the important conclusion that a combination of burnup credit and canister design modifications could ensure sub-criticality in all cases.

At the present stage, a calculation methodology for criticality safety evaluations related to dry interim storage and long-term waste disposal is under development at PSI. In particular, the application of burnup credit to criticality safety evaluations of geological repositories for long-term disposal of spent nuclear fuel was identified as being necessary for the case of PWR spent fuel assemblies (FA) operated in the Swiss reactors, but not for the case of BWR spent fuel.

This report summarises the activities and related achievements of the BUCSS-R project (BUrnup Credit System for the Swiss Reactors - Repository) in the period 2014 – 2017. The results are presented for canisters loaded with PWR  $\text{UO}_2$  spent fuel assemblies, integrating the outcome of criticality safety calculations with the uncertainties in nuclear data, fuel assembly design parameters and operating conditions as well as the burnup-induced changes in the fuel assembly geometry. Furthermore, bounding axial and radial burnup profiles and the most reactive fuel loading configuration for the canisters were taken into account.

The loading curves obtained for PWR fuel show what minimum average fuel assembly burnup is required for the given initial fuel enrichment of fresh fuel assemblies, so that  $K_{\text{eff}}$  of the canister would comply with the imposed criticality safety criterion. The loading curves presented in this work show that taking credit for the neutron absorption of non-fissile actinides only would not be sufficient to meet the criticality safety criteria for a non- mixed loading with fuel having an initial enrichment above  $\sim 3.5$  ‰, while the AC+FP approach (where the credit for neutron absorbers includes both non-fissile actinides and fission products) justifies the applicability of the canister design considered for safe disposal of spent nuclear fuel with all existing enrichments with required minimum burnups. A postulated case, consisting of FAs with 5 ‰ initial enrichment and relatively low burnup, would be the only exception not fitting the loading criteria; however, this case belongs only to a theoretical last core discharge, with, in reality, a lower enriched fuel. These loading curves can be considered as preliminary reference loading curves, since large margins for improvement were identified, in particular in relation to the treatment of uncertainties.

The criticality safety analysis for BWR fuel is not treated in the BUCSS-R project; however, work was carried out to demonstrate the fulfilment of the sub-criticality criteria without the application

of a burnup-credit approach (Gutierrez 2017), namely by considering ideal fresh (unirradiated) fuel, and without any credit from neutron poisons (e.g. gadolinium).

The case of a degraded canister/fuel configuration was out of the scope of this project phase, but will be investigated in a subsequent phase of the PSI/Nagra collaboration.

## Table of Contents

Abstract .....	I
Table of Contents .....	III
List of Tables.....	V
List of Figures .....	VI
List of Acronyms.....	IX
<b>1 Introduction .....</b>	<b>1</b>
<b>2 OECD/NEA WPNCs BUC Phase 7 benchmark analysis for decay and criticality code assessment .....</b>	<b>3</b>
2.1 Benchmark description .....	3
2.2 Methodology.....	4
2.2.1 Decay codes.....	4
2.2.2 Criticality codes.....	7
2.2.3 Nuclear data.....	7
2.3 Results of the benchmark.....	9
2.3.1 Decay calculations.....	9
2.3.1.1 Comparison of the isotopic concentrations.....	9
2.3.1.2 Isotopic concentrations evolution.....	17
2.3.1.3 Codes and decay data comparison.....	23
2.3.2 Criticality calculations for Transport/Storage cask .....	23
2.3.2.1 Comparison of the effective neutron multiplication factor.....	24
2.3.2.2 Further analysis of the results .....	27
2.4 Conclusions to Chapter 2.....	34
<b>3 Bounding case analysis of spent nuclear fuel operated in Swiss PWRs for loading in disposal canisters.....</b>	<b>35</b>
3.1 Introduction .....	35
3.2 Development of models.....	36
3.3 Development of the calculation route.....	38
3.3.1 Retrieval of nodal history .....	39
3.3.2 Lattice calculations for discharge composition estimation.....	39
3.3.3 Decay calculations after discharge .....	40
3.3.4 Criticality calculations for the disposal canister .....	40
3.4 Results .....	42
3.4.1 Fresh fuel .....	42
3.4.2 Discharged fuel.....	44
3.4.2.1 UO <sub>2</sub> fuel assembly (Case I) .....	45
3.4.2.2 ERU fuel assembly (Case II) .....	47

3.4.2.3	MOX fuel assembly (Case III) .....	48
3.4.2.4	One MOX and three UO <sub>2</sub> fuel assemblies (Case IV) .....	49
3.4.2.5	Empty position and three UO <sub>2</sub> fuel assemblies (Case V) .....	51
3.5	Conclusions to Chapter 3.....	52
<b>4</b>	<b>Preliminary reference loading curves obtained for Nagra's SNF disposal canister with the PSI BUCSS-R methodology .....</b>	<b>55</b>
4.1	Introduction .....	55
4.2	Applied criteria for criticality safety accounting for burnup credit .....	57
4.3	Modelling assumptions.....	58
4.3.1	Spatial burnup distributions.....	58
4.3.1.1	Axial distribution.....	58
4.3.1.2	Radial distribution .....	59
4.3.1.3	Impact of cooling time.....	61
4.3.1.4	Canister modelling.....	61
4.4	Results on bounding assessments .....	61
4.4.1	Axial burnup effect.....	61
4.4.2	Radial burnup effect .....	64
4.5	Assessment of uncertainties.....	65
4.5.1	Reactor operating conditions and burnup-induced changes .....	66
4.5.2	Technological tolerance impact.....	66
4.5.3	Nuclear data uncertainty impact.....	66
4.5.4	Long-term nuclide evolution .....	68
4.5.5	MCNP Monte Carlo uncertainty.....	68
4.6	Loading curve with combined uncertainty effects.....	70
4.6.1	Determination of the minimum BU required for fulfilment of the criticality safety criteria.....	70
4.6.2	Loading curve approximation.....	77
4.7	Outlook on the obtained results .....	78
<b>5</b>	<b>Conclusions.....</b>	<b>81</b>
<b>6</b>	<b>References.....</b>	<b>83</b>
<b>App. A:</b>	<b>Effect of thermal scattering data on K<sub>eff</sub> for fresh fuel.....</b>	<b>A-1</b>
<b>App. B:</b>	<b>International Guidelines and Standards for BUC Implementation .....</b>	<b>B-1</b>

## List of Tables

Tab. 2-1:	Actinide only burnup credit nuclides.....	3
Tab. 2-2:	Actinide plus fission products burnup credit nuclides.....	4
Tab. 2-3:	Convergence for Pu-238 concentration (at/b/cm) with time step in SDC. ....	6
Tab. 2-4:	Relative error (J311-E71ref/E71ref) (%) of isotopic concentrations.....	10
Tab. 2-5:	Relative error (SNF-E71ref/E71ref) (%) of isotopic concentrations.....	12
Tab. 2-6:	Relative error (SDC-E71ref/E71ref) (%) of isotopic concentrations. ....	14
Tab. 2-7:	Relative error (CINDER-E71ref/E71ref) (%) of isotopic concentrations. ...	15
Tab. 2-8:	Relative error (E71ref-bench/bench) (%) of isotopic concentrations.....	16
Tab. 2-9:	Relative error (J311-E71/E71) (%) of Tc-99 isotopic concentrations. ....	21
Tab. 2-10:	Relative error (J311-E71/E71) (%) of Am-243 isotopic concentrations. ....	22
Tab. 2-11:	$K_{eff}$ values for fresh fuel calculation with MCNP6.....	24
Tab. 2-12:	$K_{eff}$ values for fresh fuel calculation with SERPENT2.....	24
Tab. 3-1:	Time positions where decayed compositions are computed.....	40
Tab. 3-2:	Actinides only (AC) burnup credit nuclides. ....	40
Tab. 3-3:	Actinides plus fission products (AC+FP) burnup credit nuclides. ....	41
Tab. 3-4:	$K_{eff}$ values for canister configurations with fresh fuel. ....	43
Tab. 4-1:	Artificial axial burnup profile for a SIMULATE3 model with 40 axial fuel nodes (bottom to top).....	58
Tab. 4-2:	Artificial axial burnup profile for a SIMULATE3 model with 38 axial fuel nodes (bottom to top).....	59
Tab. 4-3:	Decay times considered after discharge [years]. ....	61
Tab. 4-4:	Data on $(K_{axial}-K_{nominal}) \times 10^5$ (pcm) for 4.94 w/o AC.....	62
Tab. 4-5:	Data on $(K_{axial}-K_{nominal}) \times 10^5$ (pcm) for 4.94 w/o AC+FP.....	62
Tab. 4-6:	Data on $(K_{axial}-K_{nominal}) \times 10^5$ (pcm) for 3.5 w/o AC.....	63
Tab. 4-7:	Data on $(K_{axial}-K_{nominal}) \times 10^5$ (pcm) for 3.5 w/o AC+FP.....	63
Tab. 4-8:	Data on $(K_{radial}-K_{nominal}) \times 10^5$ (pcm) for 4.94 w/o AC.....	64
Tab. 4-9:	Data on $(K_{radial}-K_{nominal}) \times 10^5$ (pcm) for 4.94 w/o AC+FP. ....	64
Tab. 4-10:	Data on $(K_{radial}-K_{nominal}) \times 10^5$ (pcm) for 3.5 w/o AC.....	65
Tab. 4-11:	Data on $(K_{radial}-K_{nominal}) \times 10^5$ (pcm) for 3.5 w/o AC+FP.....	65
Tab. 4-12:	Available UQ (Uncertainties Quantification) data on operating conditions and BU-induced geometry changes, in pcm.....	66
Tab. 4-13:	Estimated nuclear data-related uncertainties of $k_{eff}$ after discharge (no decay). ....	67

Tab. 4-14:	Estimated nuclear data-related uncertainties of $k_{eff}$ after 50'000 years decay.....	68
Tab. 4-15:	Summary of all total uncertainty components.....	69
Tab. 4-16:	Minimum burnup required for meeting the criticality safety criteria.....	77

## List of Figures

Fig. 2-1:	Evolution of actinides with the largest change in their concentrations relative to the average of computed values.....	17
Fig. 2-2:	Evolution of actinides with slight changes in concentrations relative to the average of computed values.....	18
Fig. 2-3:	Evolution of fission products and minor actinides with notable changes in their concentrations relative to the average of computed values.....	19
Fig. 2-4:	$K_{eff}$ computed with MCNP6 for the three libraries and benchmark average with actinides only composition (actinides only case).....	25
Fig. 2-5:	$K_{eff}$ computed with SERPENT2 for the three libraries and benchmark average with actinides only composition (actinides only case).....	25
Fig. 2-6:	$K_{eff}$ computed with MCNP6 for the three libraries and benchmark average with actinides plus fission products composition (actinides plus fission products case).....	26
Fig. 2-7:	$K_{eff}$ computed with SERPENT2 for the three libraries and benchmark average with actinides plus fission products composition (actinides plus fission products case).....	27
Fig. 2-8:	$K_{eff}$ computed with SERPENT2 for the three libraries using Am-241 data from ENDF/B-VII.1 only, for actinides only composition.....	28
Fig. 2-9:	$K_{eff}$ computed with SERPENT2 for the three libraries using Am-241 data from ENDF/B-VII.1 only, for actinides plus fission products composition.....	28
Fig. 2-10:	Am-241 cross section on different cross section evaluations.....	29
Fig. 2-11:	$K_{eff}$ deviations to benchmark average computed with SERPENT2.....	30
Fig. 2-12:	$K_{eff}$ deviations to benchmark average computed with SERPENT2 and actinides only, using Am-241 data from ENDF/B-VII.1.....	30
Fig. 2-13:	$K_{eff}$ deviations to benchmark average computed with SERPENT2 and actinides plus fission products, using Am-241 data from ENDF/B-VII.1....	31
Fig. 2-14:	$K_{eff}$ deviations to benchmark average computed with SERPENT2 and actinides only, using Am-241 and Pu-241 data from ENDF/B-VII.1.....	32
Fig. 2-15:	$K_{eff}$ deviations to benchmark average computed with SERPENT2 and actinides plus fission products, using Am-241 and Pu-241 data from ENDF/B-VII.1.....	32
Fig. 2-16:	Gd-155 cross section on different cross section evaluations.....	33

Fig. 2-17:	Np-237 cross section on different cross sections evaluations.....	33
Fig. 3-1:	Main dimensions of the carbon steel disposal canister ( $R_{in} = 41$ cm, $R_{out} = 55$ cm, Box Centre - Centre (C-C) Separation = 17.9 cm). ....	37
Fig. 3-2:	Radial (left) and axial (right) view of the canister model loaded with fresh $UO_2$ fuel. ....	38
Fig. 3-3:	Computational scheme for burnup credit in a disposal application. ....	39
Fig. 3-4:	Difference between $K_{eff}$ computed with the reference axial detail and $K_{eff}$ computed with a coarser mesh ( $UO_2$ fuel). ....	42
Fig. 3-5:	Evolution of $K_{eff}$ for the intact canister loaded with spent $UO_2$ fuel. ....	45
Fig. 3-6:	Reactivity inserted by use of AC+FP against AC for a $UO_2$ fuel loading. ...	46
Fig. 3-7:	Evolution of $K_{eff}$ for the intact canister loaded with mixed burnup $UO_2$ fuel (first burnup value for one position, second value for three remaining).....	47
Fig. 3-8:	Evolution of $K_{eff}$ for the intact canister loaded with ERU fuel.....	47
Fig. 3-9:	Reactivity inserted by use of AC+FP for an ERU fuel loading.....	48
Fig. 3-10:	Evolution of $k_{eff}$ for the intact canister loaded with MOX fuel. ....	48
Fig. 3-11:	Reactivity inserted by use of AC+FP for a full MOX fuel loading. ....	49
Fig. 3-12:	Evolution of $K_{eff}$ for the intact canister loaded with one low burnup MOX (18 GWd/t) and three $UO_2$ fuel at different burnups. ....	50
Fig. 3-13:	Reactivity inserted by use of actinides plus fission products for a MOX- $UO_2$ fuel loading. ....	50
Fig. 3-14:	Evolution of $k_{eff}$ for the intact canister loaded with 3 $UO_2$ assemblies and one empty position. ....	51
Fig. 3-15:	Reactivity inserted by use of actinides plus fission products for a 3 $UO_2$ assemblies loading with one empty position. ....	51
Fig. 3-16:	Evolution of minimum burnup credit required to comply with a $k_{eff}$ value below 0.95 within the geological disposal timescale (AC case). ....	52
Fig. 3-17:	Evolution of minimum burnup required to comply with a $K_{eff}$ value below 0.95 within the geological disposal timeframe (AC+FP case).....	53
Fig. 4-1:	Schematic concept of the PSI BUCSS-R methodology.....	56
Fig. 4-2:	Illustration of the radial burnup profile specification in MCNP6 models (here: U-235 atomic density). ....	60
Fig. 4-3:	Presently employed ND stochastic sampling methodology.....	67
Fig. 4-4:	Impact of the burnup profiles and the total uncertainty on the canister $k_{eff}$ value. ....	69
Fig. 4-5:	Illustration of determination of the minimum burnup required for fuel to meet .....	70
Fig. 4-6:	Determination of the limiting BU for 2.5 % PWR $UO_2$ fuel. ....	71
Fig. 4-7:	Determination of the limiting BU for 3.2 % PWR $UO_2$ fuel. ....	72

Fig. 4-8:	Determination of the limiting BU for 3.5 w/o PWR UO <sub>2</sub> fuel. ....	73
Fig. 4-9:	Determination of the limiting BU for 4.1 w/o PWR UO <sub>2</sub> fuel. ....	74
Fig. 4-10:	Determination of the limiting BU for 4.3 w/o PWR UO <sub>2</sub> fuel. ....	75
Fig. 4-11:	Determination of the limiting BU for 4.94 w/o PWR UO <sub>2</sub> fuel.....	76
Fig. 4-12:	Loading curve with all conservative effects for discharged spent fuel.....	77
Fig. 4-13:	Impact of different modelling components and options on the BU limits....	78

## List of Acronyms

ANSI:	American National Standards Institute
BU:	Burnup
BUC:	Burnup Credit
CSE:	Criticality Safety Evaluation
DBE:	Deutsche Gesellschaft zum Bau und Betrieb von Endlagern für Abfallstoffe mbH
DIN:	Deutsches Institut für Normung
DOE:	Department of Energy of the U.S.A
EBS:	Engineered Barrier System
EGBUC:	Expert Group on Burnup Credit Criticality Safety at the OECD/NEA
EOL:	End of Life
ENSI:	Eidgenössisches Nuklearsicherheitsinspektorat / Swiss Federal Nuclear Safety Inspectorate
EPRI:	Electric Power Research Institute
ERU:	Enriched Reprocessed Uranium
FEP:	Features, Events and Processes
GDF:	Geological Disposal Facility
GWd:	Gigawatt days
HLW:	High-Level Waste
ILW:	Long-Lived Intermediate-Level Waste
IRSN:	Institut de Radioprotection et de Sûreté Nucléaire
KKG:	Kernkraftwerk Gösgen (Gösgen NPP)
MOX:	Mixed uranium and plutonium oxide fuel
MPI:	Message Passing Interface
MTU:	Metric Ton of Uran
NEA:	Nuclear Energy Agency
ORNL:	Oak Ridge National Laboratory
PIE:	Post-Irradiation Examination
QA:	Quality Assurance
RCA:	Radiochemical Assay data
RWMD:	Radioactive Waste Management Directorate
SNF:	Spent Nuclear Fuel
tHM:	Tonnes of Heavy Metal, measured in the initial fresh fuel composition
TSL:	Thermal Scattering Law data
UOX:	Uranium Oxide fuel

UO <sub>2</sub> :	Uranium dioxide
USL:	Upper Subcritical Limit
YMP:	Yucca Mountain Project
ZWIBEZ:	Waste storage facility located at the Beznau nuclear power plant
ZWILAG:	Centralised interim storage facility located in Würenlingen, operational since 2002

# 1 Introduction

In deep geological repositories for radioactive waste, a significant number of spent nuclear fuel assemblies are foreseen for disposal. The Swiss National Cooperative for the Disposal of Radioactive Waste (Nagra) plans to submit a general licence application for the site of a deep geological repository for the disposal of spent fuel, high-level and low- and intermediate-level wastes (for individual L/ILW and HLW repositories as well as for a combined repository) by around 2022. One of the requirements for the design of the repository is the safety of the installations (encapsulation facility and repository) from the point of view of a possible criticality excursion.

For the reasons above, the criticality safety issue for the disposal of canisters for spent fuel was investigated preliminarily by Nagra in 2002 in the context of the safety assessment of a repository for spent fuel and high-level waste in the Opalinus Clay (Kühl et al. 2012b). The results of this study were not considered sufficiently developed for the detailed design of canisters and for a systematic and comprehensive application of burnup credit to all Swiss spent fuel assemblies. However, the project came to the important conclusion that a combination of burnup credit and canister design modifications could ensure sub-criticality in all cases.

A general framework agreement between the Laboratory for Reactor Physics and Systems Behaviour (LRS) in the PSI Nuclear Energy and Safety Research Department (NES) and Nagra has been established for collaboration in the area of reactor physics and safety analyses related to the Swiss Light Water Reactors (LWR). The scope of the programme was to develop an advanced methodology, based on state-of-the-art reactor physics codes and in line with the latest international programs, for criticality safety evaluations (CSE) including Burnup Credit (BUC) of disposal canisters with spent nuclear fuel (SNF) aimed at deep geological disposal. The long-term objective is to allow the methodology to be used as the basis for supporting Nagra's safety assessments for long-term criticality scenarios that will be required firstly for the general licensing and the later construction licensing of a Swiss repository.

A comprehensive state-of-the-art BUC methodology for application to Swiss interim storage facilities, referred to as the BUCSS methodology (BUrnup Credit System for the Swiss Reactors), was already under development at the beginning of the project and was then extended to long-term disposal applications, namely BUCSS-Repository (BUCSS-R).

The studies are performed for a reference canister loaded with PWR UO<sub>2</sub> spent fuel assemblies, integrating the outcome of criticality safety calculations with the uncertainties in nuclear data, fuel assembly design parameters and operating conditions as well as the burnup-induced changes in the fuel assembly geometry. Furthermore, bounding axial and radial burnup profiles and the most reactive fuel loading configuration for the canisters were taken into account.

The achievements of the project have been documented as PSI technical reports delivered to Nagra. This report summarises the activities and related achievements of the BUCSS-R project over the last three years. Three main sections are dedicated to each corresponding PSI technical report. **Chapter 2** discusses the report "OECD/NEA WPNCB BUC Phase 7 benchmark analysis for decay and criticality code assessment", **Chapter 3** the "Bounding case analysis of spent nuclear fuel operated in Swiss PWRs and loaded in disposal canisters" and **Chapter 4** "Preliminary reference loading curves obtained for Nagra's SNF disposal canister with the PSI BUCSS-R methodology". The loading curves obtained for PWR fuel show what minimum average fuel assembly burnup is required for the given initial fuel enrichment of fresh fuel assemblies so that the neutron multiplication factor ( $K_{\text{eff}}$ ) of the canister would comply with the

imposed criticality safety criterion. These loading curves can be considered as preliminary reference loading curves.

The criticality safety analysis for BWR fuel was not considered in the PSI/Nagra collaboration, however work was carried out to demonstrate the fulfilment of the sub-criticality criteria without the employment of the burnup-credit approach, namely by considering ideal fresh fuel (Gutierrez 2017).

The case of a degraded canister/fuel configuration was out of the scope of this project phase, but will be investigated in a subsequent phase of the PSI/Nagra collaboration.

## 2 OECD/NEA WPNCs BUC Phase 7 benchmark analysis for decay and criticality code assessment

At the beginning of the BUCSS-R project, the performance of the available decay/burnup and criticality safety codes had to be evaluated. In this report, the Burnup Credit (BUC) Criticality Safety Benchmark Phase 7 organised by the OECD/NEA (NEA 2012) has been employed to evaluate decay calculation results for the following codes:

- CINDER1.05 (Wilson et al. 2007)
- CASMO5 (CASMO5 2012)
- SERPENT2 (SERPENT 2015)

The computed isotopic compositions have then been used for the assessment of the criticality calculations with MCNP6 (Pelowitz 2014) and SERPENT2, while employing the most recent ACE cross section libraries from:

- ENDF/B VII.1 (ENDFB7 2014)
- JEFF 3.2 (JEFF 2014b)
- TENDL 2013 (Koning 2012)

### 2.1 Benchmark description

The objective of this benchmark is to evaluate the ability of the computer codes and the associated nuclear data to predict spent fuel isotopic compositions and  $K_{\text{eff}}$  values in a generic spent fuel cask configuration (transport/storage cask), but at a time scale relevant to SNF disposal.

Participants performed decay and criticality calculations at 30 post-irradiation time steps, up to one million years. Although isotopes relevant for public dose were also considered, the focus was on burnup-credit isotopes to be considered for criticality calculations. The  $K_{\text{eff}}$  values for fresh fuel compositions were also reported.

Average values and related standard deviations were reported in the final comparison for each quantity (with 4 significant digits in all cases).

The initial discharge composition is representative of a PWR assembly of 4.5 %<sub>0</sub> initial enrichment in U-235 and 50 GWd/MTU burnup. The  $K_{\text{eff}}$  values were computed taking credit only for the actinides (11 isotopes) or for the actinides plus fission products (30 isotopes), and including the O-16 (stable) present in the compositions. The isotopes included for each type of calculation are listed in Tab. 2-1 and Tab. 2-2.

Tab. 2-1: Actinide only burnup credit nuclides.

U-233	U-234	U-235	U-236	U-238	Pu-238
Pu-239	Pu-240	Pu-241	Pu-242	Am-241	

Tab. 2-2: Actinide plus fission products burnup credit nuclides.

U-233	U-234	U-235	U-236	U-238	Np-237	Pu-238	Pu-239	Pu-240
Pu-241	Pu-242	Am-241	Am-242m	Am-243	Mo-95	Tc-99	Ru-101	Rh-103
Ag-109	Cs-133	Nd-143	Nd-145	Sm-147	Sm-149	Sm-150	Sm-151	Sm-152
Eu-151	Eu-153	Gd-155						

The transport/storage cask is assumed to be loaded with intact standard  $17 \times 17$  PWR fuel assemblies; all the dimensions for the fuel pins and the guide tubes are described in the final report (NEA 2012). The assemblies are situated in a borated stainless steel basket inside a stainless steel (SS304) cask forming an array. The cask is flooded with water and the temperature of the cask is assumed to be 293K. All the material compositions are given and the isotopic compositions for each metallic species were taken from the IUPAC Technical Report (Berglund 2011) when needed.

## 2.2 Methodology

### 2.2.1 Decay codes

Four codes have been considered in the decay calculations: CINDER 1.05, the decay module within SERPENT2, the two decay modules inside CASMO5, and the CINDER version included inside MCNP6.

The reasons for employing these codes are related, in principle, to their availability at LRS, which should also facilitate a future coupling to the fuel burnup sequence for the Swiss power plants and the sensitivity and uncertainty analysis methodologies under development. Besides, these codes are employed worldwide, which ensures a better quality and continued development or maintenance.

#### CINDER-1.05

CINDER90 is the latest version of CINDER available from the NEA Data Bank, in particular the code CINDER90 version 7.4.2 is compiled with the highest precision available. The method of resolution of this code is based on the linearization of the Markov chains plus an automatic procedure to simplify the chain depth depending on a user-given accuracy parameter (Wilson 2007). The decay data used by CINDER90 are based on ENDF/B-VI plus other sources when ENDF/B values were not available.

Apart from the compilation of CINDER from the original package, a set of initial runs was computed to characterise the convergence properties of the solution.

For the benchmark, two calculations were performed: one including only the original time positions where results were included in the benchmark and another halving the time steps by including intermediate points in the original time mesh. The results showed deviations in terms of relative errors below  $10^{-3}$ , so the method is quite independent of the time step.

Also, some sensitivity studies on the error tolerance parameters were performed. In summary, default parameters can be considered reliable for the calculation scope. Even a relaxation of

tolerances could be envisioned to improve execution speed, although running time is already reasonable.

### **CINDER inside MCNP6/MCNPX**

Several years ago, CINDER90 was included inside the MCNPX code for transmutation and burnup calculations. Because CINDER90 integration into MCNP6 has been recently revised (Fensin 2012), it is possible that the cinder.dat file in the MCNP6 distribution already contains updated data from ENDF/B-VII.1, so the results of MCNP6 decay calculations could slightly differ from the values produced by CINDER90.

### **CASMO-5**

CASMO-5 is a "two-dimensional characteristics based neutron and gamma transport theory lattice physics code with depletion capability". To perform decay calculations of the fuel, it includes a Shutdown Cooling Calculation option (SDC), in principle prepared for long outages or intervals between cycles. We have used this ability to perform decay calculations for long periods using a single fuel pin model, as the geometry considered plays no role in the decay results.

CASMO-5 also includes a SNF-lite option provided for scoping studies, but not as rigorous as the stand-alone SNF application which requires SIMULATE power histories to correct for the real cycle operation. Nevertheless, calculations with this option output the isotopic concentrations of the decayed nuclides and have also been benchmarked. The latest available version of the code has been used for the calculations.

Regarding the time step dependence of both methods, it was found that the solution from SNF-lite was totally independent of the time steps, while for the SDC method the results are time step dependent. This is an important drawback for this method when considering a time period over thousands of years.

The simulations became quite long with the SDC method, as the period of time considered increased. Therefore, comparison with other results is provided only for a period of 1'000 years in this case. SNF-lite was, on the contrary, very fast. Calculations for a 10-year period using 10, 100, 1'000 and 2'000 steps in SDC show the following values in Tab. 2-3 for the final concentration of Pu-238.

Tab. 2-3: Convergence for Pu-238 concentration (at/b/cm) with time step in SDC.

Number of steps	Pu-238 conc (*1.E+6)	Relative error (%)	Execution time (min)	Extrapolated execution time to 1'000 years (min)
SERPENT (ref.)	9.24504	-	-	0.5
10	8.97073	-2.96	0.5	50
100	9.20392	-0.44	3.5	350
1'000	9.24074	-0.05	37	3'700
2'000	9.24288	-0.02	77	7'700
SNF	9.24584	0.01	0.1	0.1

Based on the first results of the convergence comparison for SDC in 10 years, a time step of 100 homogeneous intervals in these 10 years should be used for high accuracy (error below 1 %). A similar study was performed until the position of 100'000 years was reached, then computation time became prohibitive.

## SERPENT2

SERPENT2 is provided with a decay calculation module used in principle for burnup calculations. The decay calculation in SERPENT uses "an advanced matrix exponential solution based on the Chebyshev Rational Approximation Method (CRAM)", which has been shown to be fast and accurate (Pusa 2013) when coupled to the transport solution for core burnup calculations.

However, the code can be instructed to run only the decay calculation without predictor-corrector transport calculations in between. In this case, the classical Transmutation Trajectory Analysis (TTA) or linear chains method is activated internally (Isotalo 2013), the same as for CINDER, the differences between these codes probably being only the decay data employed.

Unlike CINDER or CASMO, the user has the flexibility to choose the decay data library, which allows the user to compare and analyse the impact of each library. Thus, both decay libraries ENDF/B-VII.1 and JEFF-3.1.1, including the spontaneous fission yield data, were employed in the decay calculations. The differences between the solutions from the two libraries were minor, as reported below.

Again, these calculations were prepared from a criticality calculation input file, adding the card "*set decstep*" with the corresponding time positions and the criticality calculation was exchanged with a null external source calculation, although this step may be not necessary when using the "*decstep*" card.

### 2.2.2 Criticality codes

Monte Carlo neutron transport codes have been chosen as candidates for the criticality calculations, among them MCNP6 and SERPENT2. The main reason for this choice is related to the geometry of the model as well as the complexity of the material composition and also to allow the possibility of using continuous energy and the most up to date cross section libraries.

#### MCNP6

MCNP6 is actually a merge of MCNP5 and MCNPX, so it shares the capabilities of both; it is a reference code for criticality calculations. It is extensively validated and has a huge user community which ensures constant development and improvement.

The distribution of the code includes up to date cross section libraries and new capabilities which could be important in the future, such as the calculation of sensitivity coefficients of  $K_{\text{eff}}$  to the nuclear parameters useful for uncertainty propagation and the ability to use unstructured mesh files to model the geometry. The MCNP code is intended to be the code used at PSI for criticality safety and burnup credit applications, including uncertainty propagation.

#### SERPENT2

SERPENT is a neutron transport code for calculation of models typical of reactor physics problems (Leppänen 2007). In this sense, it is less complex than MCNP6 and the source of the code is readily available to PSI and the code licence is free and easy to obtain.

Two versions of the code are available. The version used for this work is SERPENT2, as it is the version currently supported and under continuous development. SERPENT2 has recently included the union operator for the geometry description, so it is becoming equivalent to MCNP in that sense. The porting of CAD mesh files to describe the geometry is also in preparation. An alpha version is already available at PSI, in order to compute the adjoint flux and then the sensitivities of  $K_{\text{eff}}$  to some reactions.

### 2.2.3 Nuclear data

The nuclear data employed in the calculations are as important as the codes benchmarked. In this case, three distributions have been considered: ENDF/B-VII.1, JEFF-3.2 and TENDL2013. A first estimation of the accuracy of the calculations when applied to a real problem is part of the main goal.

#### ENDF/B-VII.1

The decay and neutron cross section library files of this evaluated library version have been obtained through two paths. One is the data directly bound to the MCNP6 distribution, which includes neutron cross sections directly in ACE format, and the decay data contained in the cinder.dat file (this is mainly ENDF/B-VI.8). The other way is through the files posted in the American National Nuclear Data Center (NNDC), in ACE format for the neutron cross sections. The decay data and the fission yields were also obtained from the NNDC (ENDFB7 2014).

The data provided together with the MCNP6 code included, for the first time, thermal scattering data processed in continuous energy, which has been used in the calculations with MCNP6.

During the checking of the output files, a minor error was encountered and corrected in the heading of the thermal scattering  $S(\alpha,\beta)$  data corresponding to uranium in  $\text{UO}_2$ .

At the time, this version of the library was used for  $K_{\text{eff}}$  calculations, the continuous energy version of the library was employed with MCNP6 and the discrete energy version with SERPENT2, as the latter was not yet able to correctly read the continuous energy representation. In practice, it has been checked that the results from both approaches are similar, regardless of the Monte Carlo code used.

Data are also available in the thermal scattering libraries for hydrogen in  $\text{H}_2\text{O}$ , oxygen in  $\text{UO}_2$ , and iron (Fe-56). All these were included in the simulation when using these libraries (see Appendix A on the assessment of the effect of thermal scattering on  $K_{\text{eff}}$ ).

NNDC cross sections were discarded from the study and only the values from the MCNP6 distribution were considered after calculations with the fresh fuel. For the use of the MCNP6 ACE files in SERPENT, a modified version of the files was generated, as recent library modifications have not yet been taken into account in SERPENT2. This modification was only performed on the files for 293K used in the calculations.

During the cross section preparations, the `xmdirconvert.pl` script taken from the SERPENT web page was adapted to translate the `xmdir` file to the `xpdata` file taking into account the Am-242 metastable identification number used in MCNP6, which is 95242 instead of 95642, which is used for Am-242 in its ground state.

### **JEFF-3.2**

The latest neutron data from the JEFF database were released in Version 3.2 (to be downloaded from the NEA web page<sup>1</sup> (JEFF 2014b)). It is worth noting that these data only include thermal scattering libraries for hydrogen in water, in contrast to the more complete information in ENDF/B-VII.1. On the other hand, the decay data and fission yields are still those from the JEFF-3.1.1 release (Kellett 2009).

A modified version of the library including the evaluation of Am-241 from ENDF/B-VII.1 was also employed in the simulations. Actually, only the `xpdata` file used in SERPENT2 was modified for this purpose.

### **TENDL2013**

The TALYS-based evaluated nuclear data library (TENDL, Koning 2012) released a new version in late 2013. The approach used here to generate the neutron cross sections is, in principle, independent from ENDF/B or JEFF evaluations. In this sense, this library could be a good indicator for possible needs for improvement in the evaluated nuclear data, although the results should always be considered cautiously. This distribution did not include decay data. It also did not include the thermal scattering  $S(\alpha,\beta)$  data, and the data from ENDF/B-VII.1 were taken instead.

For the creation of the `xmdir` file from the original distribution files, a script `set-xmdir.sh` was prepared. Also, the original `xmdirconvert.pl` script was corrected to translate the `xmdir` file to the

---

<sup>1</sup> Downloaded from NEA. Status 28.02.2014.

xpdata file accordingly when second metastable isotopes were present in the library (as in the current case).

For reasons provided below, updated versions of some ACE files were requested from the TENDL team to include probability tables for some main actinides. This is signalled in the library with the ptable label for the xsdir and xpdata files.

## **2.3 Results of the benchmark**

### **2.3.1 Decay calculations**

The decay calculations were performed with all the codes listed in section 2.2.1. For SERPENT2, it was also possible to consider different decay data files and these results are also presented.

#### **2.3.1.1 Comparison of the isotopic concentrations**

The comparison begins with a code-to-code approach to identify discrepancies between methods and/or data, then proceeds with a comparison to the average benchmark results.

The results from SERPENT2 using the decay data from ENDF/B-VII.1 (E71ref) have been taken as terms of reference for the code-to-code comparison. These values have been shown to be reliable and they will be used for the global comparison with the benchmark average values and later for the criticality calculations.

The input file for SERPENT2 was optimised to output the densities of all the isotopes listed in the benchmark specification, the ones important for criticality and also the ones related to radiation exposure. However, the analysis will stick to the isotopes employed in the criticality safety calculations.

SERPENT2 results, with and without consideration of the spontaneous fission yield data files, produced the same concentrations, with discrepancies below 0.1 % in all cases. To have an idea of the impact of this deviation, we consider the isotope with the highest relative sensitivity, U-235, with  $\sim 0.425$  after 1 million years of decay. Considering a  $K_{\text{eff}}$  of approximately 0.75 and the  $\Delta N/N$  in the concentration of 0.001 (this is the 0.1 %), the  $\Delta k$  gives 32 pcm. On the other hand, we obtain a  $\Delta k$  of 12 pcm for Pu-239, where  $\Delta N/N$  is equal to 0.001 for the highest  $K_{\text{eff}}$  position (0.85), at the highest sensitivity position.

Calculations employing ENDF/B (E71) and JEFF (J311) evaluations were also compared. Tab. 2-4 includes the relative differences in percentage between both, and only the isotopes with differences above 0.1 % are included.

Tab. 2-4: Relative error (J311-E71ref/E71ref) (%) of isotopic concentrations.

Time	Tc-99	Sm-149	U-233	Np-237	Pu-238	Pu-240	Pu-241	Am-241	Am-243
0	0.00	0.00	0.00	0.00	0.00	0.00	0.00	0.00	0.00
1	0.00	-0.54	0.00	0.00	0.00	0.00	0.01	-0.14	0.00
2	0.00	-0.54	0.00	0.00	0.00	0.00	0.03	-0.18	0.00
5	0.00	-0.54	0.00	0.00	0.00	0.00	0.07	-0.20	0.00
10	0.00	-0.54	0.00	0.00	0.00	0.01	0.14	-0.19	0.00
20	0.00	-0.54	0.00	-0.01	0.00	0.01	0.27	-0.15	0.00
40	0.00	-0.54	0.00	-0.02	0.00	0.01	0.54	-0.08	0.00
60	0.00	-0.54	0.00	-0.02	0.00	0.00	0.82	-0.04	0.00
80	0.00	-0.54	0.00	-0.02	0.00	0.00	1.09	-0.01	0.00
100	0.00	-0.54	0.00	-0.02	0.00	0.00	1.36	0.00	0.00
120	0.00	-0.54	0.00	-0.02	0.00	0.00	1.64	0.01	0.00
150	0.00	-0.54	0.16	-0.03	0.00	0.00	2.04	0.02	0.00
200	0.00	-0.54	0.16	-0.03	0.00	0.00	2.57	0.02	0.00
300	0.00	-0.54	0.16	-0.02	0.00	0.00	0.00	0.03	0.00
500	0.00	-0.54	0.16	-0.02	0.01	0.00	0.00	0.04	0.00
1'000	0.00	-0.54	0.17	-0.01	0.06	0.00	0.00	0.08	-0.01
2'000	0.01	-0.54	0.18	0.00	0.00	0.01	0.00	0.16	-0.01
5'000	0.02	-0.54	0.18	0.00	0.00	0.01	0.00	0.30	-0.03
8'000	0.04	-0.54	0.19	0.00	0.00	0.02	0.00	0.07	-0.05
10'000	0.04	-0.54	0.19	0.00	0.00	0.03	0.00	0.05	-0.07
15'000	0.07	-0.54	0.19	0.00	0.00	0.05	0.00	0.05	-0.10
20'000	0.09	-0.54	0.19	0.00	0.00	0.06	0.00	0.05	-0.13
25'000	0.11	-0.54	0.19	0.00	0.00	0.08	0.00	0.00	-0.17
30'000	0.13	-0.54	0.19	0.00	0.00	0.09	0.00	0.00	-0.20
40'000	0.18	-0.54	0.19	0.00	0.00	0.12	0.00	0.00	-0.27
45'000	0.20	-0.54	0.19	0.00	0.00	0.14	0.00	0.00	-0.30
50'000	0.22	-0.54	0.19	0.00	0.00	0.15	0.00	0.00	-0.33
100'000	0.45	-0.54	0.19	-0.01	0.00	0.30	0.00	0.00	0.00
500'000	2.25	-0.54	0.19	-0.03	0.00	0.00	0.00	0.00	0.00
1'000'000	4.54	-0.54	0.17	-0.06	0.00	0.00	0.00	0.00	0.00

In the table, some errors drop to zero; this is because a threshold on the error calculation has been set up, respectively reached. Whenever the isotope concentration falls below  $10^{-9}$  at/b/cm, the error is set to 0.0. This prevents computing very high relative errors for isotope concentrations which would be negligible in the criticality calculations.

Explanations should be found at least for the most notable deviations in Tc-99, Sm-149 and Pu-241; reasons will be given in the next section of analysis. It will be shown that the deviations are in any case negligible in the  $K_{\text{eff}}$  calculations in section 2.3.2.

The next comparison in Tab. 2-5 includes the results of CASMO5 with the SNF-lite option (SNF) against the reference results. The decay data in CASMO5 also come from the ENDF/B library. In this case, all the isotopes required for the "actinides only" burnup credit approach (see Tab. 2-1) can be found in the output. However, from the isotopes required for the "actinides plus fission products" burnup credit approach (see Tab. 2-2) only the values for Tc-99, Sm-147, Sm-151, Np-237, Am-242m and Am-243 are found.

Tab. 2-5: Relative error (SNF-E71ref/E71ref) (%) of isotopic concentrations.

Time	Tc-99	U-233	U-234	U-235	Np-237	U-238	Pu-240	Pu-241	Am-241	Pu-242
0	0.00	0.00	0.00	0.00	0.00	0.00	0.00	0.00	0.00	0.00
1	0.06	0.00	-0.02	-0.01	-0.01	-0.01	-0.01	0.00	-0.21	-0.01
2	0.06	0.00	-0.03	-0.01	-0.01	-0.01	-0.02	0.03	-0.27	-0.01
5	0.06	0.00	-0.05	-0.02	-0.01	-0.01	-0.01	0.09	-0.31	-0.01
10	0.06	0.00	-0.08	-0.01	-0.02	-0.01	-0.01	0.19	-0.30	0.00
20	0.06	0.00	-0.13	-0.01	-0.02	-0.01	-0.01	0.39	-0.24	0.01
40	0.06	0.00	-0.19	-0.01	-0.04	-0.01	-0.01	0.79	-0.13	0.03
60	0.06	0.00	-0.23	-0.02	-0.04	-0.01	-0.01	1.19	-0.07	0.05
80	0.06	0.00	-0.26	-0.01	-0.04	-0.01	-0.01	1.60	-0.03	0.06
100	0.06	0.00	-0.28	-0.02	-0.05	-0.01	-0.02	2.01	-0.01	0.08
120	0.06	0.00	-0.29	-0.02	-0.05	-0.01	-0.01	2.41	0.00	0.09
150	0.06	0.20	-0.30	-0.01	-0.04	-0.01	-0.01	3.01	0.01	0.11
200	0.06	0.18	-0.32	-0.02	-0.04	-0.01	-0.01	3.80	0.01	0.13
300	0.06	0.17	-0.33	-0.02	-0.03	-0.01	-0.01	0.00	0.02	0.16
500	0.06	0.16	-0.34	-0.03	-0.03	-0.01	-0.01	0.00	0.02	0.19
1'000	0.06	0.16	-0.34	-0.04	-0.03	-0.01	-0.01	0.00	0.04	0.21
2'000	0.06	0.17	-0.34	-0.06	-0.04	-0.01	-0.01	0.00	0.08	0.20
5'000	0.06	0.17	-0.34	-0.16	-0.07	-0.01	0.00	0.00	0.15	0.18
8'000	0.06	0.17	-0.34	-0.27	-0.10	-0.01	0.01	0.00	0.03	0.17
10'000	0.06	0.18	-0.34	-0.35	-0.12	-0.01	0.01	0.00	0.02	0.16
15'000	0.06	0.18	-0.34	-0.53	-0.15	-0.02	0.03	0.00	0.02	0.15
20'000	0.06	0.18	-0.34	-0.70	-0.17	-0.02	0.04	0.00	0.01	0.15
25'000	0.06	0.17	-0.34	-0.84	-0.19	-0.02	0.06	0.00	0.00	0.14
30'000	0.06	0.17	-0.34	-0.97	-0.19	-0.02	0.07	0.00	0.00	0.14
40'000	0.06	0.18	-0.33	-1.17	-0.21	-0.02	0.10	0.00	0.00	0.14
45'000	0.06	0.17	-0.33	-1.25	-0.21	-0.02	0.12	0.00	0.00	0.14
50'000	0.06	0.18	-0.33	-1.32	-0.21	-0.02	0.13	0.00	0.00	0.14
100'000	0.06	0.17	-0.31	-1.63	-0.22	-0.03	0.28	0.00	0.00	0.14
500'000	0.06	0.16	-0.19	-1.72	-0.24	-0.07	0.00	0.00	0.00	0.13
1'000'000	0.05	0.13	-0.06	-1.72	-0.27	-0.09	0.00	0.00	0.00	0.13

Larger deviations are found for U-235 at the end of the period and for Pu-241 as it decays away. Overall, the agreement is quite good, but not all the information needed for the criticality calculation is present.

The comparison with CASMO5 results obtained with the SDC option was performed up to  $10^5$  years (very long computational time), with increasing time steps when permitted. In this sense, iterative refinement of the mesh steps was performed until convergence was checked, simple refinement of the time mesh along the whole period not really being practical, as this led to simulations taking several days. Here, values for all the considered isotopes were available.

In the following Tab. 2-6, only isotopes with relative errors above 1 % have been included and the threshold to set the error to 0.0 was lowered to  $10^{-8}$ . This relaxation is related to the inaccuracy introduced by the time-dependent solution which has been found to be quite dependent on the time step.

Tab. 2-6: Relative error (SDC-E71ref/E71ref) (%) of isotopic concentrations.

Time	Sm-149	Gd-155	U-233	U-234	Pu-238	Pu-239	Pu-240	Am-241	Am-243
0	0.0	0.0	0.0	0.0	0.0	0.0	0.0	0.0	0.0
1	0.0	0.0	0.0	0.0	0.0	0.0	0.0	0.0	0.0
2	0.0	0.0	0.0	0.0	0.0	0.0	0.0	0.0	0.0
5	0.0	0.0	0.0	0.0	0.0	0.0	0.0	0.0	0.0
10	0.0	0.0	0.0	0.0	0.0	0.0	0.0	0.0	0.0
20	0.0	0.0	0.0	0.0	-0.1	0.0	0.0	0.0	0.0
40	0.0	0.0	0.0	-0.1	-0.1	0.0	0.0	0.0	0.0
60	0.0	0.0	0.0	-0.1	-0.1	0.0	0.0	0.0	0.0
80	0.0	0.0	0.0	-0.1	-0.1	0.0	0.0	0.0	0.0
100	0.0	0.0	0.0	-0.1	-0.1	0.0	0.0	0.0	0.0
120	0.0	0.0	0.0	-0.1	-0.1	0.0	0.0	0.0	0.0
150	0.0	0.0	0.0	-0.2	-0.2	0.0	0.0	0.0	0.0
200	0.0	0.0	0.0	-0.2	-0.2	0.0	0.0	0.0	0.0
300	0.0	0.0	0.0	-0.2	-0.3	0.0	0.0	0.0	0.0
500	-0.1	0.0	0.0	-0.2	-0.7	0.0	0.0	0.0	0.0
1'000	-0.1	-0.1	-0.1	-0.3	0.0	0.0	0.0	0.0	0.0
2'000	-0.2	-0.2	-0.1	-0.3	0.0	0.0	0.0	0.0	0.0
5'000	-0.6	-0.4	-0.3	-0.3	0.0	0.0	0.0	3.6	0.0
8'000	-0.9	-0.7	-0.2	-0.4	0.0	0.0	0.0	0.0	0.0
10'000	-1.1	-0.9	-0.2	-0.4	0.0	0.0	0.0	0.0	0.0
15'000	-1.7	-1.4	-1.8	-0.6	0.0	0.0	0.0	0.0	0.0
20'000	-2.4	-1.9	-1.4	-0.7	0.0	0.0	0.1	0.0	0.1
25'000	-3.0	-2.4	-1.1	-0.8	0.0	0.0	0.1	0.0	0.2
30'000	-3.7	-2.9	-0.9	-0.9	0.0	0.0	0.3	0.0	0.3
40'000	-5.1	-4.0	-0.7	-1.1	0.0	0.0	0.8	0.0	0.9
45'000	-5.8	-4.5	-0.7	-1.3	0.0	0.0	1.3	0.0	1.4
50'000	-6.5	-5.1	-0.6	-1.4	0.0	0.1	2.0	0.0	2.3
100'000	-13.7	-10.7	-0.4	-2.7	0.0	1.1	0.0	0.0	0.0

The increasing deviations for Sm-149 and Gd-155 are, in principle, due to error accumulation from previous time step solutions. This is because they increase for further positions in time and remain close to zero in the first years when the time steps are refined.

In contrast, the minor deviations for the actinides are almost certainly due to differences in the decay constant values employed in the CASMO5 library. Note also that the discrepant isotopes are not the same as in the SNF calculation, in particular the Pu-241 difference does not appear here; this suggests that the decay data source is different for both methods.

The comparison against CINDER-1.05 (see Tab. 2-7) shows good agreement; an explanation should be found only for the deviation in the density of Pu-241.

Tab. 2-7: Relative error (CINDER-E71ref/E71ref) (%) of isotopic concentrations.

Time	Gd-155	U-233	U-234	Np-237	Pu-240	Pu-241	Am-241
0	0.00	0.00	0.00	0.00	0.00	0.00	0.00
1	-0.14	0.00	0.00	0.00	0.00	0.02	-0.21
2	-0.14	0.00	0.00	0.00	0.00	0.04	-0.26
5	-0.11	0.00	0.00	0.00	0.00	0.10	-0.30
10	-0.07	0.00	0.00	0.00	0.00	0.20	-0.29
20	-0.03	0.00	0.00	-0.01	0.00	0.40	-0.23
40	0.00	0.00	0.00	-0.02	0.00	0.81	-0.12
60	0.00	0.00	0.00	-0.02	0.00	1.22	-0.06
80	0.00	0.00	0.00	-0.03	0.00	1.63	-0.02
100	0.00	0.00	0.00	-0.03	0.00	2.04	0.00
120	0.00	0.00	0.00	-0.03	0.00	2.45	0.01
150	0.00	0.16	0.00	-0.03	0.00	3.05	0.02
200	0.00	0.16	0.00	-0.02	0.00	3.84	0.02
300	0.00	0.16	0.00	-0.02	0.00	0.00	0.02
500	0.00	0.17	0.00	-0.02	0.00	0.00	0.03
1'000	0.00	0.17	0.00	-0.01	0.00	0.00	0.05
2'000	0.00	0.18	0.00	0.00	0.01	0.00	0.09
5'000	0.00	0.18	0.00	0.00	0.02	0.00	0.16
8'000	0.00	0.19	0.00	0.00	0.02	0.00	0.04
10'000	0.00	0.19	0.00	0.00	0.03	0.00	0.03
15'000	0.00	0.19	0.00	0.00	0.05	0.00	0.02
20'000	0.00	0.19	0.00	0.00	0.06	0.00	0.02
25'000	0.00	0.19	0.00	0.00	0.08	0.00	0.00
30'000	0.00	0.19	0.01	0.00	0.09	0.00	0.00
40'000	0.00	0.19	0.01	0.00	0.12	0.00	0.00
45'000	0.00	0.19	0.01	0.00	0.14	0.00	0.00
50'000	0.00	0.19	0.01	0.00	0.16	0.00	0.00
100'000	0.00	0.18	0.02	-0.01	0.31	0.00	0.00
500'000	0.00	0.17	0.10	-0.03	0.00	0.00	0.00
1'000'000	0.00	0.14	0.13	-0.06	0.00	0.00	0.00

The final comparison concerns MCNP6, namely the CINDER module. A comparison of both solutions showed good agreement, below 0.05 % in all cases, which is due to the convergence tolerances or to the fact that the stand-alone version of CINDER was compiled with "quadruple" precision variables. The only deviation is that of the Gd-155 concentration, which peaks at around 1 % in the first year and then vanishes. The comparison to the SERPENT2 solution is not shown as it is redundant and very similar to the table values above; again, only the Gd-155 concentration deviation is new. There are therefore no notable modifications in the CINDER version in MCNP6.

Finally, the SERPENT2 solution with ENDF/B-VII.1 (E71ref) was used as a term of reference for the benchmark comparison (average values from all participants), as shown in Tab. 2-8. Except for a few cases, deviations are rather minor, which gives confidence in this solution, but also in most of the previous ones for which the comparisons showed good agreement.

Tab. 2-8: Relative error (E71ref-bench/bench) (%) of isotopic concentrations.

Time	Tc-99	Sm-151	Eu-151	Gd-155	U-233	U-234	Np-237	Pu-238	Pu-241	Pu-242	Am-241	Am-242
0	0.00	0.00	-0.01	0.00	0.00	0.00	-0.01	0.00	0.01	-0.03	0.00	0.00
1	0.01	0.00	-0.30	0.34	0.00	0.00	0.02	0.00	-0.02	-0.02	0.25	0.00
2	0.01	0.00	-0.31	0.33	0.00	0.00	0.01	0.00	-0.05	-0.02	0.31	-0.01
5	0.01	0.01	-0.36	0.26	0.00	0.01	0.00	0.00	-0.11	-0.02	0.37	-0.02
10	0.01	0.02	-0.36	0.19	0.00	0.00	0.01	0.00	-0.24	-0.02	0.35	-0.03
20	0.00	0.04	-0.34	0.07	0.00	0.01	0.03	-0.01	-0.48	-0.02	0.27	-0.04
40	0.00	0.09	-0.30	0.02	0.00	0.01	0.02	-0.01	-0.91	-0.02	0.15	-0.10
60	0.01	0.13	-0.28	0.01	0.00	0.01	0.01	-0.01	-1.36	-0.02	0.08	-0.14
80	0.00	0.17	-0.27	0.00	0.00	0.01	0.01	0.00	-1.78	-0.02	0.02	-0.20
100	0.01	0.21	-0.24	0.00	0.00	-0.01	0.04	-0.01	-2.27	-0.02	-0.01	-0.24
120	0.00	0.26	-0.22	0.00	0.00	0.03	0.02	0.00	-2.74	-0.02	-0.01	-0.28
150	0.01	0.32	-0.20	0.00	-0.59	0.03	-0.34	-0.02	-3.37	-0.02	-0.02	-0.37
200	0.00	0.42	-0.16	0.00	-0.59	0.04	-0.31	-0.04	-4.24	0.02	-0.02	-0.50
300	0.00	0.65	-0.09	0.00	-0.67	0.03	-0.26	-0.03	0.00	0.01	-0.02	-0.79
500	0.00	1.08	-0.03	0.00	-0.55	0.00	-0.23	-0.07	0.00	-0.01	0.01	-1.32
1000	0.00	0.00	0.00	0.00	-0.43	-0.01	-0.17	-0.30	0.00	0.01	0.03	0.00
2000	0.00	0.00	0.01	0.00	-0.37	0.03	-0.16	0.00	0.00	-0.01	-0.02	0.00
5000	0.00	0.00	0.01	0.00	-0.35	0.02	-0.15	0.00	0.00	-0.02	0.12	0.00
8000	-0.01	0.00	0.01	0.00	-0.32	0.01	-0.15	0.00	0.00	0.02	0.51	0.00
10'000	-0.01	0.00	0.01	0.00	-0.31	-0.02	-0.16	0.00	0.00	-0.02	0.95	0.00
15'000	-0.02	0.00	0.01	0.00	-0.34	0.03	-0.16	0.00	0.00	-0.03	2.82	0.00
20'000	-0.01	0.00	0.01	0.00	-0.32	0.03	0.00	0.00	0.00	-0.03	2.80	0.00
25'000	-0.03	0.00	0.01	0.00	-0.28	0.05	0.00	0.00	0.00	-0.02	0.00	0.00
30'000	-0.04	0.00	0.01	0.00	-0.27	0.08	0.00	0.00	0.00	-0.01	0.00	0.00
40'000	-0.03	0.00	0.01	0.00	-0.24	0.06	0.00	0.00	0.00	-0.01	0.00	0.00
45'000	-0.05	0.00	0.01	0.00	-0.23	0.08	0.00	0.00	0.00	-0.03	0.00	0.00
50'000	-0.05	0.00	0.01	0.00	-0.17	0.11	0.00	0.00	0.00	-0.04	0.00	0.00
100'000	-0.09	0.00	0.01	0.00	-0.21	0.18	0.01	0.00	0.00	-0.03	0.00	0.00
500'000	-0.53	0.00	0.01	0.00	-0.15	1.33	0.02	0.00	0.00	-0.25	0.00	0.00
1'000'000	-1.03	0.00	0.01	0.00	-0.11	3.86	0.05	0.00	0.00	-0.51	0.00	0.00

From this comparison, U-234, Pu-241, Am-241 and Am-242m suffer the highest deviations, but less than 5 %. These deviations will not be further investigated as it can be difficult to track their origin from the average of the participants.

### 2.3.1.2 Isotopic concentrations evolution

The results of these decay calculations, namely isotopic concentrations, are used in the criticality calculations implying a changing value of  $K_{\text{eff}}$ . In order to better understand the origin of the  $K_{\text{eff}}$  trend, the isotopic concentration evolution has been plotted as an informative and potentially useful tool.

Relative concentrations ( $\bar{N}_i$ ), calculated as shown in Equations (2.1) and (2.2), are used in the graphics for illustration purposes. The sample mean  $\bar{N}$  is obtained by all concentration calculated for an individual isotope ( $N_i$ ) at a defined instant  $i$  normalised to the number of calculations ( $T$ ).

$$\bar{N} = \frac{1}{T} \sum_{i=1 \dots T} N_i \quad (2.1)$$

$$\bar{N}_i = \frac{N_i}{\bar{N}} \quad (2.2)$$

Fig. 2-1 shows the evolution of actinides (for a limited set of nuclides, i.e. set 1) with the largest change in their concentrations relative to the average of the computed values. For a better understanding, the isotopes are illustrated in different plots, according to the magnitude of the relative change computed. The comparison of different nuclide evolutions is done on a qualitative basis, but nonetheless illustrates the criticality behaviour. In particular, Fig. 2-1 illustrates that the change in  $K_{\text{eff}}$  for the first 100 years could be driven by the change in Pu-241 concentration together with the influence of Am-241 and Pu-238. Until the first 1'000 years, Am-241 and Pu-238 can play a role and, from 1'000 years on, the change in U-233 concentration could have a major influence on the evolution of  $K_{\text{eff}}$ .

However, in order to better understand the influence of these isotopic evolutions on criticality behaviour, a sensitivity study of  $K_{\text{eff}}$  to the concentrations of each isotope, for each time position, needs to be carried out. Results on the treatment of the sensitivities to nuclide total cross section as a function of decay time can be found in NEA (2012). From these analyses, we can conclude that, of the isotopes in Fig. 2-1 (nuclides with the largest relative change grouped in set 1), Pu-238, Pu-241 and Am-241 will have an impact on the time evolution of  $K_{\text{eff}}$ , while the change in the U-233 concentration will have a negligible impact on  $K_{\text{eff}}$ .

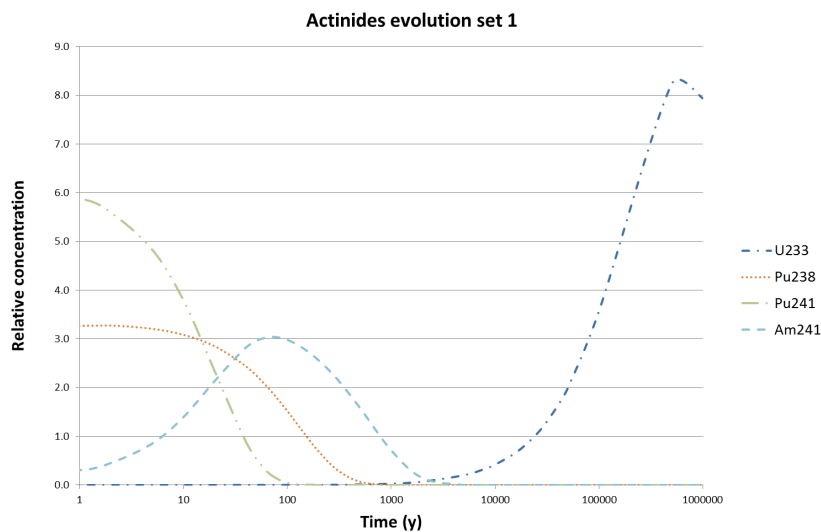


Fig. 2-1: Evolution of actinides with the largest change in their concentrations relative to the average of computed values.

Fig. 2-2 shows the relative concentration evolutions for the other actinides considered (nuclides with slight relative change; grouped in set 2) on a logarithmic scale. The changes in these concentrations would start to have a possible impact after the first 1'000 years. After approximately 10'000 years, the concentrations of U-234, Pu-239, Pu-240 and Pu-242 start to decrease in the material compositions; from the sensitivity values, only Pu-239 and Pu-240 will notably impact  $K_{eff}$  evolution. The concentration of U-235 rises and that of U-236 stabilises and decreases slowly; from the sensitivities, U-235 will have a strong impact on  $K_{eff}$  at the end of the period.

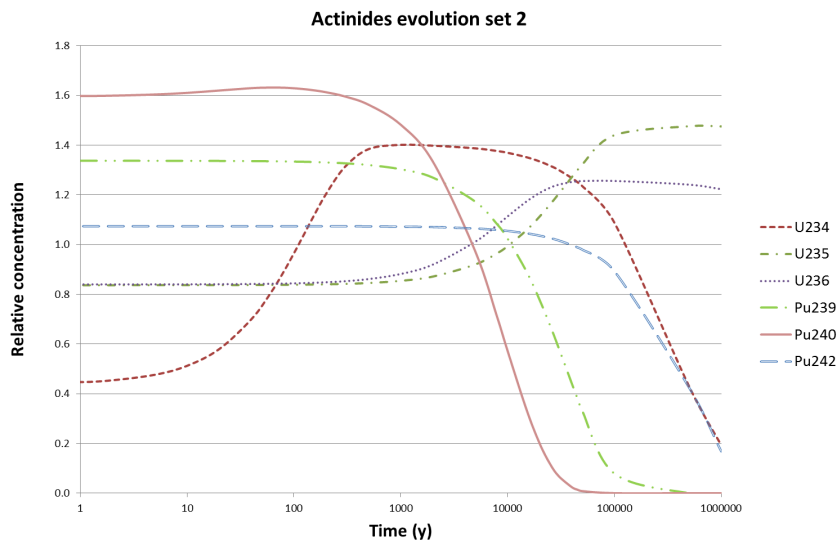


Fig. 2-2: Evolution of actinides with slight changes in concentrations relative to the average of computed values.

Fig. 2-3 shows the evolution of fission products and minor actinides, according to Tab. 2-2, needed if treating the "actinides plus fission products" burnup-credit case. In the first 1'000 years, Sm-151 and Am-242m vanish from the material with small impact on  $K_{eff}$ . Am-243 takes almost until 100'000 years to disappear, but its importance is also low. Tc-99 is the most long-lived fission product of the group studied, starting to disappear after 10'000 years until the end of the 1 million year period. Also the sensitivity of  $K_{eff}$  is low. However, Gd-155 and Sm-147 show an increase in the first decade and Eu-151 and Np-237 in the first hundreds of years. They then stabilise, except Np-237 which starts to decline after 100'000 years, becoming the only isotope to which  $K_{eff}$  results are sensitive from 1'000 years on.

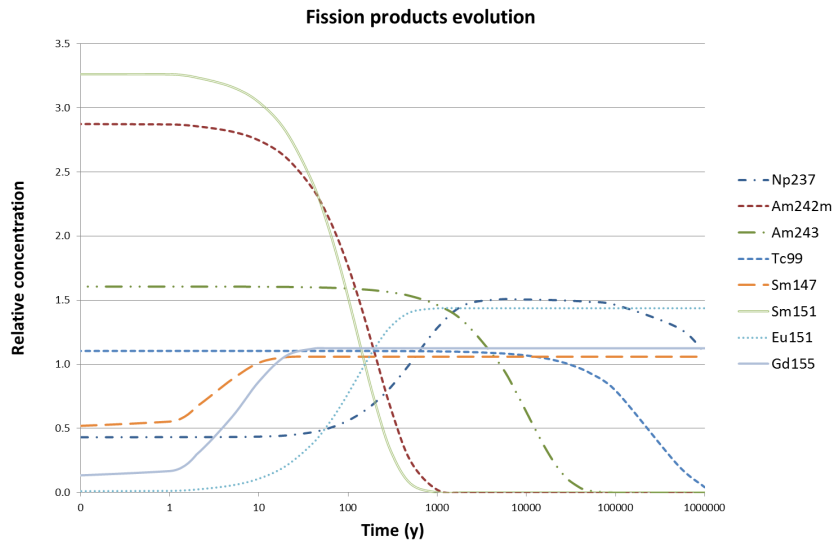


Fig. 2-3: Evolution of fission products and minor actinides with notable changes in their concentrations relative to the average of computed values.

A dedicated analysis of the more relevant nuclides is given below.

### Plutonium-241 decay constant

Noticeable relative differences for the computed Pu-241 concentration was found between the different results of the decay calculations.

First the values obtained with SERPENT2 and the JEFF-3.1.1 decay data yield final concentrations higher than the corresponding ENDF/B-VII.1-based concentrations (see Tab. 2-4). The parent nuclide for Pu-241 is Cm-245 and its half-life of 8'500 years is much longer than the 100 years needed for Pu-241 to disappear, and the values of the decay constant for this isotope are the same in both evaluations. Therefore, decay data are not the reason for the difference in the computed values.

On the other hand, the half-life of Pu-241 in JEFF-3.1.1 is  $14.33 \text{ y} \pm 0.04 \text{ y}$ , and the value in ENDF/B-VII.1 is  $14.290 \text{ y} \pm 0.006 \text{ y}$ . Pu-241 will therefore decay faster using ENDF/B data and this is confirmed from the calculations.

Next, the comparison in Tab. 2-5 included SNF results, again with a behaviour similar to that in the JEFF calculations, so this code should again be using a different decay constant. On the other hand, SDC results in Tab. 2-6 agree well with latest ENDF/B data, and we know ENDF/B-VII.0 data have already been included.

The values calculated using the latest ENDF/B were then compared to the CINDER results, observing again the same behaviour (see Tab. 2-6). In this case, we know that the data come from the ENDF/B-VI.8 evaluation, which included a decay constant value of  $14.35 \text{ y} \pm 0.1 \text{ y}$ . This agrees with the stronger discrepancy encountered with JEFF data, because of the longer half-life.

As a matter of fact, the discrepancy from SNF-lite results for Pu-241 is similar to that of CINDER, surely indicating that ENDF/B-VI.8 data are also being used in this module, although for other isotopes other data may have been employed. In fact, not all deviations are similar, which means

that this could be an effect of the calculation methodology or even of the precision of the employed variables.

As a conclusion, a lesson learned is to pay attention to the accompanying uncertainties. All three values are consistent as the nominal value of each evaluation is within the uncertainty band of the other two. Since the lowest uncertainty is related to the value from ENDF/B-VII.1, this library should be considered as the reference, at least for this isotope. All differences within the benchmark come from participants using less accurate JEFF or older ENDF data.

### **Technetium-99 decay constant**

A growing discrepancy between JEFF and ENDF/B results was also observed for Tc-99. This isotope is not bred by any parent in this case. The half-life in JEFF-3.1.1 is  $214'000 \text{ y} \pm 8'000 \text{ y}$ , and in ENDF/B-VII.1  $211'105 \text{ y} \pm 1'200 \text{ y}$ . This agrees with higher concentrations after decay computed with JEFF data. Again, ENDF/B-VII.1 data are the reference because of the lower uncertainties in the decay constants and the deviations in the benchmark average come from participants employing JEFF data.

Considering the chain  $\text{Mo-99} \rightarrow \text{Tc-99}$ , the differences in Tc-99 concentrations obtained with SERPENT2 using JEFF and ENDF values are compared in Tab. 2-9 against the related differences resulting from an analytical calculation performed with the same data from JEFF and ENDF. Both calculations show the same range of relative error.

Tab. 2-9: Relative error (J311-E71/E71) (%) of Tc-99 isotopic concentrations.

Time (y)	Computed	Analytical
0	0.00	0.00
1	0.00	0.00
2	0.00	0.00
5	0.00	0.00
10	0.00	0.00
20	0.00	0.00
40	0.00	0.00
60	0.00	0.00
80	0.00	0.00
100	0.00	0.00
120	0.00	0.00
150	0.00	0.00
200	0.00	0.00
300	0.00	0.00
500	0.00	0.00
1'000	0.00	0.00
2'000	0.01	0.01
5'000	0.02	0.02
8'000	0.04	0.04
10'000	0.04	0.04
15'000	0.07	0.07
20'000	0.09	0.09
25'000	0.11	0.11
30'000	0.13	0.13
40'000	0.18	0.18
45'000	0.20	0.20
50'000	0.22	0.22
100'000	0.45	0.44
500'000	2.25	2.22
1'000'000	4.54	4.24

### Americium-243 decay constant

For Am-243, the JEFF half-life is approximately  $7'365.0 \text{ y} \pm 21.9 \text{ y}$  and ENDF/B is  $7'370.1 \text{ y} \pm 15.0 \text{ y}$ , and the differences in their decay calculations can be explained on the basis of this half-life difference. However, it is not so clear which nominal value is the best, although the uncertainty in the ENDF decay constant is half of the uncertainty in the JEFF decay constant.

Considering the chain Pu-243 → Am-243, the differences in Am-243 concentrations obtained with SERPENT2 using JEFF and ENDF values are compared in Tab. 2-10 with the related differences resulting from an analytical calculation performed with the same data from JEFF and ENDF. Both calculations show the same range of relative error.

Tab. 2-10: Relative error (J311-E71/E71) (%) of Am-243 isotopic concentrations.

Time (y)	Computed	Analytical
0	0.00	0.00
1	0.00	0.00
2	0.00	0.00
5	0.00	0.00
10	0.00	0.00
20	0.00	0.00
40	0.00	0.00
60	0.00	0.00
80	0.00	0.00
100	0.00	0.00
120	0.00	0.00
150	0.00	0.00
200	0.00	0.00
300	0.00	0.00
500	0.00	0.00
1'000	-0.01	-0.01
2'000	-0.01	-0.01
5'000	-0.03	-0.03
8'000	-0.05	-0.05
10'000	-0.07	-0.07
15'000	-0.10	-0.10
20'000	-0.13	-0.13
25'000	-0.17	-0.16
30'000	-0.20	-0.20
40'000	-0.27	-0.26
45'000	-0.30	-0.28
50'000	-0.33	-0.30
100'000	0.00	-0.06
500'000	0.00	0.00
1'000'000	0.00	0.00

### **Build-up of samarium-149**

Samarium-149 is stable, but a deviation is observed already in the first decay year between JEFF and ENDF-based calculations, which then remains constant. Therefore, some parent isotope with a short half-life should be identified as responsible. It can be confirmed that for all isotopes in the Sm-149 decay chain (considering all the isotopes present in the initial spent fuel composition), the decay constants were the same in JEFF-3.1.1 as well as ENDF/B-VII.1. The only exception is for Sm-149 itself, which is considered stable in ENDF/B, but radioactive in JEFF, with a half-life of  $2 \times 10^{15}$  years. This is several orders of magnitude higher than the next higher value of its parent Pm-149, which is 2.21 days.

Comparing the linear system values in the TTA solution method used in SERPENT2, it was found that the matrix condition was very poor for the JEFF coefficient for samarium. A fix-up was introduced to nullify decay constants lower than  $10^{-19}$  seconds, which in practice makes the samarium isotope be considered as stable with a decay constant of the order of  $10^{-23}$  seconds. After this change, the relative errors between JEFF and ENDF/B remain as in Tab. 2-4, except that the discrepancy for Sm-149 disappeared.

#### **2.3.1.3 Codes and decay data comparison**

In summary, SERPENT2 and CINDER (in- or outside MCNP6) are both good candidates for decay calculations, although the decay data used by CINDER are outdated. Also, the decay data from JEFF-3.1.1 are adequate if compared to ENDF/B-VII.1, but the latter should be preferred because of lower uncertainties. In general, the latter also has data with high accuracy for the decay heat (not related to this study).

SERPENT2 has the advantage of availability of the source code and the possibility to implement any set of decay data.

For CASMO5, the values from the SNF-lite method are accurate but several fission products are not present in the output file and could not be compared. Also, the decay constants seem to be outdated. It may be relevant to mention that the results from the SDC calculation showed a doubtful accuracy when the time step is enlarged; additionally, long running times are needed to reach positions far in time. In principle, CASMO5 does not seem to be a good candidate for the implementation of the BUCSS-R sequence; nevertheless, it could be considered as a tool for verification of the sequence after the translation step.

### **2.3.2 Criticality calculations for Transport/Storage cask**

The criticality calculations were performed for all the cross section libraries and code combinations available with the isotopic compositions calculated with SERPENT2 and ENDF/B-VII.1 decay data as input.

First, a single fuel pin in infinite lattice was employed to obtain preliminary results from the setup of each pair of code-library combinations. An early estimate of the agreement between MCNP6 and SERPENT2 was found using the same library and checking the differences between the neutron data distributions using the same code. After the pin calculations, a full cask configuration was developed according to the benchmark requirements (21 FA, 17×17 PWR), and the study was revisited and expanded as reported in the following.

### 2.3.2.1 Comparison of the effective neutron multiplication factor

Each run used 150 inactive cycles and 2'000 active cycles, with 10'000 histories per cycle. The initial fission source was set up at every fuel pin position in the lattice, following constant probabilities in the radial and axial positions of the pin and the default Watt fission spectrum for energy. All the cases were run in parallel with OpenMP.

For the spent fuel case, since the calculations are performed over a large time scale, each input "fission source" is taken from the previously converged problem. The initial spent fuel case already used the fresh fuel case fission source from file.

The  $K_{\text{eff}}$  values for the fresh fuel problem, as specified in the benchmark, are given first in Tab. 2-11 and Tab. 2-12.

Tab. 2-11:  $K_{\text{eff}}$  values for fresh fuel calculation with MCNP6.

Library	ENDF/B-VII.1 (MCNP6)	JEFF-3.2	TENDL13	ENDF/B-VII.1 (NNDC)
$K_{\text{eff}}$	1.15008	1.15040	1.14941	1.14990
$2\sigma$	0.00034	0.00032	0.00034	0.00034

Tab. 2-12:  $K_{\text{eff}}$  values for fresh fuel calculation with SERPENT2.

Library	ENDF/B-VII.1 (MCNP6)	JEFF-3.2	TENDL13	ENDF/B-VII.1 (NNDC)
$K_{\text{eff}}$	1.15028	1.15043	1.14924	1.14967
$2\sigma$	0.00032	0.00034	0.00034	0.00034

For the benchmark calculations on a fuel cask configuration, the ENDF/B-VII.1 data from MCNP6 were used.

The results for the fresh fuel calculation between MCNP6 and SERPENT2 show good agreement, overlapping the uncertainty bands for each calculation. A slight difference between ENDF and JEFF results exists, however, for the JEFF case where only thermal scattering data for hydrogen in water are being used; in the other cases, all the available TSL (Thermal Scattering Law data) are employed with ENDF data (see Appendix A for more details about the effect of thermal scattering data on  $K_{\text{eff}}$ ).

Fig. 2-4 shows the evolution of  $K_{\text{eff}}$  as computed with MCNP6 (M6) for the three cross section libraries considered, for the case of actinides only. The results include the  $2\sigma$  uncertainty bands from the Monte Carlo result, which are not noticeable. Also, the benchmark average value is shown for comparison together with its  $2\sigma$  deviation as computed from all participants' results.

From this figure, the results for the first decades and after 1'000 years are all within the uncertainty band of the benchmark average result. However, in the period close to 100 years a discrepancy between the average benchmark value and the results from JEFF-3.2 (J32) and TENDL-2013 (T13) exists. It can be seen from Fig. 2-4 that the latter is outside the deviation band.

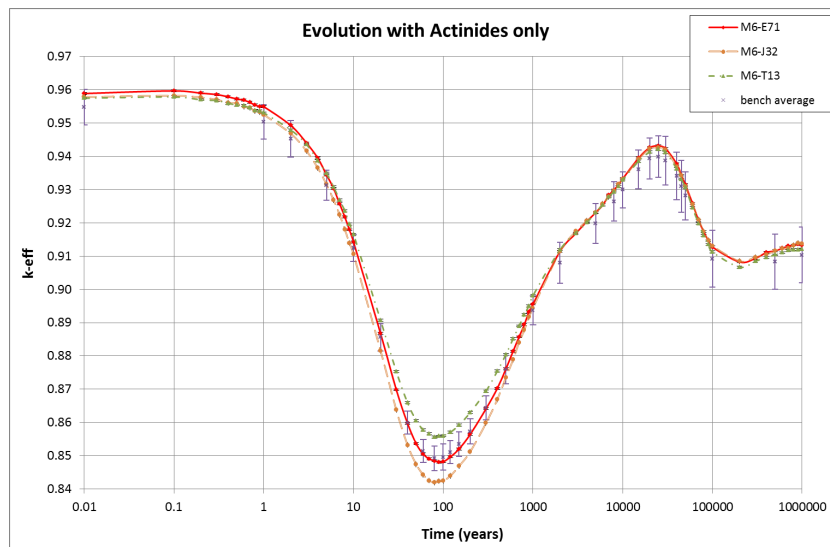


Fig. 2-4:  $K_{\text{eff}}$  computed with MCNP6 for the three libraries and benchmark average with actinides only composition (actinides only case).

For completeness, the results from SERPENT2 (S2) are also included here, for the same situation, as shown in Fig. 2-5.

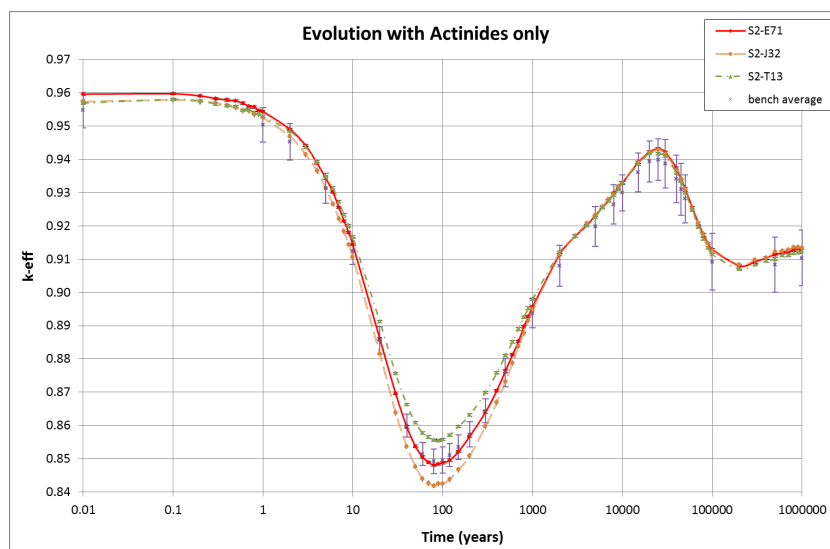


Fig. 2-5:  $K_{\text{eff}}$  computed with SERPENT2 for the three libraries and benchmark average with actinides only composition (actinides only case).

Calculations were also performed for the actinides plus fission products case, as indicated in the benchmark specifications. The evolution of the effective neutron multiplication factor with this set of isotopes shows a similar trend to the calculations including the actinides only, but  $K_{\text{eff}}$  reaches lower values due to the poisoning effect of the fission products (see Fig. 2-6 for the MCNP6 case). In particular, the increase in  $K_{\text{eff}}$  after 100 years is very much reduced by the fission products effect.

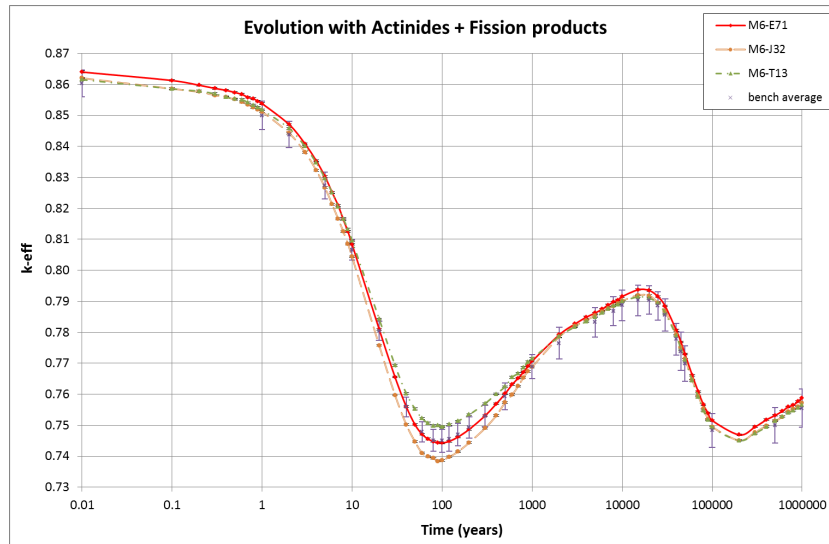


Fig. 2-6:  $K_{\text{eff}}$  computed with MCNP6 for the three libraries and benchmark average with actinides plus fission products composition (actinides plus fission products case).

As for the actinides only case, apart from the slight deviations of the results from one library to the others, the same discrepancy appears around 100 years.

The same calculations were done using SERPENT2, as shown Fig. 2-7, for the actinides plus fission products case.

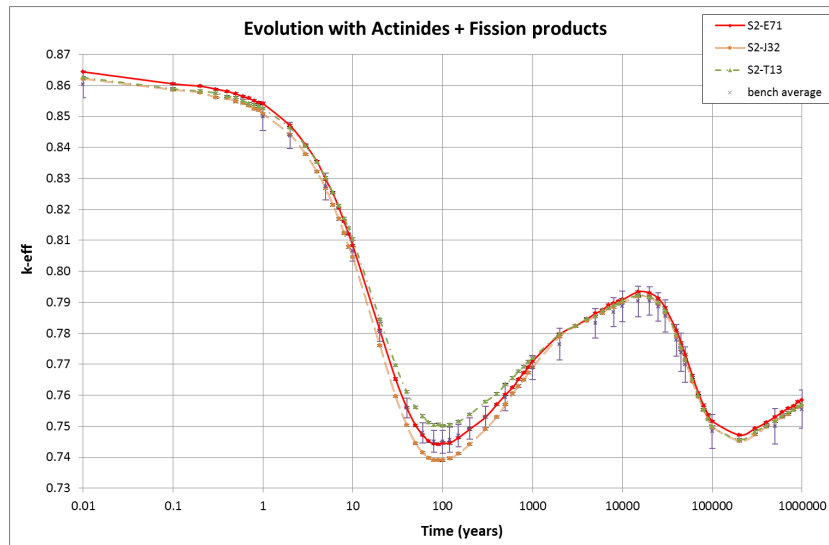


Fig. 2-7:  $K_{\text{eff}}$  computed with SERPENT2 for the three libraries and benchmark average with actinides plus fission products composition (actinides plus fission products case).

### 2.3.2.2 Further analysis of the results

Effective neutron multiplication factors can be computed accurately with SERPENT2 or MCNP6, with a similar statistical uncertainty for a given number of histories and cycles. The computing time for each case is around 10 minutes for SERPENT2 and close to 20 minutes for MCNP6, using 12 processors in parallel.

Both codes are being maintained and developed, but in practice SERPENT2 offers the advantage of availability of the source, open use with no fees, and the possibility to run in parallel on large clusters with MPI interface. In contrast, the MPI version of MCNP6 is not available in the official distribution. In principle, developments for both codes should be maintained where possible.

#### Effect of americium-241 on deviations

The observed deviation of the results for the three libraries after 100 years are of about the same magnitude, but opposite in direction: TENDL-2013 cross sections yield a higher  $K_{\text{eff}}$  value, whilst JEFF-3.2 yields a lower  $K_{\text{eff}}$  value. From the previous analysis on isotopic time evolution, as shown in Fig. 2-1, Am-241 reached its peak concentration exactly in this same period, around 100 years after storage, and the concentration takes the parabolic shape of  $K_{\text{eff}}$ ; therefore, the sensitivity of  $K_{\text{eff}}$  to this isotope is remarkable.

Starting from this consideration, the same calculations were performed substituting the Am-241 cross section in JEFF-3.2 and TENDL-2013 with the ACE library file in ENDF/B-VII.1. The results of this test are given in Fig. 2-8 and Fig. 2-9 respectively, showing that the agreement in  $K_{\text{eff}}$  value is improved to the point where all results are now within the benchmark deviation band.

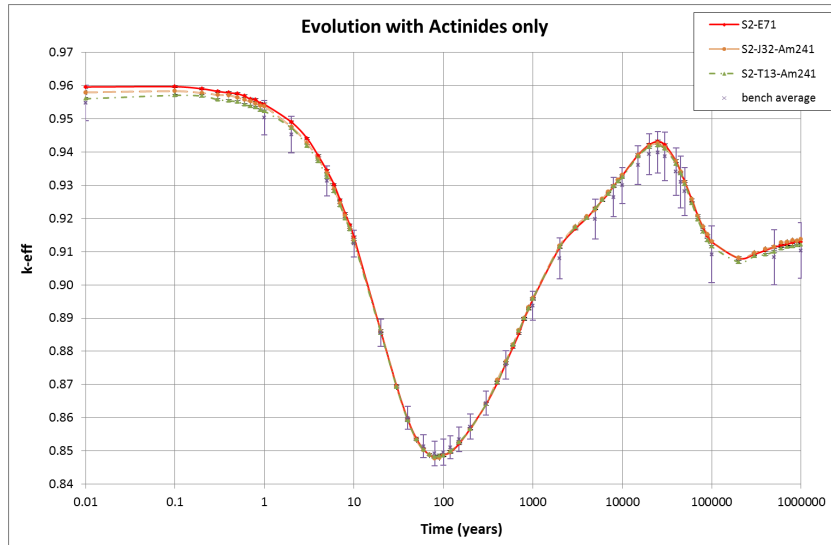


Fig. 2-8:  $K_{eff}$  computed with SERPENT2 for the three libraries using Am-241 data from ENDF/B-VII.1 only, for actinides only composition.

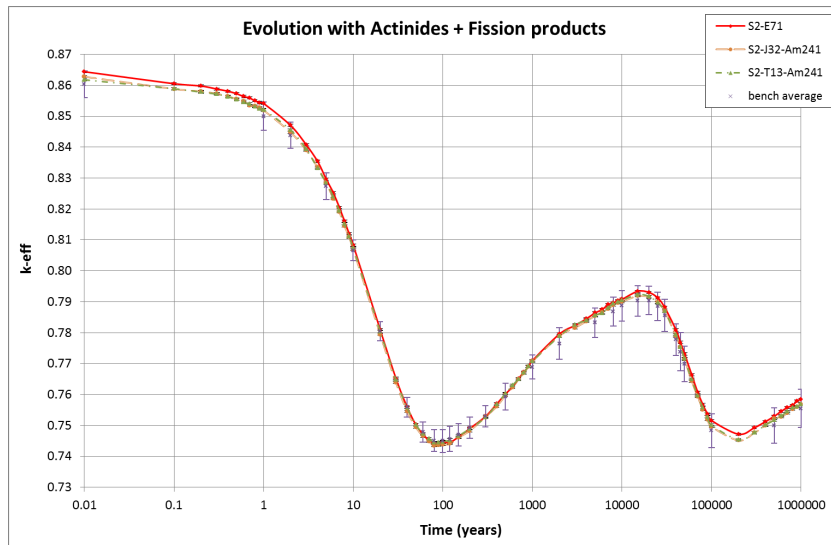


Fig. 2-9:  $K_{eff}$  computed with SERPENT2 for the three libraries using Am-241 data from ENDF/B-VII.1 only, for actinides plus fission products composition.

In the beginning, it was observed that the TENDL-2013 data for some isotopes, including Am-241, lacked the probability tables for the unresolved resonance region. A new update to these files was obtained for some of these isotopes, although a new calculation of the  $K_{\text{eff}}$  evolution showed almost no change in the results, and the discrepancy in TENDL-2013 remained unsolved.

As shown in Fig. 2-10, the cross section value for Am-241 has been updated from JEFF-3.1.2 to JEFF-3.2, and is now slightly higher than the ENDF/B-VII.1 value; this is in agreement with the lower  $K_{\text{eff}}$  computed. On the contrary, the value from TENDL-2013 is lower than the other two, also indicated by the higher computed  $K_{\text{eff}}$ .

According to the recent update, the value for Am-241 has been updated based on experiments with MOX fuel to improve the agreement with the measurements (Noguere 2012). Based on this consideration, it would be reasonable to take the JEFF-3.2 results as the reference. The deviation of TENDL-2013 at 100 years is 1'000 pcm, while the deviation of ENDF/B-VII.1 is 500 pcm.

In any case, all three nominal values are within the uncertainty band associated with ENDF data, and a conclusive statement cannot be made.

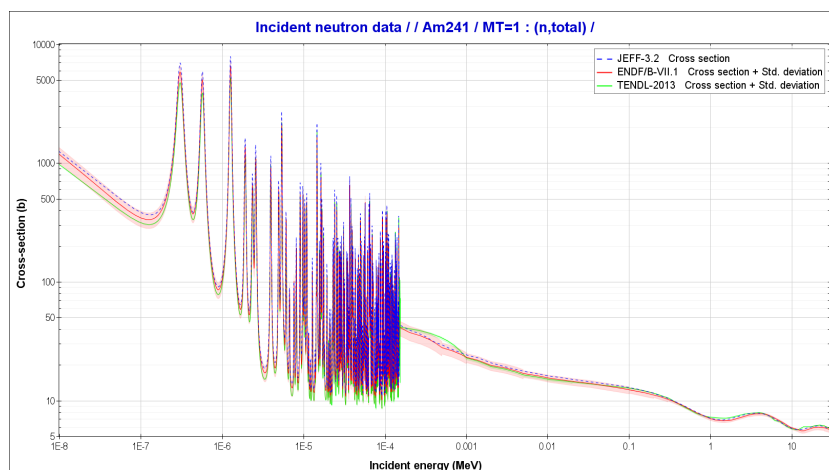


Fig. 2-10: Am-241 cross section on different cross section evaluations.

Figs. 2-11 and 2-12 show the deviations of the computed SERPENT2 solutions again using the three libraries with the benchmark average solution. The results given from MCNP6 are not presented as the behaviour is similar. The uncertainty bands are not shown in these graphs (but were already highlighted in Fig. 2-5 and Fig. 2-9), however the  $2\sigma$  of the new results is around 30 pcm, while the deviation of the average benchmark values is between 300 and 900 pcm.

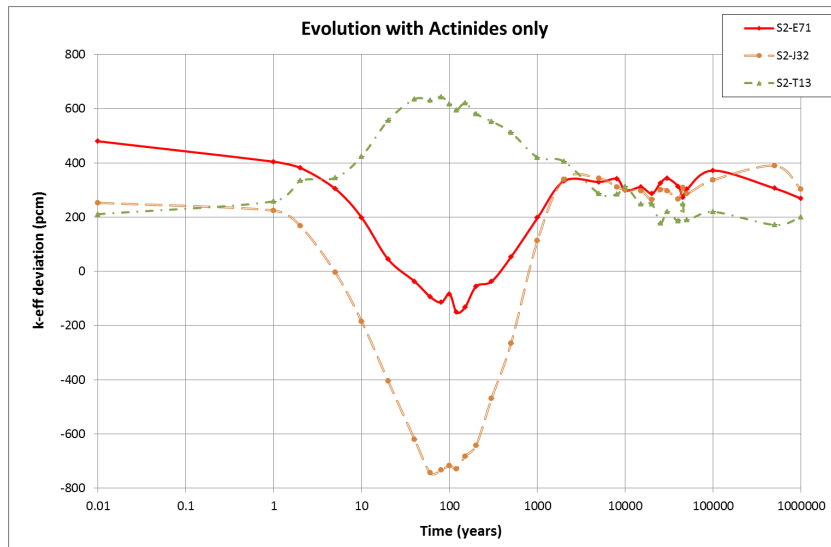


Fig. 2-11:  $K_{eff}$  deviations to benchmark average computed with SERPENT2.

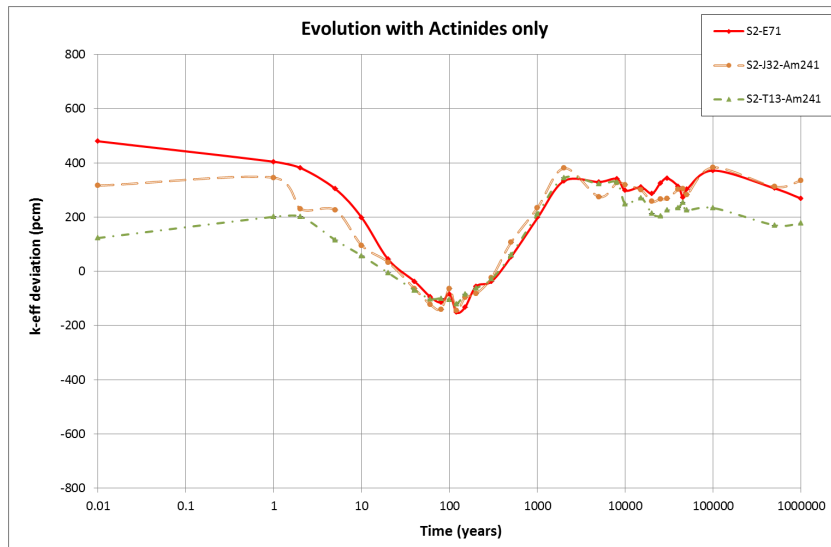


Fig. 2-12:  $K_{eff}$  deviations to benchmark average computed with SERPENT2 and actinides only, using Am-241 data from ENDF/B-VII.1.

Fig. 2-12 suggests that some differences in the cross sections still exist (and these are for some isotopes relevant to the early phase of the decay period) between ENDF and JEFF and also for TENDL (at the early and late phase of the decay period).

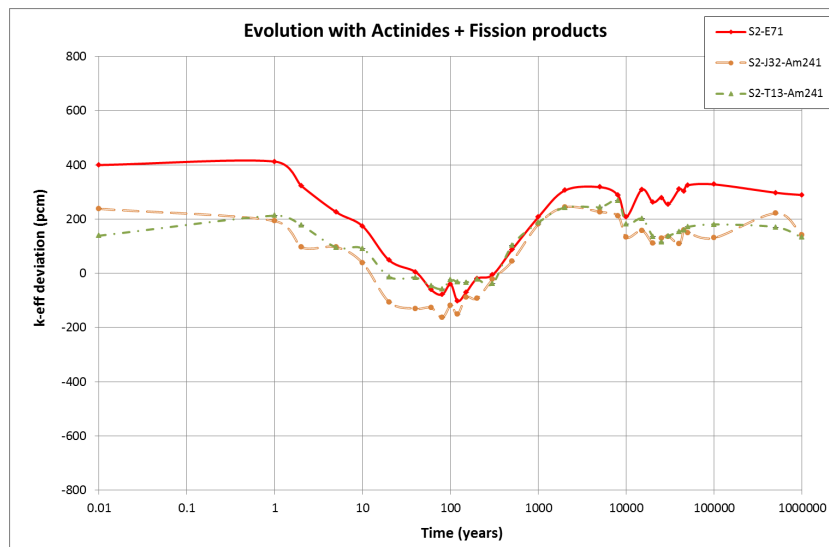


Fig. 2-13:  $K_{\text{eff}}$  deviations to benchmark average computed with SERPENT2 and actinides plus fission products, using Am-241 data from ENDF/B-VII.1.

Finally, the results including the fission products are given in Fig. 2-13, with the Am-241 effect eliminated. The graph shows that a significant difference exists between the cross sections for the fission products in ENDF and JEFF. The deviation of TENDL nevertheless remains quite similar to the actinides only case.

### Effect of plutonium-241 on deviations

As observed in Fig. 2-1, two actinides have a significant evolution in the first hundred years, which matches with the behaviour of  $K_{\text{eff}}$ , as observed in Fig. 2-2. The former, Am-241, was treated in the previous section. The second isotope, which could explain deviations in  $K_{\text{eff}}$  between libraries, would be Pu-241, as the sensitivities to Pu-238 and U-233 are both lower than this.

The same type of study as presented for Am-241 was performed for Pu-241, employing the ACE file from ENDF/B-VII.1 with the three library evaluations. The ACE file from ENDF/B-VII.1 for Am-241 was also kept. Fig. 2-14 and Fig. 2-15 show the deviations obtained against the average results of the benchmark, for the actinides only and actinides plus fission products cases.

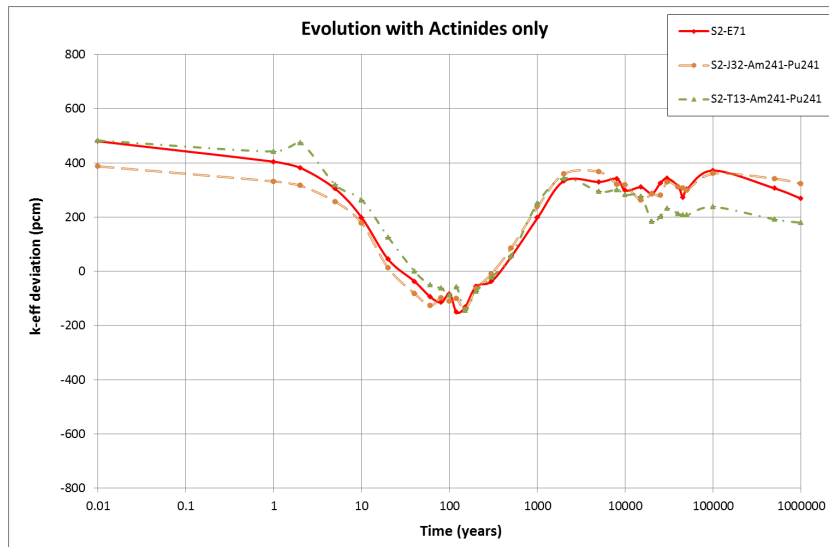


Fig. 2-14:  $K_{\text{eff}}$  deviations to benchmark average computed with SERPENT2 and actinides only, using Am-241 and Pu-241 data from ENDF/B-VII.1.

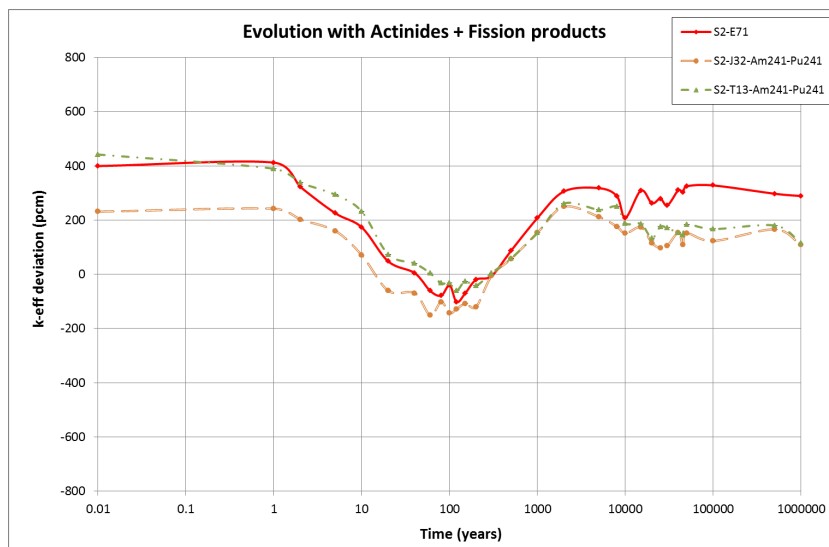


Fig. 2-15:  $K_{\text{eff}}$  deviations to benchmark average computed with SERPENT2 and actinides plus fission products, using Am-241 and Pu-241 data from ENDF/B-VII.1.

For the case of actinides only, the match between ENDF/B and JEFF is very much improved, although a slight deviation remains in the first 10 years. Reasons for this are unclear.

With actinides only, TENDL maintains a deviation from 20'000 years to 1 million years, indicating a deviation of the cross sections for some already stabilised actinide, probably U-236.

For the case of actinides plus fission products, JEFF deviates from the ENDF/B results for the whole 1 million year period, therefore Gd-155 and Np-237 are good candidates for this effect.

Also, the deviations in TENDL could be explained with these isotope cross sections, at least to the same extent.

The plot of the Gd-155 capture cross section in Fig. 2-16 shows discrepancies for the three evaluations from 0.1 keV, which supports its candidature.

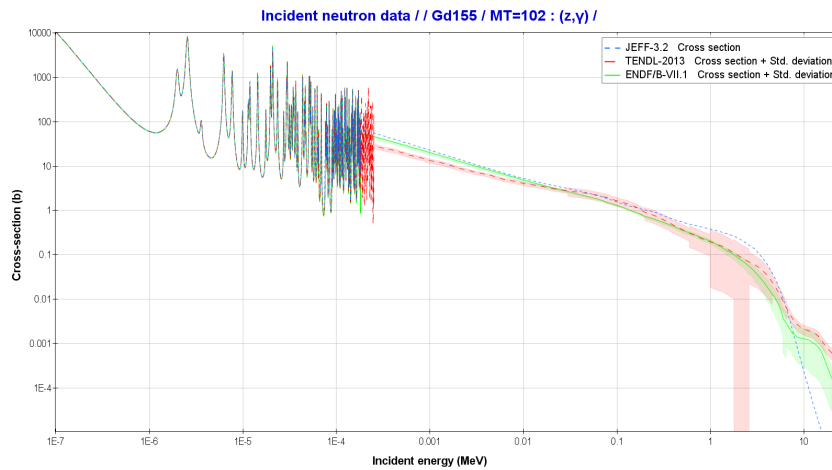


Fig. 2-16: Gd-155 cross section on different cross section evaluations.

Also, the plot for Np-237 in Fig. 2-17 shows significant differences in the resonance region, a candidate for improvement in JEFF.

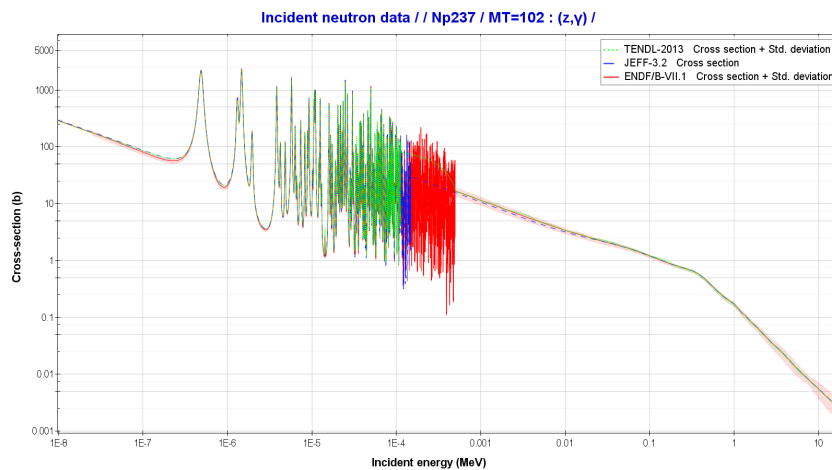


Fig. 2-17: Np-237 cross section on different cross sections evaluations.

## 2.4 Conclusions to Chapter 2

The WPNCS BUC Phase 7 benchmark, organised by the OECD/NEA, was used to evaluate the ability of decay codes to predict the concentrations of isotopes important for burnup-credit application and the ability of criticality codes to predict  $K_{\text{eff}}$  values for the geological disposal timeframe.

The results of the benchmark for the decay calculations showed a good agreement with the other participants, on average. The main deviation was found for the Pu-241 decay chain and, to a lesser extent, for other chains, although these deviations can be explained with the nuclear decay dataset. It can be noted that ENDF/B-VII.1 decay data are, to date, the best available for the type of calculations considered, since they have the lowest uncertainty in nominal values and because the JEFF nominal data do not lie within the ENDF uncertainty bands, suggesting that the JEFF values may be incorrect.

Given the performance of the SERPENT2 decay module, it seems that this is the best solution for the decay calculations. SERPENT also allows the implementation of decay data in ENDF format from any source.

SERPENT2 can perform criticality calculations coupled with decay calculations. However, MCNP was chosen as the reference code for criticality calculations, due to the worldwide establishment and reliability of the code, even if the SERPENT2 criticality calculations were satisfactory enough.

Cross section data comparisons showed good agreement in a rough sense for the three distributions considered, although JEFF-3.2 seems up to now to be the most accurate library and better adapted when including MOX fuels. ENDF data remain valid as the uncertainty band contains JEFF nominal values, while the JEFF data do not include uncertainty bands in cross sections. As for the benchmark results, a new solution with slight deviations from the benchmark average for the decay part has been computed with ENDF/B-VII.1 decay data, but with a significant difference for the  $K_{\text{eff}}$  results compared to the latest JEFF-3.2 cross sections.

### **3 Bounding case analysis of spent nuclear fuel operated in Swiss PWRs for loading in disposal canisters**

The determination of the final loading curves for SNF to be loaded in disposal canisters is preceded by a preliminary study, namely the evaluation of bounding and/or conservative conditions.

Criticality margins have been computed for PWR fuel assemblies using realistic irradiation conditions for different enrichments, burnup levels, fuel assembly designs and fuel compositions. The results are bounding in the sense of employing the highest possible enrichment of fuel irradiated in the Swiss power plants, but can also be considered as a best estimate as real operational data were used for the burnup calculations.

Calculations were performed for the "actinides only" case and for the "actinides plus fission products" case. The inclusion of some minor actinides and fission products in the latter approach shows an increase of at least 4'000 pcm in the criticality margin in general, and this contribution rises during the disposal period.

From these preliminary results, even considering the effect of the fission products, it is clear that PWR fuel cannot be loaded into the canisters without taking credit for the burnup and preferably loading them in a mixed configuration of different burnup levels. The option of some canisters being not fully loaded could be an alternative approach, but would be also challenging from another point of view (logistics and cost optimisation).

#### **3.1 Introduction**

The application of burnup credit in post-closure disposal applications requires the establishment of a well-defined methodology aiming to ensure the fulfilment of all safety requirements needed for spent nuclear fuel disposal. According to the different phases of the burnup credit analysis process, i.e. preparation of models, depletion, criticality calculations and final implementation, it is appropriate to consolidate the first three phases into the methodology, which leads to the final implementation phase based on the determination of the final loading curves.

For the specific case at hand in this report, namely the application of burnup credit to long-term disposal of PWR spent nuclear fuel, the preparation of the methodology has consisted of the analysis of the Nagra canister concept (Patel et al. 2012) and the fuel assembly designs corresponding to the Gösgen nuclear power plant (KKG). The loaded canister is assumed to be flooded with water entering through a postulated breach, as is the case for the Swedish design and related criticality assessment (SKB 2010).

For the depletion phase, the fuel assembly depletion code CASMO5 was employed with feedback from the reactor code SIMULATE-3 (SIMULATE 1995) by means of the BOHR tool. The development of a best-estimate methodology together with uncertainty propagation methodologies based on Monte Carlo sampling was under development at the time of the BUCSS-R project duration (Leray 2015).

Between depletion calculations and the criticality calculations, a decay phase is introduced for the study of the long-term evolution of the fuel composition. The decay calculation module within the code SERPENT2, in accordance with the studies described in Chapter 2 and in Herrero (2016), leads to best-estimate results, whereby decay data uncertainties influence the fuel composition

used for the criticality calculations only marginally (Diez 2016). Indeed, the depletion route determines the uncertainties in fuel composition.

For the criticality calculation case, the Monte Carlo transport code MCNP6 allows many approximations in the simulation of the system to be avoided, and it is again part of a best-estimate calculation approach, incorporating Monte Carlo propagated nuclear data uncertainties (Zhu 2015) and technological uncertainties (Pecchia 2015).

Results are presented using the above-described methodology for different loading configurations of the canister, including:

- 4 similar UO<sub>2</sub> fuel assemblies
- 4 similar ERU fuel assemblies
- 4 similar MOX fuel assemblies
- 1 MOX fuel assembly and 3 similar UO<sub>2</sub> fuel assemblies
- 3 similar UO<sub>2</sub> fuel assemblies and an empty position

### 3.2 Development of models

The fuel assemblies selected for the study are those used in KKG, being representative of the highest enrichments and highest burnups among all Swiss fuels. However, the operating history employed by the code to deplete the fuel is based on realistic core conditions, and these conditions are not bounding for the final fuel composition. However, the uncertainties related to the depletion routes and corresponding fuel composition are considered later in Chapter 4 and used to develop the fuel loading curve.

Three fuel assemblies were considered for the analysis:

- I. UOX 4.94 w/o U-235
  - II. MOX 4.80 w/o Pu<sub>fiss</sub>
  - III. ERU 4.599 w/o U-235 Equivalent
- (I) The UO<sub>2</sub> assembly is formed by a 15 × 15 array of fuel pins (with 20 guide tubes) which contains fuel homogeneously enriched at 4.94 w/o and operated up to 5 cycles, reaching discharge burnups of 17.61, 33.82, 50.47, 61.92 and 72.75 GWd/t.
  - (II) The MOX fuel assembly contains a distribution of three slightly different enrichments inside the assembly, with the central rod empty, i.e. flooded with water. The chosen assembly was operated to burnups of 18.10, 34.78, 44.96 and 51.72 GWd/t.
  - (III) The ERU fuel assembly is similar in structure to the UO<sub>2</sub> fuel assembly and was operated to burnups of 17.27, 34.58, 50.10, 56.04 and 61.72 GWd/t.

The disposal canister is basically a carbon steel cylinder, almost 5 metres long and designed to fit 4 PWR fuel assemblies in 4 separate carbon steel boxes inserted and welded (see Fig. 3-1). The analysis performed in Chapter 4 refers wholly to this disposal canister concept.

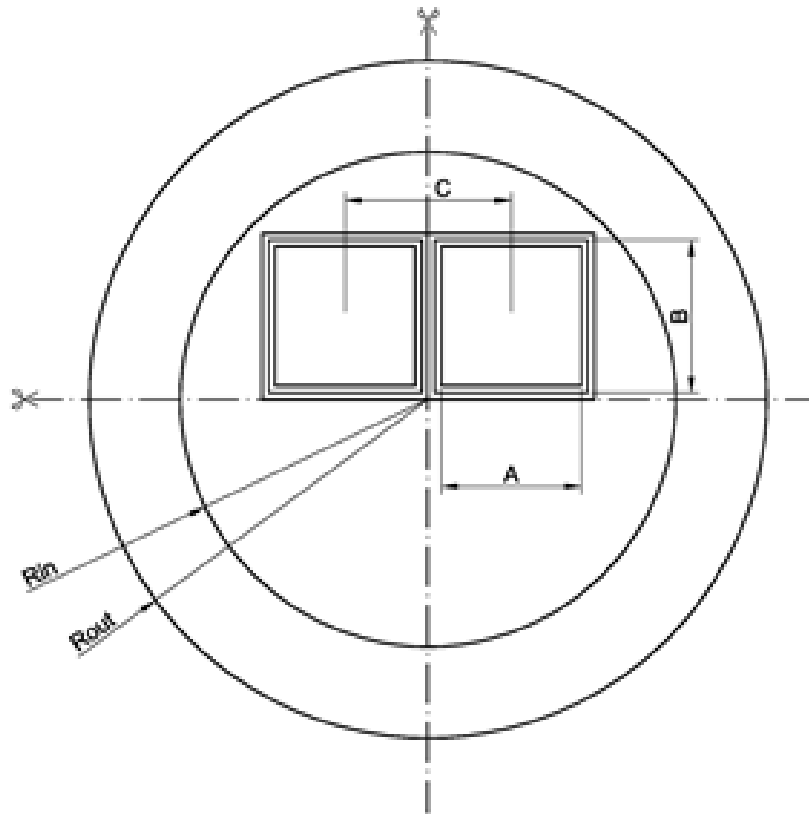


Fig. 3-1: Main dimensions of the carbon steel disposal canister ( $R_{in} = 41$  cm,  $R_{out} = 55$  cm, Box Centre - Centre (C-C) Separation = 17.9 cm).

Half model sector with symmetry axes.

As optimum moderation conditions must be assumed in the criticality safety assessment, the loaded canister is assumed to be flooded with water entering through a postulated breach in the canister. However, fuel or canister degradation scenarios are not considered in this study.

The boundary conditions considered for the calculations are that the canister is emplaced in the repository; therefore, a 35 cm layer of bentonite clay, saturated with water, is included in the model. However, the impact of the bentonite on the reactivity is negligible for a flooded canister. Other conservative assumptions are already present in the model, such as the low material temperature or the presence of water without diluted minerals.

The assemblies loaded in the canister are assumed to come from the same batch, i.e. with the same nuclear and mechanical design. The design of the FA in the model corresponds to that employing the highest enrichment and operated reaching high burnups. For a representative and individual assembly of a given batch, the irradiation history is reconstructed using real plant operation data (all assemblies in the canister share the same properties).

Fig. 3-2 (left) shows the MCNP model for the canister loaded with a homogeneous composition. The axial mesh employed to describe the fuel composition variation is shown in Fig. 3-2 (right).

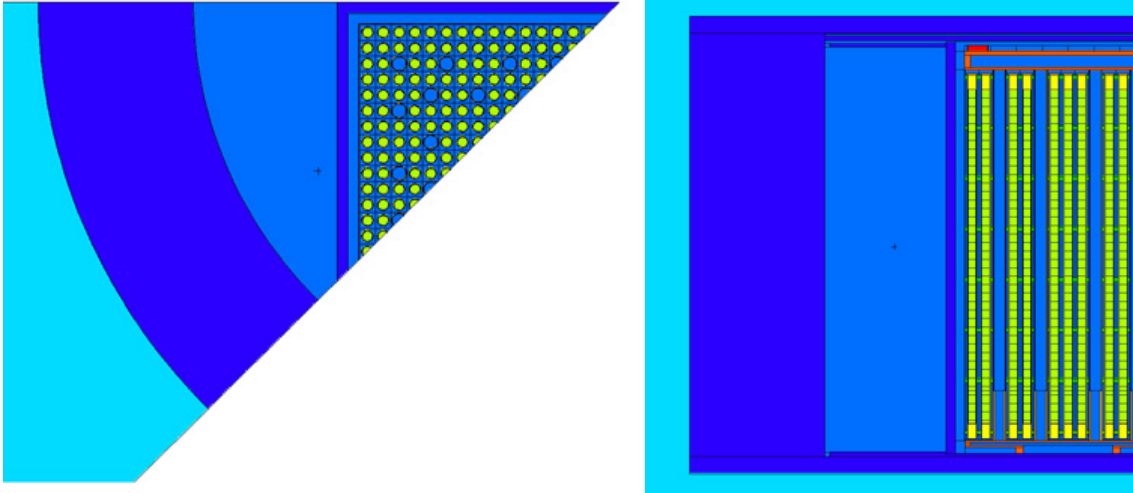


Fig. 3-2: Radial (left) and axial (right) view of the canister model loaded with fresh  $\text{UO}_2$  fuel.

### 3.3 Development of the calculation route

The computational scheme developed and implemented at PSI begins with a suite of reference CASMO5/SIMULATE-3 core models which are continuously developed and validated for all Swiss reactors and all operated cycles within the PSI CMSYS platform (Ferroukhi 2008). These core models thus provide realistic estimations of the operating histories, including in-core depletion as well as shutdown cooling between cycles, for all individual fuel assemblies.

The main data defining the fuel/core operational conditions are retrieved from CASMO5/SIMULATE-3 by the BOHR tool and used to rerun CASMO5 depletion FA calculations with realistic boundary conditions instead of nominal plus branch conditions as in the standard execution chain with SIMULATE-3. In this way, pin-by-pin and axially detailed burnt compositions can be obtained.

In the next step, the burnt compositions are input to SERPENT2 to compute the change in the isotopic concentrations after different decay periods. The coupling between the basic MCNP canister model and the fuel composition is performed with the COMPLINK tool (Pecchia 2015b), which imports detailed fuel compositions for every assembly to define a complete canister loading.

The MCNP model of the canister loaded with burnt fuel assemblies is then used to compute the  $K_{\text{eff}}$  of the system at different time steps during decay, aiming to assess whether the system remains subcritical in the postulated case of a flooded canister. Fig. 3-3 illustrates the scheme and related processes, which are described in the following subsections.

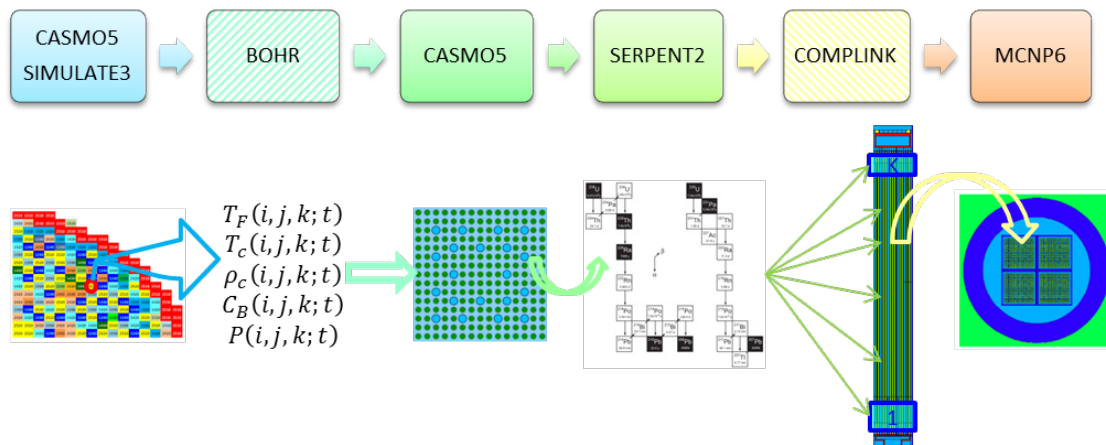


Fig. 3-3: Computational scheme for burnup credit in a disposal application.

### 3.3.1 Retrieval of nodal history

The sequence of calculations begins with the generation of the data library using CASMO5 2D lattice calculations performing a burnup calculation at nominal conditions, plus the corresponding branch calculations for the state points. The nuclear data library employed in this step is based on ENDF/B-VII.0. The spacers are smeared along the full axial length of the fuel assembly, which complies with the SIMULATE-3 model requirements. Every fuel assembly type is computed, and the initial isotopic composition is taken from the final state of the previous cycle.

The fuel burnup along the reactor cycle operation is computed with SIMULATE-3. From these results, the values of the state parameters are retrieved for every fuel assembly and axial elevation at different cycle instants. The explicit spacer model for the neutronics solution is activated in SIMULATE-3.

The BOHR tool is employed for the extraction of the required values from SIMULATE, which provides the values of nodal power, fuel temperature, coolant temperature and density, as well as boron concentration for every axial and radial location in the nodal calculation. Also, the presence of inserted control rods during the operation is taken into account.

### 3.3.2 Lattice calculations for discharge composition estimation

In order to extract and make use of the composition for every fuel pin at the discharge burnups and for every elevation, new 2D lattice calculations are performed with CASMO5. During every time interval, the temperatures and densities employed are equalled to the values computed during the cycle calculation from SIMULATE-3. The nuclear data library used is based on ENDF/B-VII.1.

The spacer mass is again smeared along the whole axial length, introducing an approximation to realistic conditions. Additional approximations are that irradiation-induced changes in the fuel assembly structures and materials are currently not taken into account. More importantly, it must also be underlined that the CASMO5 reconstructed depletion calculations are performed using single assembly reflected models, i.e. without accounting for a realistic leakage term representative of the 3D environment under which the assembly was irradiated.

### 3.3.3 Decay calculations after discharge

From the detailed burnup results, the compositions obtained are decayed over a one million year period using the Transmutation Trajectory Analysis algorithm programmed in the Monte Carlo burnup code SERPENT2 (Leppänen 2013). The decay data from ENDF/B-VII.1 are employed and concentrations are computed at the time positions specified in Tab. 3-1. The fuel pin compositions in the fuel assembly decay at every axial elevation after discharge.

Tab. 3-1: Time positions where decayed compositions are computed.

Case	Time (y)	Case	Time (y)	Case	Time (y)
0	0	10	120	20	15'000
1	1	11	150	21	20'000
2	2	12	200	22	25'000
3	5	13	300	23	30'000
4	10	14	500	24	40'000
5	20	15	1'000	25	45'000
6	40	16	2'000	26	50'000
7	60	17	5'000	27	100'000
8	80	18	8'000	28	500'000
9	100	19	10'000	29	1'000'000

### 3.3.4 Criticality calculations for the disposal canister

Each particular MCNP model, which includes the spent fuel compositions for every discharge burnup at the end of each fuel operation cycle and for each decay period, is generated starting from a base input file with the canister model loaded with fuel assemblies of equal uniform composition corresponding to fresh fuel. The tool COMPLINK developed at PSI is used for this purpose.

Only the isotopes usually considered for burnup credit calculations are included in the fuel composition for the calculation. Two sets of isotopes are considered, customarily named the actinides only (AC) and the actinides plus fission products (AC+FP) groups; Tab. 3-2 and 3-3 list both sets, to which oxygen isotopes O-16 and O-17 are also added<sup>2</sup>. Curium isotopes should be added to the list mainly for MOX fuels.

Tab. 3-2: Actinides only (AC) burnup credit nuclides.

U-233	U-234	U-235	U-236	U-238	Pu-238
Pu-239	Pu-240	Pu-241	Pu-242	Am-241	Cm-242
Cm-243	Cm-244	Cm-245	Cm-246		

<sup>2</sup> The CASMO5 version used does not separate oxygen into its three natural isotopes, but uses a homogenised cross section of O-16 and O-17, ignoring O-18. The latest version (not used here) finally also splits O-18 and includes the separated cross sections. The impact on results is negligible.

Tab. 3-3: Actinides plus fission products (AC+FP) burnup credit nuclides.

U-233	U-234	U-235	U-236	U-238	Np-237	Pu-238	Pu-239
Pu-240	Pu-241	Pu-242	Am-241	Am-242m	Am-243	Cm-242	Cm-243
Cm-244	Cm-245	Cm-246	Mo-95	Tc-99	Ru-101	Rh-103	Ag-109
Cs-133	Nd-143	Nd-145	Sm-147	Sm-149	Sm-150	Sm-151	Sm-152
Eu-151	Eu-153	Gd-155					

The nuclear data from ENDF/B-VII.1 coming with the MCNP6 distribution have been used in the calculations. The canister and fuel geometry are considered constant over time, which is a common approach in this type of criticality safety assessment. The material temperature is 293.16 K everywhere and corresponding densities and dimensions are employed.

The criticality eigenvalue is computed with 65 inactive cycles and 30 active cycles to obtain  $K_{\text{eff}}$  with an uncertainty in the range of approximately  $\pm 40$  pcm<sup>3</sup>; the number of inactive cycles was chosen following the MCNP recommendation based on the Shannon entropy estimation of the fission distribution. All the cycles are run with 200'000 neutron histories each to overcome possible problems with the fission source convergence in the inactive cycles as further explained in Appendix B.

In order to reduce computational costs, the MCNP model of the active zone was reduced to 22 layers compared to the reference SIMULATE-3 core model based on 40 axial nodes in the active part. Apart from the two layers at the bottom and top of the active zone as well as at the interface between the standard guide tube size diameter and the dashpot region, all other SIMULATE-3 layers were collapsed in a pairwise manner, meaning an averaging of the two node compositions into layers of 17.9 cm in the MCNP model. This number of layers was supposedly enough to capture the end-effect (Wagner 2003).

During the calculation of reference results using the most accurate representation available, i.e. the 40 axial layers from the SIMULATE-3 results plus an additional layer from splitting the node where the dashpot region ends, a difference was found between the reference results and those from the 22 layer model. The computed  $K_{\text{eff}}$  value for low burnup UO<sub>2</sub> fuel (17.61 and 33.82 GWd/t) was higher using the simplified axial mesh, but above 50.47 GWd/t the computed criticality eigenvalue in the reference model was higher, as represented in Fig. 3-4. Simplifications which are not bounding conservative in all the parametric space should not be adopted. Therefore, all the results in the report are obtained using the most detailed axial mesh available.

<sup>3</sup> The latest calculations were performed with 80 inactive cycles and 60 active cycles, leaving the Monte Carlo uncertainty in the range of  $\pm 30$  pcm. This change was included to improve the initial fission source convergence and eliminate some bias in the calculations which could be noticeable for the actinides plus fission products calculations and alarming in the case of mixed MOX and UO<sub>2</sub> fuel configurations.

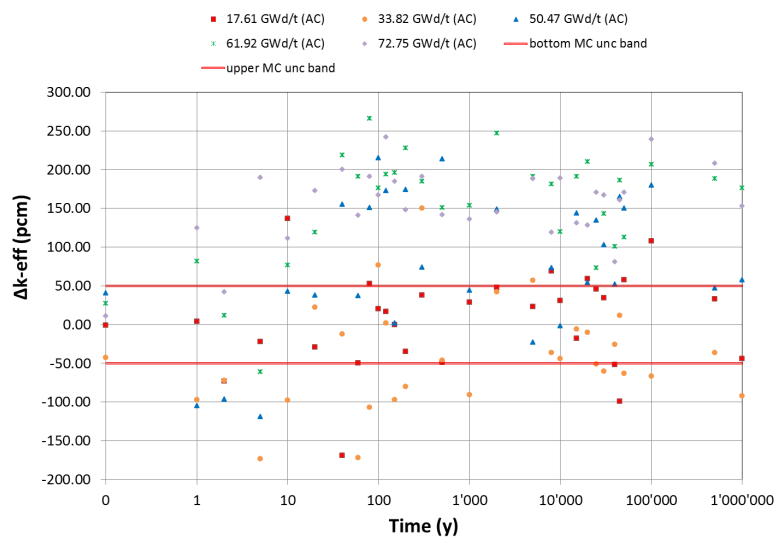


Fig. 3-4: Difference between  $K_{\text{eff}}$  computed with the reference axial detail and  $K_{\text{eff}}$  computed with a coarser mesh ( $\text{UO}_2$  fuel).

## 3.4 Results

### 3.4.1 Fresh fuel

First, a set of calculations has been performed to determine if the global reactivity of the fresh fuel configuration reaches the Upper Subcritical Limit (USL), which was estimated preliminarily here. In case this reactivity is below the desired threshold (e.g. 0.95 if only the administrative margin is considered), then the fuel could be loaded in the canister without further need for burnup credit. Normally this is not the case for PWR fuel, but rather only for very low enrichments typical of the first operational cycles.

The analysis is, indeed, useful to compare the behaviour of different fuel configurations, including the following:

- I. 4  $\text{UO}_2$  fuel assemblies
- II. 4 ERU fuel assemblies
- III. 4 MOX fuel assemblies
- IV. 1 MOX and 3  $\text{UO}_2$  fuel assemblies
- V. 1 empty position and 3  $\text{UO}_2$  fuel assemblies

Configurations with 4 MOX fuel assemblies loaded in a canister are not considered feasible, as their contributions to the total heat load is too high according to the Nagra safety assessment. In fact, a heat load of 1.5 KW is considered the maximum for the disposal canister to ensure the functionality of the engineered barrier system (canister-bentonite-Opalinus Clay). The mixed loading of one MOX with 3  $\text{UO}_2$  is, however, considered in the Nagra concept design.

Several boundary conditions are considered for the bounding analysis. The configurations considered are the following:

- The canister in dry conditions (actually filled with helium gas)
- The canister flooded with water at 293.16 K
- The canister flooded with the fuel assemblies displaced diagonally towards the centre of every fuel box
- The canister flooded with the fuel assemblies displaced diagonally towards the outer part of the fuel box

The calculated  $K_{\text{eff}}$  value for each of these cases is presented in Tab. 3-4, together with reactivity data on fuel configuration displacement, i.e. inwards and outwards against a flooded centred case. The Monte Carlo standard deviation value is below 30 pcm for all cases.

Tab. 3-4:  $K_{\text{eff}}$  values for canister configurations with fresh fuel.

<b>Boundary conditions</b>	<b>UO<sub>2</sub></b>	<b>ERU</b>	<b>MOX</b>	<b>1-MOX + 3-UO<sub>2</sub></b>	<b>1 empty + 3-UO<sub>2</sub></b>
Helium filled	0.21146	0.20772	0.26259	0.20743	0.17861
Flooded centred	1.09513	1.08022	0.96180	1.07035	1.02971
Flooded inwards	1.12903	1.11227	0.98601	1.10079	1.04864
<i>Δ in-centred (pcm)</i>	<i>3'390</i>	<i>3'205</i>	<i>2'421</i>	<i>3'044</i>	<i>1'893</i>
Flooded outwards	1.04355	1.02920	0.91990	1.02301	0.99541
<i>Δ out-centred (pcm)</i>	<i>-5'158</i>	<i>-5'103</i>	<i>-4'190</i>	<i>-4'734</i>	<i>-3'430</i>

The canister in dry conditions is clearly subcritical for any combination of fresh fuel, but not for flooded conditions. All calculated  $K_{\text{eff}}$  values are above the hypothetical administrative margin (0.95), and the  $K_{\text{eff}}$  increases notably if a less favourable position of the assemblies inside the canister is considered (inwards). The importance of the distance between assemblies for the  $K_{\text{eff}}$  is clearly reflected in the table. This also means that the material of the wall boxes has a small impact on decoupling the neutron fluxes of each assembly, so that the loading position of the assemblies in the canister seems to be important for the reactivity in flooded conditions.

### 3.4.2 Discharged fuel

Given the results from the previous section, burnup credit would be a reasonable solution to try to obtain a lower but more realistic  $K_{\text{eff}}$  value for the canister loaded with spent fuel and thus to satisfy the upper criticality limit. The burnup credit approach can reduce the reactivity of the system as a consequence of the presence of neutronic poisons (minor actinides and fission products) as well as including the depletion of multiplicative material (major actinides)<sup>4</sup>. The impact on reactivity has been evaluated for both actinides only (AC) and actinides plus fission products (AC+FP) cases (see the set of isotopes in Tab. 3-2 and Tab. 3-3).

For this calculation, the same configurations (as the fresh fuel case) are used, as follows:

- I. 4 UO<sub>2</sub> fuel assemblies
- II. 4 ERU fuel assemblies
- III. 4 MOX fuel assemblies
- IV. 1 MOX and 3 UO<sub>2</sub> fuel assemblies
- V. 1 empty position and 3 UO<sub>2</sub> fuel assemblies

However, in this case the canister is loaded with spent fuel compositions at different discharge times, i.e. with different burnups, and at different times covering the one million year period from Tab. 3-1.

It is worth noting that the following results are still preliminary, because the upper criticality limit is still not computed and the administrative margin does not incorporate all sources of uncertainty.

---

<sup>4</sup> Although some amount of fissile major and minor actinides is produced during reactor operation, the net reactivity effect with fuel burnup is negative.

### 3.4.2.1 UO<sub>2</sub> fuel assembly (Case I)

For the burnt fuel configurations, analyses were conducted for each of the assembly-averaged burnup levels reached after one cycle irradiation, starting thus from 17.61 GWd/t at the end of the first cycle to 72.75 GWd/t, at discharge after 5 cycles (EOL). The calculated curves of the  $K_{\text{eff}}$  evolution are plotted in Fig. 3-5, for a flooded canister at different instants during decay of the isotopes, for both AC and AC+FP cases. The observed behaviour is in line with already published results for the same situation (Wagner 2003b).

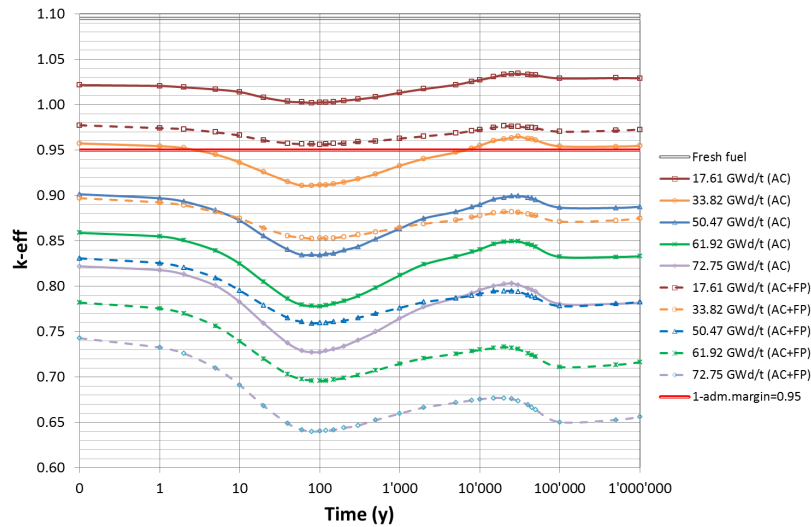


Fig. 3-5: Evolution of  $K_{\text{eff}}$  for the intact canister loaded with spent UO<sub>2</sub> fuel.

An almost constant difference of about 20'000 pcm can be observed between the first and last cycle assembly-averaged burnup levels, with other discharge burnups lying in between these. The difference between the AC approach and the AC+FP approach shows an increase of around 4'200 pcm just after discharge, up to 5'400 pcm at the end of the one million year period (for the 17.6 GWd/t fuel). The impact increases with burnup; the differences between AC+FP and AC cases and related time evolution are given in Fig. 3-6.

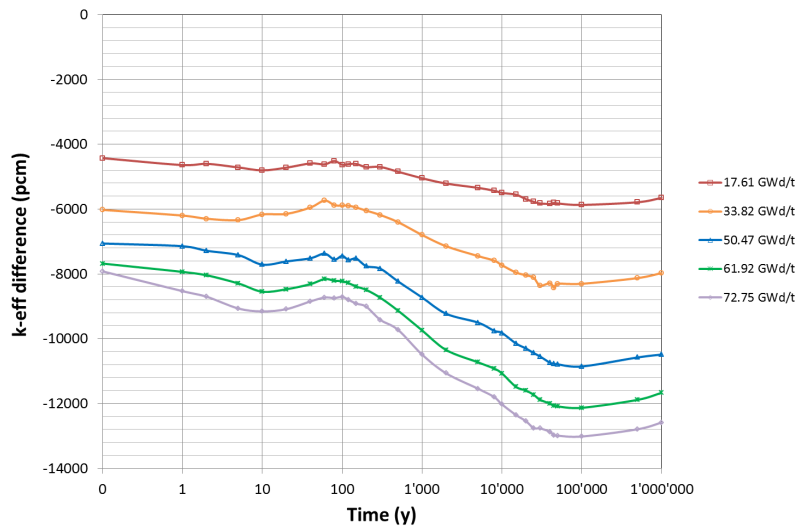


Fig. 3-6: Reactivity inserted by use of AC+FP against AC for a UO<sub>2</sub> fuel loading.

If the administrative limit of 0.95 is considered (without further uncertainties), spent fuel with a burnup of less than 24 GWd/t (for the AC+FP case) would not meet the limit specification for loading, unless a mixed configuration with higher burnup fuel were considered. If an AC approach were considered, a burnup higher than approximately 38 GWd/t needs to be reached. The reactivity of the system after 10'000 years could reach a value above that from initial discharged fuel for the AC approach. Again, these results are still preliminary, because the upper criticality limit is still not computed and the administrative margin does not incorporate all sources of uncertainty.

A mixed burnup configuration was investigated. One fuel assembly at low burnup (17.61 GWd/t) is considered in mixed loading with the other three fuel assemblies of higher burnups. The results in Fig. 3-7 show that high burnup fuels are needed (above 50 GWd/t) when taking credit only for actinides, and that the reactivity of this less burnt fuel dominates the total reactivity of the system.

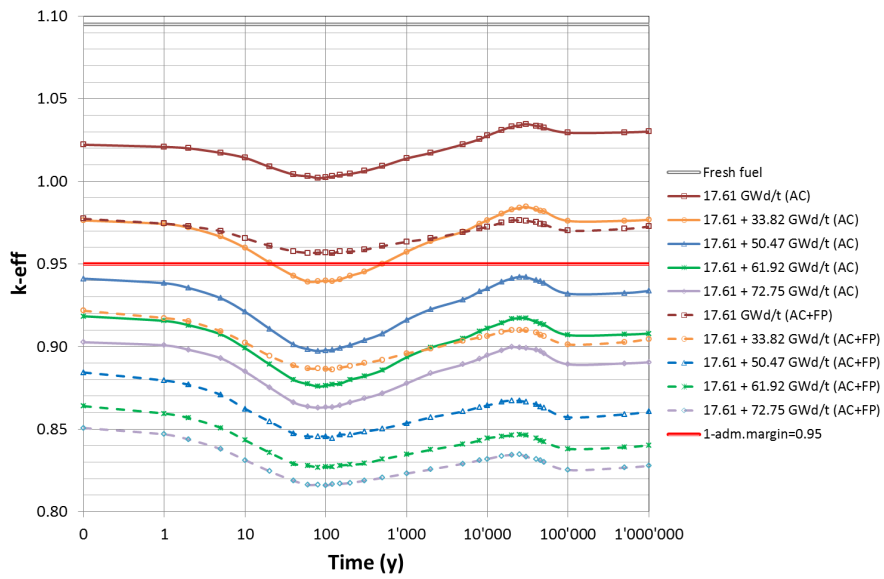


Fig. 3-7: Evolution of  $K_{eff}$  for the intact canister loaded with mixed burnup  $UO_2$  fuel (first burnup value for one position, second value for three remaining).

### 3.4.2.2 ERU fuel assembly (Case II)

The ERU fuel assembly corresponds to fuel enriched to 4.6 w/o  $^{235}U_{eq}$  and operated to 61.72 GWd/t. The evolution of  $K_{eff}$  through time, shown in Fig. 3-8 for both AC and AC+FP cases, is fairly similar to that for the  $UO_2$  fuel.

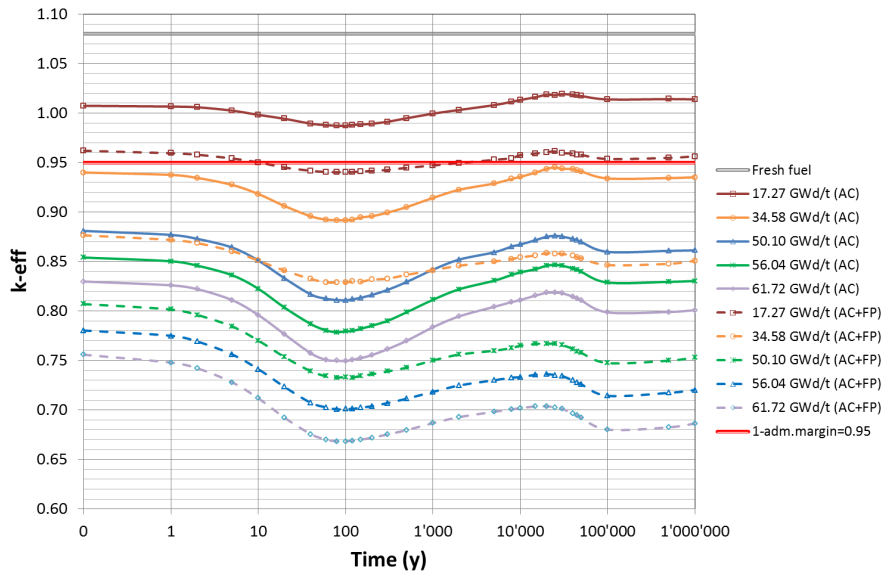


Fig. 3-8: Evolution of  $K_{eff}$  for the intact canister loaded with ERU fuel.

The reactivity difference between the actinides only and the actinides plus fission products approach, presented in Fig. 3-9, shows that, at least for the ERU case considered, the impact of the actinides plus fission products approach is less significant with increasing burnups.

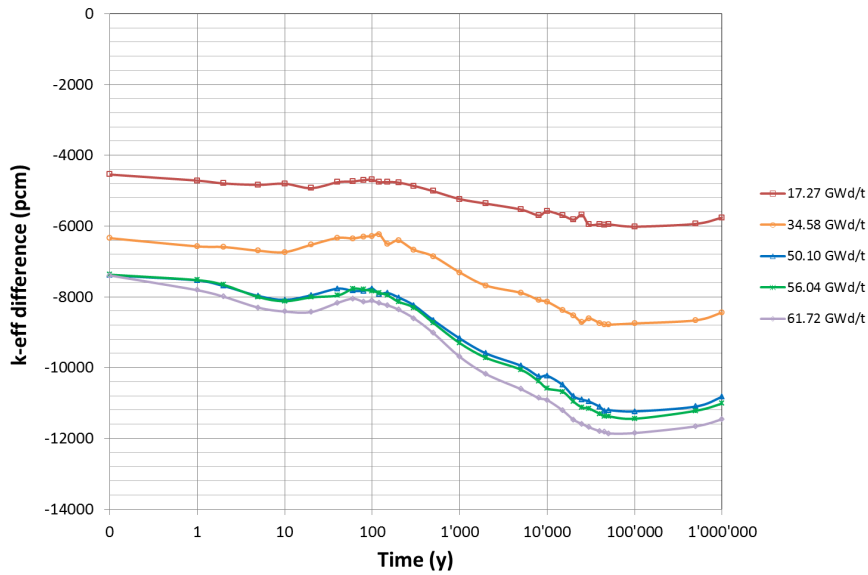


Fig. 3-9: Reactivity inserted by use of AC+FP for an ERU fuel loading.

### 3.4.2.3 MOX fuel assembly (Case III)

The canister is loaded with four MOX FAs. The MOX fuel assembly corresponds to fuel enriched to 4.8 <sup>w</sup>/<sub>0</sub> Pu<sub>fiss</sub> and operated to 51.72 GWd/t. The evolution of K<sub>eff</sub> through time in Fig. 3-10 has stronger dip and peak reactivities around 100 and 10'000 years respectively. Notable is that the reactivity peak after thousands of years would be higher than any previous reactivity value calculated for the AC case, meaning that using the discharge compositions without decay would not be a bounding assumption for the whole disposal period for the intact canister model.

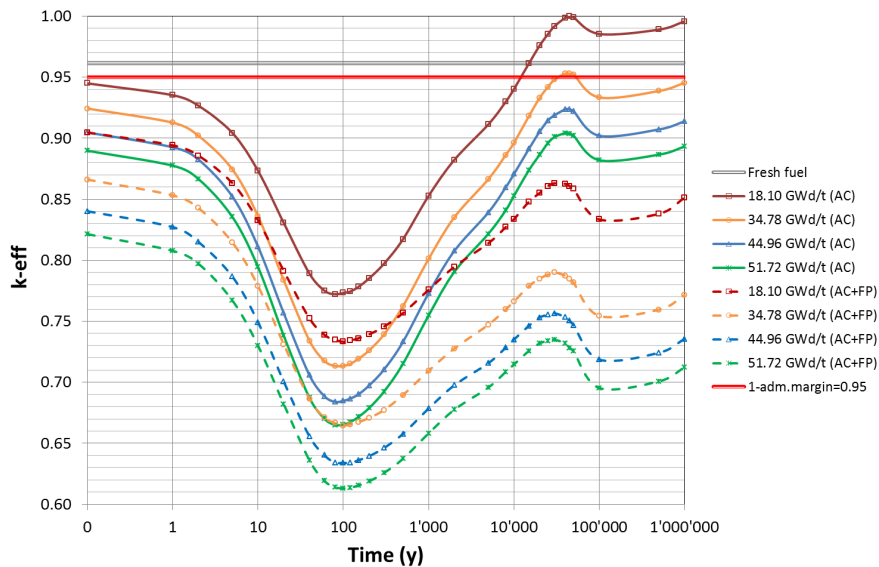


Fig. 3-10: Evolution of k-eff for the intact canister loaded with MOX fuel.

On the other hand, the impact of considering additional minor actinides and fission products in the fuel composition also has a stronger impact on the reactivity than for  $\text{UO}_2$  fuel, and this impact is more important at later periods, thus reducing the reactivity peak below former values in time (see Fig. 3-11). Therefore, the use of the discharge compositions would be bounding conservative for the AC+FP approach. Again, stagnation with increasing burnup of the impact of including the minor actinides and fission products in the compositions is observed as for the ERU fuel.

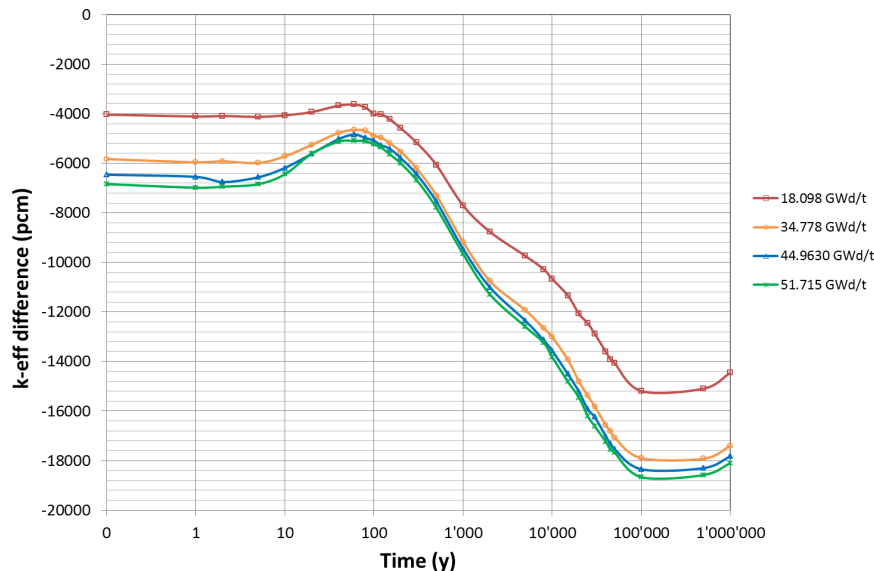


Fig. 3-11: Reactivity inserted by use of AC+FP for a full MOX fuel loading.

#### 3.4.2.4 One MOX and three $\text{UO}_2$ fuel assemblies (Case IV)

In this model, the canister is loaded with one MOX and three  $\text{UO}_2$  fuel assemblies.

Fig. 3-12 shows the reactivity evolution for the canister loaded with low burnup fuel (18 GWd/t) together with three  $\text{UO}_2$  assemblies at different burnup levels. The main findings from these graphs are:

1. The second reactivity peak after 10'000 years of the mixed load canister, characteristic of MOX fuels, is also above the first reactivity peak (the one after discharge), which implies that the second will be bounding.
2. The reactivity of the system is dominated by the three  $\text{UO}_2$  assemblies and there is not much difference in the reactivity level of the system through increasing the burnup of the MOX assembly.

The AC approach would require  $\text{UO}_2$  fuel burnt to around 40 GWd/t and AC+FP approach would require 20 GWd/t.

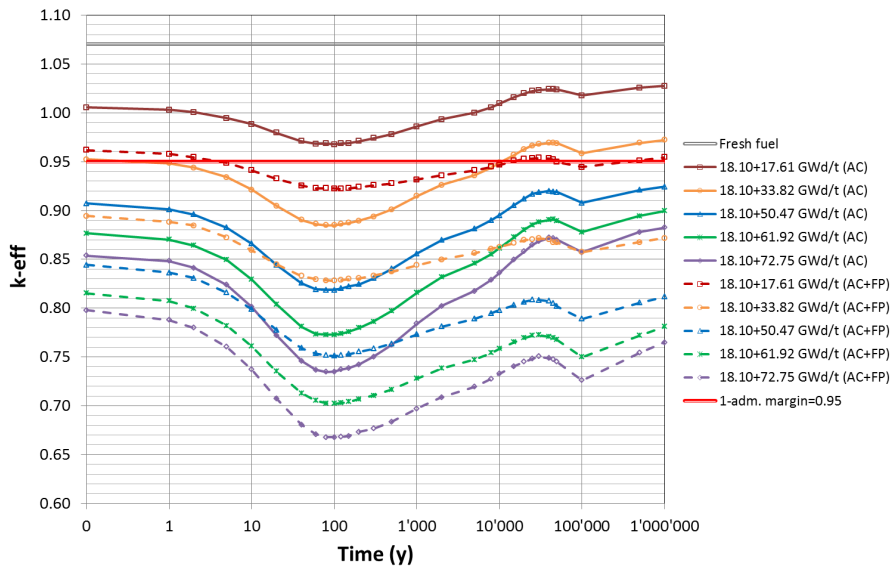


Fig. 3-12: Evolution of  $K_{eff}$  for the intact canister loaded with one low burnup MOX (18 GWd/t) and three  $UO_2$  fuel at different burnups.

The fission product impact on reactivity follows the same trend as the canisters loaded only with  $UO_2$  or that with MOX fuel only (see Fig. 3-13). The influence of the neutron spectra is not very significant from this specific point of view.

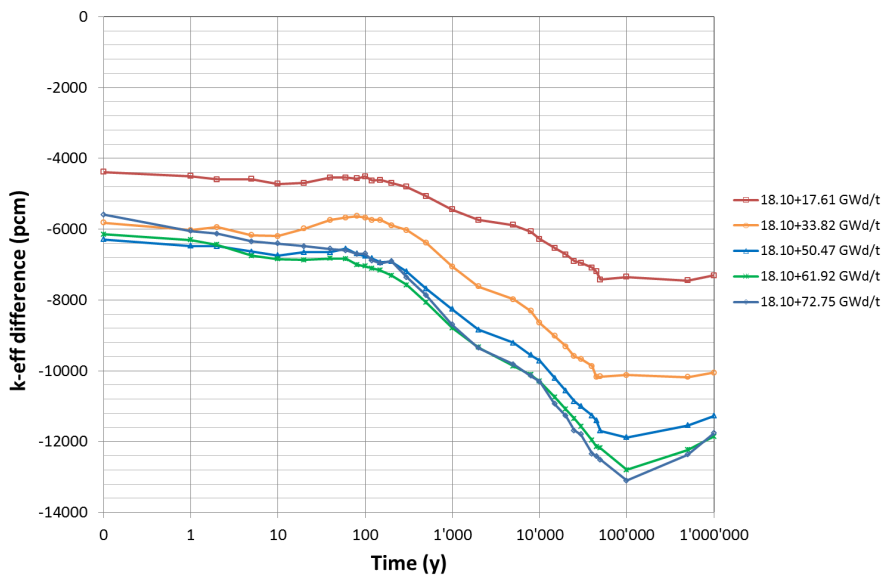


Fig. 3-13: Reactivity inserted by use of actinides plus fission products for a MOX- $UO_2$  fuel loading.

### 3.4.2.5 Empty position and three UO<sub>2</sub> fuel assemblies (Case V)

The analysis for the case of a canister loaded only with three UO<sub>2</sub> fuel assemblies is presented here. The empty position is assumed to be also flooded with water. The results plotted in Fig. 3-14 show that fuel with a limiting burnup of 19 GWd/t can be considered if using the AC approach and 10 GWd/t for the AC+FP approach. The contribution of additional minor actinides and fission products to reactivity is shown in Fig. 3-15, which is not significantly different from the case with four UO<sub>2</sub> assemblies.

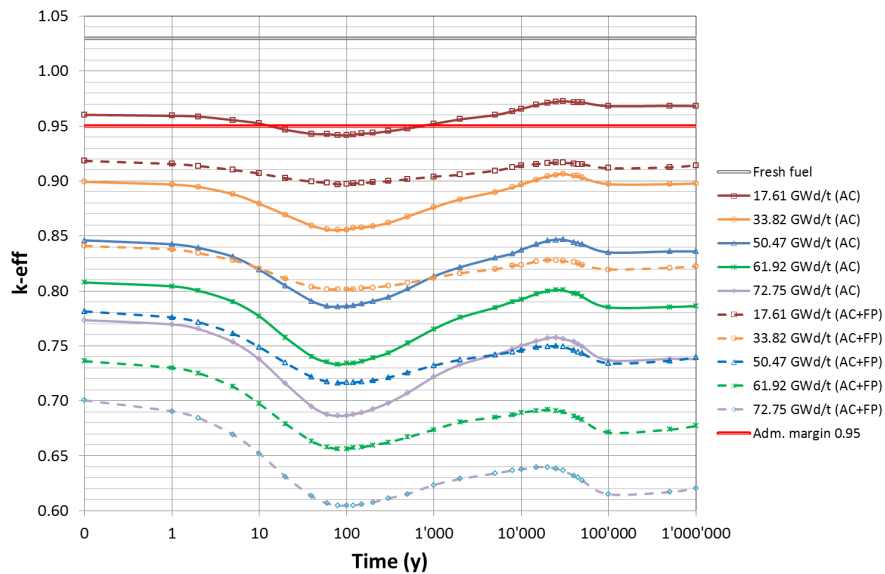


Fig. 3-14: Evolution of  $k_{\text{eff}}$  for the intact canister loaded with 3 UO<sub>2</sub> assemblies and one empty position.

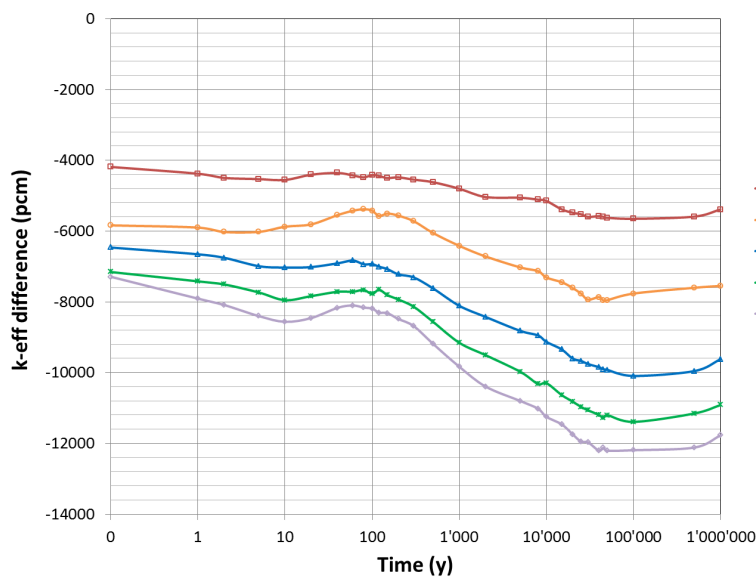


Fig. 3-15: Reactivity inserted by use of actinides plus fission products for a 3 UO<sub>2</sub> assemblies loading with one empty position.

### 3.5 Conclusions to Chapter 3

A calculational route has been developed to extract detailed axial and radial pin-by-pin spent fuel compositions from lattice calculations based on realistic cycle operating conditions. This allows more realistic axial burnup profiles to be considered and, if the neighbourhood effect is included later, also more realistic radial profiles, together with a more accurate estimation of the burnup history. Such capabilities are of importance for the selection of bounding fuel assembly designs, burnup profiles and burnup conditions as well as initial compositions, which are the basis of subsequent loading curve calculations.

The elements of the methodology have been presented and were applied to conduct bounding analyses of the canister design under consideration in Switzerland for geological disposal, using representative fuel assemblies operated in a Swiss PWR. Assemblies of the different types of fuel encountered in the operation, i.e. UO<sub>2</sub>, MOX and ERU, are studied using the highest enrichments used to date and operated to the highest burnups to properly study their behaviour.

The main findings of the work are that UO<sub>2</sub> fuel could be problematic if featuring low burnups, while MOX fuel suffers a rise in  $K_{eff}$  in later time periods after disposal, which may violate the upper criticality limit. ERU fuel has a similar behaviour to the UO<sub>2</sub> fuel. Mixing of UO<sub>2</sub> and MOX fuel in the canisters could be a good compromise to keep reactivity below the safety margin.

Fig. 3-16 summarises the minimum burnup credit which would be required for every type of loaded nuclear fuel considered in this study, if credit for actinides only (AC) is given. Loadings of UO<sub>2</sub> fuel operated for just one cycle could be allowed only if mixed with 3 other assemblies having burnups above 45 GWd/t<sub>HM</sub> (note that the second reactivity peak is decisive for the AC approach).

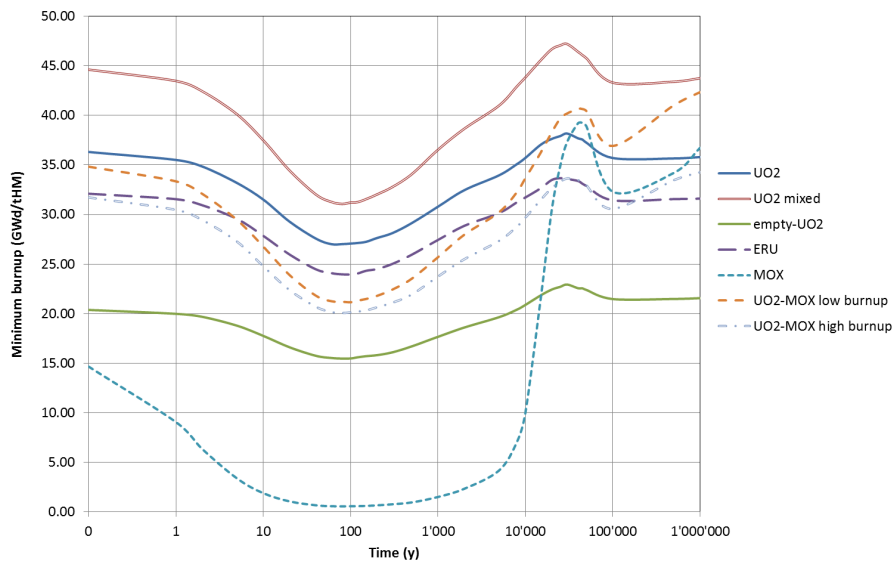


Fig. 3-16: Evolution of minimum burnup credit required to comply with a  $k_{eff}$  value below 0.95 within the geological disposal timescale (AC case).

It can be seen from Fig. 3-16 that the minimum burnup required for a homogeneous burnup  $\text{UO}_2$  fuel loading is not always above the minimum burnup required for the canisters filled with MOX fuel (mixed  $\text{UO}_2/\text{MOX}$  case or full MOX case), since the second reactivity peak in the MOX cases is very high.

Fig. 3-17 represents the minimum burnup if the effect of the fission products and some additional minor actinides are included in the spent fuel composition (AC+FP). The mixed burnup loading ( $1\text{MOX} + 3\text{UO}_2$ ) requires a minimum burnup of 20  $\text{GWd}/t_{\text{HM}}$  for the  $\text{UO}_2$  fuel (fuel operated for at least two operating cycles). In this case, the burnup credit required for canisters loaded with MOX fuel would be dominated by the reactivity at discharge ( $\sim 27 \text{GWd}/t_{\text{HM}}$ ) and it will not be higher than the corresponding  $\text{UO}_2$  case, the latter being approx. 24  $\text{GWd}/t_{\text{HM}}$ .

Finally, one should bear in mind that all these results imply that the fuel matrix is still intact, maintaining the actinides and fission products mixture even after 100'000 years, which is far from the normal fuel assembly design target, which ensures fuel assembly integrity during irradiation in the core but not for geological disposal timeframes.

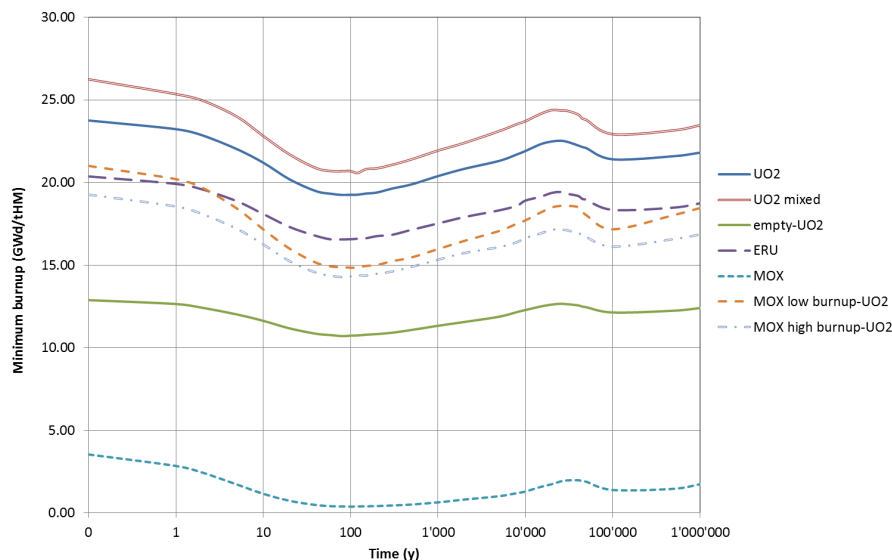


Fig. 3-17: Evolution of minimum burnup required to comply with a  $K_{\text{eff}}$  value below 0.95 within the geological disposal timeframe (AC+FP case).

The main driving parameter for criticality in the current canister design is the distance between the fuel assemblies, due to the compact configuration (and also because neutronic poisons are not present in the canister's basket material). Fresh fuel calculations indicate a difference of between 0.02 and 0.04 (2 to 4 %) in  $K_{\text{eff}}$  values for nominal and displaced configurations, which is very important.

An indicative Upper Subcritical Limit of 0.95 was considered, corresponding to an administrative margin of 0.05. However, the USL value will be lower for the real application, since bias and other uncertainties must be included. On the other hand, the administrative margin for disposal applications could be lower than 0.05, but this needs to be defined by the competent authority (ENSI).

The bounding analyses consisted of assessing the multiplication factor variation as a function of discharge burnup and decay time, ranging from fresh fuel conditions and best-estimate burnt fuel

configurations. The results derived in this study are already indicative of which configurations will not be allowed for a fuel canister loading. These best-estimate analyses are employed and complemented by bias and uncertainty quantifications in the following sections to produce conservative fuel burnup loading curves. Further use of bounding assumptions will also be used when required.

The results obtained with the described codes and nuclear data libraries are in line with analyses performed for other canister designs (Wagner 2003b), and indicate that the inclusion of the fission products in the burnup credit methodology for disposal could result in loading curves where 2-cycle operated fuel assemblies could be safely loaded. However, the margin is very close to the limit and once the biases, uncertainties and bounding assumptions are introduced for the loading curve generation, it will be further reduced.

Fuel with low burnup (corresponding to one cycle of operation) cannot be loaded to fill all the positions of the same canister, and the study of mixed burnup, mixed UO<sub>2</sub>-MOX or empty positions in the configuration show that this low burnup fuel could meet the requirement in some mixed configurations.

## **4 Preliminary reference loading curves obtained for Nagra's SNF disposal canister with the PSI BUCSS-R methodology**

As a main outcome of the study presented to this point, the application of burnup credit to the criticality calculations for disposal canisters is considered necessary for the safe disposal of the PWR spent fuel assemblies operated in the Swiss reactors, according to the current design concept for the Nagra disposal canister.

The application of a best-estimate computational route is now complemented with the mandatory conservative coverage in the form of either a stochastic uncertainty analysis or a bounding analysis of the parameters, as illustrated in the following sections.

Thus, the results are presented for a canister loaded with PWR  $\text{UO}_2$  spent fuel assemblies, integrating the outcome of the standard PSI criticality safety validation procedure with the estimated penalisation on the computed  $K_{\text{eff}}$  due to the uncertainties in nuclear data, fuel assembly design parameters and operating conditions as well as burnup-induced changes in the fuel assembly geometry. Furthermore, bounding axial and radial burnup profiles and the most reactive fuel loading configuration in the canister, in terms of penalising radial tilt, are taken into account accordingly.

The final loading curves obtained for PWR fuel and for the reference disposal canister (as illustrated in Fig. 3-1) show which minimum average fuel assembly burnup is required for the given original fuel enrichment of fresh fuel assemblies, so that the  $K_{\text{eff}}$  of the canister would comply with the imposed criticality safety criterion. However, the optimisation of the canister design could potentially improve the fuel loading conditions in terms of burnup requirement. A preliminary study demonstrating the plausibility of the concept can be found in Gutierrez (2017).

### **4.1 Introduction**

The final results of the PSI/Nagra research project BUCSS-R, based on the developments and findings gained in the preceding stages of the work (see Chapters 2 and 3), are reported here. The developed burnup credit methodology, complemented with uncertainty analysis of the nuclear data (DOE 1999) and accounting for conservative axial and radial burnup profiles, has been applied for the derivation of the loading curves.

Schematically, the final (as compared to Fig. 3.3) concept of the PSI BUCSS-R methodology is shown in Fig. 4-1 and more details can be found in Chapter 3 and Herrero (2015).

## BUCSS-R Methodology concept

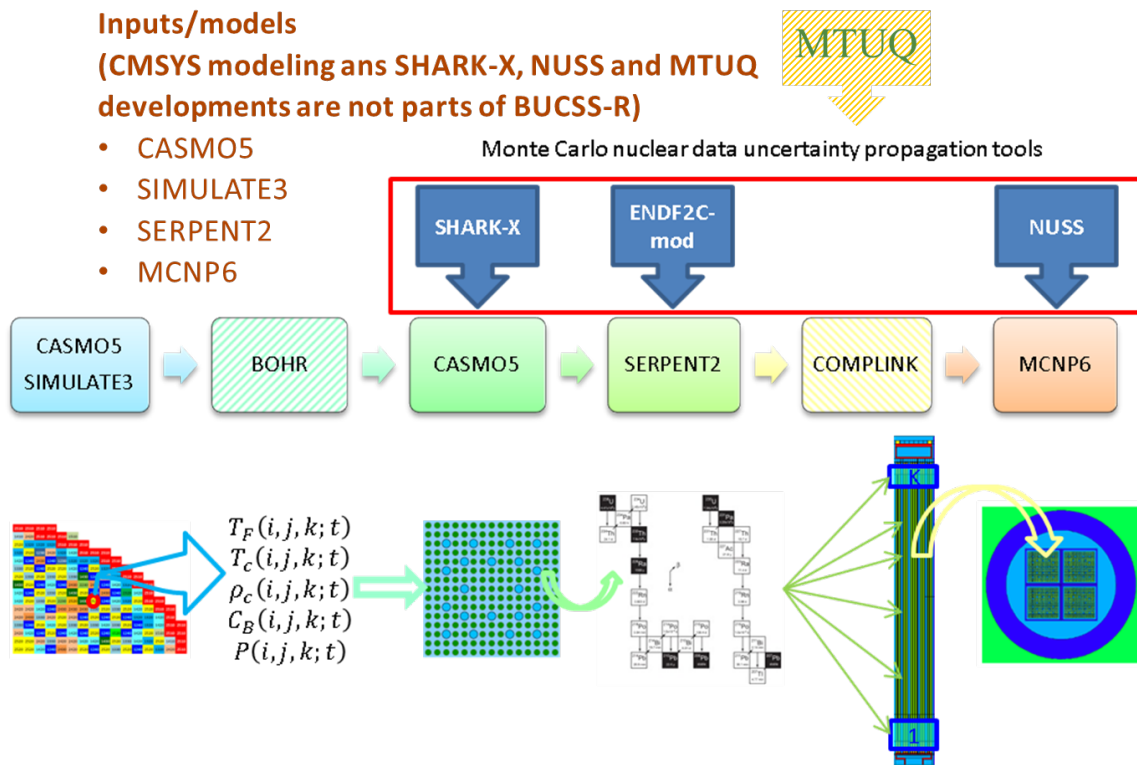


Fig. 4-1: Schematic concept of the PSI BUCSS-R methodology.

Based on the findings reported in Chapter 3 and on the Nagra criticality studies on BWR fuel configurations, which are less problematic and do not require a burnup credit approach (Gutierrez 2017), the reference disposal canister has been loaded with 4 similar PWR UO<sub>2</sub> spent fuel assemblies (i.e. the type of fuel employed at KKG) for the criticality calculations, being the most penalised configuration among those considered.

Note that the general practice in the burnup credit applications is based on choosing a set of bounding parameters for the burnup calculations in terms of power density, fuel and coolant temperatures, densities, etc., so that the reactivity at discharge for such conservative assumptions will be higher than the reactivity obtained with any possible real irradiation history. This path, however, was not adopted for the BUCSS-R project. In fact, the approach in the BUCSS-R project is different because real operational data are employed (using SIMULATE3 for accurate core follow calculations) for the fuel assemblies of different enrichments in order to estimate the loading curves on the basis of best-estimate assessments integrated with a conservative but rational treatment of the uncertainties. Therefore, at present only some representative fuel assemblies operated at KKG could be considered and explicitly analysed. It is foreseen that, in the future, the studies performed should be repeated for a statistically significant number of fuel assemblies, at least for the most reactive design/enrichment types, to allow for statistically confident verification/updating of the presently evaluated preliminary loading curves.

## 4.2 Applied criteria for criticality safety accounting for burnup credit

The criticality safety criteria applied for derivation of the loading curves can be presented with the following relation:

$$k_{eff}|_{\text{Bounding FA pos}}(BU) + \Delta k_{eff}^{Ax}(BU) + \Delta k_{eff}^{Rad}(BU) + 2\sigma_{tot}(BU) < < USL = LTB|_{AOA} - \Delta k_{eff}^{AM}, \quad (4.1)$$

where

$$\sigma_{tot}(BU) = \sqrt{\sigma_{ND}^2(BU) + \sigma_{BU-eff}^2(BU) + \sigma_{OP}^2(BU) + \sigma_{TP}^2 + \sigma_{T1/2}^2 + \sigma_{MC}^2}, \quad (4.2)$$

$$\sigma_{ND}(BU) = \sigma_{SNF-Keff}^{(SHARK-X)}(BU) + \sigma_{ND-Keff}^{(NUSS)}(BU), \quad (4.3)$$

where  $k_{eff}|_{\text{Bounding FA pos}}$  is the neutron multiplication factor corresponding to the disposal canister loaded with the spent nuclear fuel (SNF) placed in the most penalising positions considering the canister technological tolerances (see Chapter 3 for details);  $\Delta k_{eff}^{Ax}$  and  $\Delta k_{eff}^{Rad}$  are the  $k_{eff}$  penalties to cover bounding axial and radial burnup profiles, respectively; USL is the Upper Subcritical Limit (for details see Vasiliev 2015),  $\sigma_{ND}$ ,  $\sigma_{BU-eff}$ ,  $\sigma_{OP}$ ,  $\sigma_{TP}$ ,  $\sigma_{T1/2}$  and  $\sigma_{MC}$  are the uncertainties at one standard deviation level for the nuclear data (ND), burnup-induced changes (BU), operating conditions (OP), technological parameter components (TP), decay constants (half-life) and the Monte Carlo statistical uncertainty of the employed MCNP code for the criticality calculations (MC) respectively. The listed components of the  $\sigma_{tot}(BU)$  uncertainty are assumed to be random (not systematic) and uncorrelated. The resulting  $\sigma_{tot}(BU)$  is further assumed to be normally distributed. Under these conditions, the term  $2\sigma_{tot}(BU)$  in Eq. (4.1) is assumed to represent the 95 % confidence interval for  $k_{eff}$ , which is for instance in line with recommendations provided, e.g., in Dean et al. (2001) and DOE (1999).

The  $\sigma_{SNF-Keff}^{(SHARK-X)}$  nuclear data-related component is responsible for the  $k_{eff}$  uncertainty associated with the spent fuel composition (due to the propagation of nuclear data uncertainties during depletion calculations) and the  $\sigma_{ND-Keff}^{(NUSS)}$  component is the  $k_{eff}$  uncertainty due to the nuclear data uncertainties themselves. The  $LTB|_{AOA}$  parameter stands for the Lower Tolerance Bound for the particular Area of Applicability (AOA, here it is limited to LWR fuel) and its value was reported in Vasiliev (2015) as **0.99339** for the PSI CSE methodology using MCNP in conjunction with the ENDF/B-VII.1 library.  $\Delta k_{eff}^{AM}$  is the "administrative margin", normally imposed to cover unknown uncertainties to ensure subcriticality, which is assumed here to be **0.05000** (5'000 pcm) in  $\Delta k_{eff}^5$ .

<sup>5</sup> The administrative margin to criticality is set here to 5,000 pcm, however recently an administrative margin of 2,000 pcm was suggested for the very unlikely accident conditions (Mennerdahl 2012).

It is worth mentioning that the criticality safety criteria employed here and the calculation methodology applied for the derivation of the Swiss SNF loading curves are in general in compliance with the recommendations provided in German standard DIN 25712 (DIN 2007) and US ANSI/ANS Regulatory Guide 8.27 (ANS 2008). A short summary of international standards and guidelines is given in Appendix C.

### 4.3 Modelling assumptions

This section comprises most of the employed modelling and simulation assumptions. First of all, it concerns the derivation of bounding burnup profiles and the assessment of their impact on the canister  $k_{eff}$  value, to derive  $\Delta k_{eff}^{Ax}$  and  $\Delta k_{eff}^{Rad}$  penalties for Eq. (4.1). The impact of the cooling time is also addressed.

#### 4.3.1 Spatial burnup distributions

##### 4.3.1.1 Axial distribution

Axial burnup profiles for the spent fuel operated at KKG and irradiated to different average burnups were retrieved from the PSI CMSYS database which includes all the burnup values per fuel assembly at every axial node of the SIMULATE3 calculations, as described in Chapter 3. The burnup profiles were normalised with this average value and separated into two families corresponding to the models with 40 axial nodes in SIMULATE3 with active fuel regions between 358 and 352 cm height and the models with 38 axial nodes in SIMULATE3 with an active region 340 cm height. The reason for having SIMULATE3 models with different numbers of axial layers of nodes with fuel is that the active fuel length of KKG fuel assemblies changed from earlier cycles to the later ones. Therefore, in the SIMULATE3 model the older fuel assemblies have reflector segments at the 2 bottom nodes instead of the fuel nodes. It can also be noted that the older and shorter fuel assemblies had lower fuel enrichment compared to the later and longer fuel assemblies. Therefore, it is important to take into account an actual axial burnup profile for every specific enrichment for the correct derivation of the loading curves.

Following standard practice (NUREG 2003), the approach was to choose the lowest values of all the profiles for the first and the last 9 nodes, and the highest normalised burnup values of the profiles for the remaining central nodes. This resulted in the profiles defined in Tab. 4-1 and Tab. 4-2, which were both applied in this study: Tab. 4-1 for the active fuel lengths from 352 to 358 cm and Tab. 4-2 for the active fuel length of 340 cm.

Tab. 4-1: Artificial axial burnup profile for a SIMULATE3 model with 40 axial fuel nodes (bottom to top).

0.341	0.503	0.847	0.981	1.069	1.084	1.122	1.128	1.131	1.133	1.135
1.099	1.132	1.134	1.133	1.134	1.134	1.099	1.133	1.135	1.134	1.135
1.135	1.091	1.135	1.137	1.132	1.125	1.114	1.059	1.096	1.085	1.064
1.027	0.942	0.826	0.761	0.617	0.448	0.325				

Tab. 4-2: Artificial axial burnup profile for a SIMULATE3 model with 38 axial fuel nodes (bottom to top).

0.385	0.547	0.719	0.861	0.983	1.043	1.064	1.074	1.074	1.165	1.185
1.195	1.185	1.185	1.175	1.145	1.165	1.165	1.165	1.165	1.155	1.135
1.155	1.155	1.155	1.145	1.145	1.114	1.135	1.043	1.023	1.003	0.952
0.851	0.760	0.628	0.466	0.334						

The change in the bounding axial profiles with the average assembly burnup was not considered and could be a way of reducing conservatism if needed. Mass calculation with all the profiles in the database could also be a different approach for deriving bounding profiles.

#### 4.3.1.2 Radial distribution

For the radial burnup profiles within the fuel assemblies, there were no operational or CMSYS data available at the time of the study (such data could possibly be obtained by upgrading SIMULATE3 to SIMULATE5 in the CMSYS models). Therefore, as an alternative solution, the publicly open information on the bounding horizontal burnup profile reported in IAEA (2001) was employed. The bounding profile is expressed with equations (4.4) and (4.5), which were derived from real measurements (see IAEA (2001) and references therein for details), to generate a radial burnup tilt varying for each assembly row.

$$B_{rel} = \frac{B_H - B_{av}}{B_{av}} = 0.33 - \frac{0.08}{15} \cdot (B_{av} - 10) \quad (4.4)$$

$$B(n) = \left[ B_{rel} + 1 - \frac{4}{N} \cdot B_{rel} \cdot \left( n - \frac{N+2}{4} \right) \right] \cdot B_{av} \quad (4.5)$$

where  $N$  is the number of rows in the square assembly, 15 in our case;  $B_{rel}$  is the relative difference between the horizontally averaged burnup value for the half of the assembly ( $B_H$ ) with the highest burnup and the horizontally averaged assembly burnup  $B_{av}$  and  $n$  is the row number in the assembly to which the computed burnup  $B(n)$  corresponds. The second formula includes a correction of sign from the one in the original report (IAEA 2001).

It must be underlined that, in fact, CASMO5 does not allow specification of the burnup value desired for each row of the fuel assembly. To overcome this difficulty, a surrogate approach was utilised: the CASMO5 input file was modified such that the fuel composition is printed at the 15 burnup steps which correspond to the desired burnups of each of the fuel rod rows, as obtained with (4.4) and (4.5). After this, the fuel compositions from every burnup step were transferred to the SERPENT and further to the MCNP6 models row by row. In this sense, the approach differs slightly from the one described in IAEA (2001), where it was assumed that "all the fuel rods belonging to one and the same row have one and the same burnup". In the present approach, each fuel rod has its own composition, but the horizontally averaged burnup of the entire row is preserved as defined by the above procedure. However, examination of the typical ratios between the burnup value of each pin and the average assembly burnup showed that, to avoid burning the pins in the regions of higher power above the desired value for the row, a factor of 0.93 should be applied to each  $B(n)$ . This implies that the assembly burnup is lowered by 7 %, which introduces an additional conservatism in the sequence as peripheral pins typically already have a

lower burnup than average. In addition, the lowest burnup regions of the assemblies are later faced in the canister so as to produce the highest reactivity.

To illustrate the outcome of the employed methodology, Fig. 4-2 shows an example of the radial (horizontal) U-235 concentration distribution on a pin-by-pin basis within a fuel assembly axial node. For the studies on the radial burnup profiles, the quarter-symmetry sector of the canister model with a full-size single fuel assembly specification was utilised in the MCNP6 calculations.

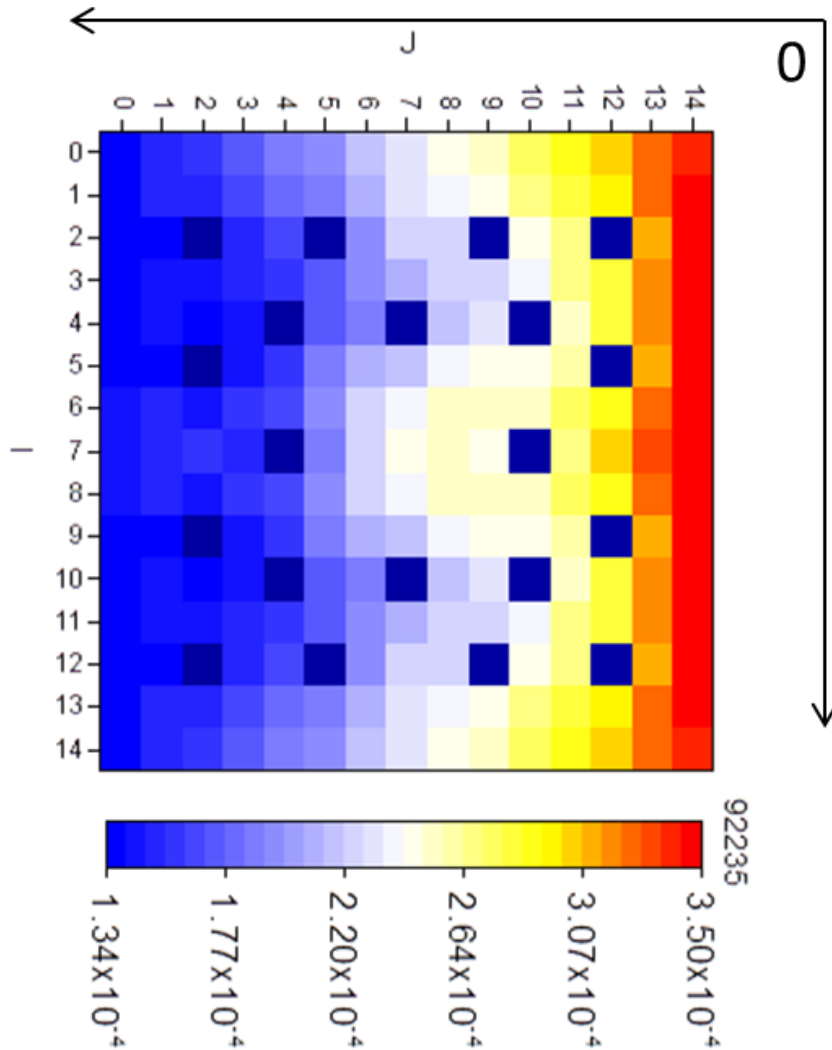


Fig. 4-2: Illustration of the radial burnup profile specification in MCNP6 models (here: U-235 atomic density).

Quarter model sector with symmetry axes.

### 4.3.1.3 Impact of cooling time

The cooling time between cycles was explicitly considered in the burnup calculations with CASMO5. In the case of actinides only credit, the impact of cooling time after discharge on the system reactivity is characterised by an initial decrease in  $K_{\text{eff}}$  in approximately the first 100 years, followed by a steady increase which reaches its maximum at around 30'000 years after discharge (see Chapter 3). The important point is that the  $K_{\text{eff}}$  value at that time for intact canister configurations could be higher than the initial  $K_{\text{eff}}$  value just after discharge, so taking this initial value cannot be considered bounding in all cases and decay calculations out to 100'000 years also need to be considered to generate the loading curves. Beyond that time, the flooded intact canister approximation would be totally unrealistic for a canister with a lifetime of approximately 10'000 years and degraded models should start to be considered in that range.

The time positions where decay compositions have been used to compute  $K_{\text{eff}}$  values are presented in Tab. 4-3.

Tab. 4-3: Decay times considered after discharge [years].

0	5	20'000	30'000	40'000	50'000
---	---	--------	--------	--------	--------

### 4.3.1.4 Canister modelling

The canister modelling includes all the details provided in Patel et al. (2012) and the detailed structure of the fuel assemblies including heads, grids and rods from the available internal documentation at PSI. For the canister loaded with the same fuel in all positions, a  $\frac{1}{8}$ <sup>th</sup> symmetry was modelled, as illustrated in Fig. 3-1. As outlined in Chapter 3, the fuel assemblies were conservatively placed towards the centre of the canister at the storage positions, as this was found to be the most reactive configuration.

## 4.4 Results on bounding assessments

Results for criticality calculations of the canister loaded with the same fuel assembly in the four positions were compiled for different enrichments covering the values employed from the initial to the latest fuel cycles of KKG.

### 4.4.1 Axial burnup effect

The results of substituting the original burnup profile by the penalising profiles while keeping the average assembly burnup are illustrated in Tab. 4-4 and Tab. 4-5, which present the reactivity added to the nominal calculations with original burnup profile for the highest enrichment with actinides only (AC) and actinides plus fission products (AC+FP) burnup credit.

Tab. 4-4: Data on  $(K_{\text{axial}}-K_{\text{nominal}}) \times 10^5$  (pcm) for 4.94 w/o AC.

	<b>Discharge burnup (GWd/tHM)</b>				
<b>Time [a]</b>	<b>17.61*</b>	<b>33.82</b>	<b>50.47</b>	<b>61.92</b>	<b>72.75</b>
0	-	983	2'359	3'604	4'737
5	-	1'273	2'752	4'141	5'322
20'000	-	1'209	2'886	4'571	6'210
30'000	-	1'197	2'930	4'675	6'414
40'000	-	1'225	2'950	4'729	6'538
50'000	-	1'213	2'993	4'901	6'693

Tab. 4-5: Data on  $(K_{\text{axial}}-K_{\text{nominal}}) \times 10^5$  (pcm) for 4.94 w/o AC+FP.

	<b>Discharge burnup (GWd/tHM)</b>				
<b>Time [a]</b>	<b>17.61*</b>	<b>33.82</b>	<b>50.47</b>	<b>61.92</b>	<b>72.75</b>
0	-	1'792	3'390	4'880	6'223
5	-	2'203	4'042	5'642	7'144
20'000	-	2'445	4'946	7'113	9'078
30'000	-	2'445	4'968	7'218	9'236
40'000	-	2'544	5'064	7'307	9'493
50'000	-	2'533	5'154	7'381	9'609

\* At the first discharge burnup of 17.61 GWd/tHM, the nominal axial burnup profile is actually more reactive than the penalising one and therefore the  $(K_{\text{axial}}-K_{\text{nominal}})$  values are not relevant for reporting for that case.

At first glance, it can be observed that the impact on reactivity is stronger for the following cases:

- Actinides plus fission products burnup credit
- Longer decay periods
- Increasing burnup

Tab. 4-6 and Tab. 4-7 show similar information for the intermediate enrichment of 3.5 w/o. In this case, the proposed profile is conservative even for the lowest burnup, so the impact of the conservative axial burnup profile is apparently also stronger with lower enrichments. As in the previous case, the added reactivity is notably larger in the actinides plus fission products approach.

Tab. 4-6: Data on  $(K_{\text{axial}}-K_{\text{nominal}}) \times 10^5$  (pcm) for 3.5 w/o AC.

Time [a]	Discharge burnup (GWd/tHM)			
	18.9	33.66	45.25	56.15
0	401	1'703	3'711	4'910
5	592	1'931	4'129	5'484
20'000	587	2'143	4'904	6'808
30'000	577	2'248	4'974	6'982
40'000	674	2'274	5'064	7'271
50'000	634	2'350	5'294	7'401

Tab. 4-7: Data on  $(K_{\text{axial}}-K_{\text{nominal}}) \times 10^5$  (pcm) for 3.5 w/o AC+FP.

Time [a]	Discharge burnup (GWd/tHM)			
	18.9	33.66	45.25	56.15
0	1'037	2'306	4'705	6'211
5	1'387	2'860	5'575	7'252
20'000	1'769	3'603	7'184	9'472
30'000	1'905	3'698	7'258	9'647
40'000	1'919	3'760	7'411	9'944
50'000	2'026	3'826	7'593	10'144

Finally, regarding the effect for the lowest enrichments of 1.9 and 2.5 w/o, the impact of the proposed profiles is not conservative and the reactivity from the nominal profile is higher and will be maintained for the final loading curves. Other profiles could be proposed to make the axial burnup profile bounding for these enrichments.

#### 4.4.2 Radial burnup effect

The calculations were repeated, this time using a full fuel assembly model in the canister with a quarter symmetry for the canister geometry, in such a way that the lowest radial burnup regions are facing the centre of the canister so as to raise reactivity. It remains to be checked if a diagonal burnup profile would be even more penalising, but the approach used already decreased the average assembly burnup by several percent as already mentioned.

Tab. 4-8: Data on  $(K_{\text{radial}}-K_{\text{nominal}}) \times 10^5$  (pcm) for 4.94 % AC.

	<b>Discharge burnup (GWd/tHM)</b>				
<b>Time [a]</b>	<b>17.61</b>	<b>33.82</b>	<b>50.47</b>	<b>61.92</b>	<b>72.75</b>
0	1'380	2'008	2'100	2'449	2'375
5	1'464	2'187	2'364	2'584	2'548
20'000	1'246	2'194	2'553	2'917	2'926
30'000	1'202	2'185	2'601	3'009	3'040
40'000	1'208	2'225	2'630	3'028	3'121
50'000	1'260	2'219	2'670	3'073	3'102

Tab. 4-9: Data on  $(K_{\text{radial}}-K_{\text{nominal}}) \times 10^5$  (pcm) for 4.94 % AC+FP.

	<b>Discharge burnup (GWd/tHM)</b>				
<b>Time [a]</b>	<b>17.61</b>	<b>33.82</b>	<b>50.47</b>	<b>61.92</b>	<b>72.75</b>
0	1'729	2'230	2'656	2'829	2'820
5	1'947	2'475	3'016	3'268	3'103
20'000	1'832	2'743	3'550	3'959	3'858
30'000	1'831	2'821	3'652	3'952	3'883
40'000	1'860	2'815	3'663	3'976	3'973
50'000	1'860	2'888	3'751	3'997	4'045

In the case of the highest enrichment of 4.94 % in Tab. 4-8 and Tab. 4-9, the reactivity impact is:

- Stronger for the actinides plus fission products burnup credit
- Increasing from lower to higher burnups
- Mainly increasing during the decay period up to 20'000 years, then stabilising

In Tab. 4-10 and Tab. 4-11, the information is shown for the intermediate burnup of 3.5 % and a similar behaviour is observed.

Tab. 4-10: Data on  $(K_{\text{radial}} - K_{\text{nominal}}) \times 10^5$  (pcm) for 3.5 w/o AC.

	<b>Discharge burnup (GWd/tHM)</b>			
<b>Time [a]</b>	<b>18.9</b>	<b>33.66</b>	<b>45.25</b>	<b>56.15</b>
0	1'966	2'278	2'866	2'780
5	2'140	2'248	2'928	2'972
20'000	2'150	2'633	3'567	3'642
30'000	2'107	2'603	3'577	3'701
40'000	2'151	2'666	3'586	3'851
50'000	2'198	2'754	3'754	3'879

Tab. 4-11: Data on  $(K_{\text{radial}} - K_{\text{nominal}}) \times 10^5$  (pcm) for 3.5 w/o AC+FP.

	<b>Discharge burnup (GWd/tHM)</b>			
<b>Time [a]</b>	<b>18.9</b>	<b>33.66</b>	<b>45.25</b>	<b>56.15</b>
0	2'339	2'511	3'210	3'163
5	2'575	2'975	3'710	3'617
20'000	2'761	3'553	4'429	4'601
30'000	2'799	3'657	4'572	4'617
40'000	2'770	3'677	4'624	4'750
50'000	2'911	3'733	4'638	4'826

As with the axial burnup profiles for the lowest enrichments of 1.9 and 2.5 w/o, the proposed radial profiles are not conservative in any case and so the nominal profiles are kept.

#### 4.5 Assessment of uncertainties

Among the uncertainties  $\sigma_{\text{tot}}$  (BU) taken into account in Eq. (4.1, 4.2 and 4.3), the following components are considered:

- ND combined impact (including decay constants) on SNF composition and  $K_{\text{eff}}$  ( $\sigma_{\text{ND}}$ )
- Operating conditions ( $\sigma_{\text{OP}}$ )
- Burnup-induced geometry changes ( $\sigma_{\text{BU-eff}}$ )
- FA design tolerances ( $\sigma_{\text{TP}}$ )
- Monte Carlo ( $\sigma_{\text{MC}}$ )

In the following subsections, quantitative assessments are given for the listed uncertainties. It must be outlined that, at present, some of the assessments provided are rather preliminary and

may require verification depending on the availability of required modelling and simulation information.

#### 4.5.1 Reactor operating conditions and burnup-induced changes

Due to the recent PSI activities devoted to extending the BOHR-CASMO tool for fuel depletion calculations under realistic operating conditions, it has become possible to investigate the impact of reactor operational parameter variations. In fact, the resulting uncertainties in the SNF can be then translated into the  $\sigma_{OP}$  and  $\sigma_{BU-eff}$  components of Eq. (2). Using PSI proprietary fuel experimental data, two types of uncertainties were assessed for a KKG fuel rod sample (15×15 fuel assembly, irradiated during 3 cycles up to the sample final burnup of 51.9 GWd/t<sub>HM</sub>):

- The related operating conditions, including boron concentration, moderator temperature, irradiation history, etc.
- The burnup-induced changes in the geometry

The final assessments accepted for the given study are shown below in Tab. 4-12.

Tab. 4-12: Available UQ (Uncertainties Quantification) data on operating conditions and BU-induced geometry changes, in pcm.

<b>Burnup</b> [GWd/t <sub>HM</sub> ]	<b>0.0 – 17.6</b>	<b>17.6 – 33.8</b>	<b>33.8 – 50.5</b>
Operating conditions	100	400	500
Burnup-induced changes	200	200	700

#### 4.5.2 Technological tolerance impact

The impact of the PWR fuel technological and manufacturing parameter tolerances on the criticality calculations was analysed at PSI/LRS and published in Pecchia (2015c). Taking into account only the fuel assembly-related uncertainties from the list of parameters used, the total  $\sigma_{TP}$  uncertainty component is assessed as only 10 pcm. In particular, the uncertainty components from all parameters listed in Fig. 9 of Pecchia (2015c), except parameters 11 and 13, should be summed as random uncorrelated uncertainties, thus leading to a total uncertainty value limited by this 10 pcm.

#### 4.5.3 Nuclear data uncertainty impact

The uncertainties in the nuclear data employed in the calculations contribute to the uncertainty in the computed  $K_{eff}$  values. Their impact was considered in the CASMO5 burnup calculations using the SHARK-X methodology (see Herrero 2016b and references therein), providing the  $\sigma_{SNF-Keff}^{(SHARK-X)}$  estimation, and in the MCNP6 criticality calculations using the NUSS methodology to assess the  $\sigma_{ND-Keff}^{(NUSS)}$  component (see again Herrero 2016b and Dean et al. 2001). For additional illustration, Fig. 4-3 shows the scheme of the ND-related uncertainties (given as covariance matrices (CM)) propagation in compliance with the flowchart of Fig. 4-1.

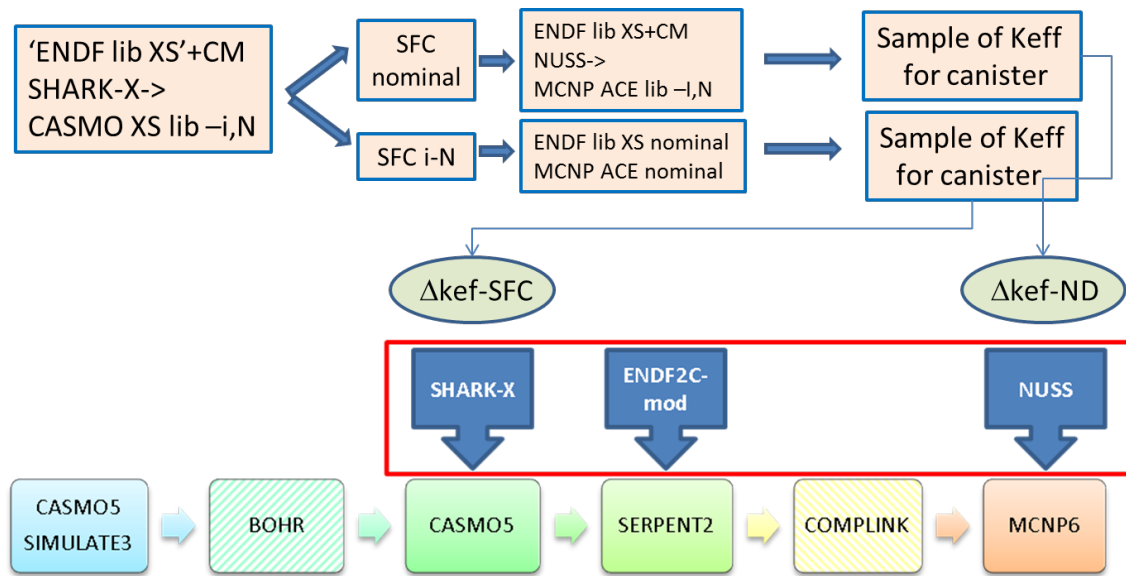


Fig. 4-3: Presently employed ND stochastic sampling methodology.

The Monte Carlo uncertainty sampling method employed to obtain the estimated uncertainty in  $K_{eff}$  requires a very large number of calculations and has thus been realised only for the 4.94  $w_0$  fuel enrichment case.

Tab. 4-13 and Tab. 4-14 show the estimated  $\sigma_{SNF-Keff}^{(SHARK-X)}$  and  $\sigma_{ND-Keff}^{(NUSS)}$  values for the fuel just after discharge and after 50'000 years of decay; uncertainties from all AC and FP are considered. The direct effect from nuclear data in the MCNP6 calculation is similar in both periods and slightly decreases with the burnup level attained, and the indirect effect of nuclear data contained in the isotopic uncertainties increases slightly with decay time. These observations are valid for  $UO_2$  fuel. Details of the performed calculations are given in Herrero (2015) and Herrero (2016b).

Tab. 4-13: Estimated nuclear data-related uncertainties of  $k_{eff}$  after discharge (no decay).

Exposure (GWd/tHM)	$\sigma_{SNF-Keff}^{(SHARK-X)}$	$\sigma_{ND-Keff}^{(NUSS)}$
0	-	0.00367
17.61	0.00162	0.00311
33.82	0.00258	0.00304
50.47	0.00358	0.00298
61.92	0.00437	0.00295
72.75	0.00526	0.00288

Tab. 4-14: Estimated nuclear data-related uncertainties of  $k_{eff}$  after 50'000 years decay.

Exposure (GWd/tHM)	$\sigma_{SNF-Keff}^{(SHARK-X)}$	$\sigma_{ND-Keff}^{(NUSS)}$
0	-	0.00367
17.61	0.00249	0.00332
33.82	0.00396	0.00318
50.47	0.00536	0.00301
61.92	0.00635	0.00287
72.75	0.00738	0.00271

It should be noted that the considered uncertainty components  $\sigma_{SNF-Keff}^{(SHARK-X)}$  and  $\sigma_{ND-Keff}^{(NUSS)}$  must be correlated since the underlying nuclear data are the same for the independent estimations performed for both the components. However, at present the correlation level is unknown. In the ideal case, all calculations should be done in a single set using the same original perturbation factors for the nuclear data in both the depletion and the criticality calculations; however this will involve significant additional computation burdens. Therefore, it will be conservative to assume a full correlation between both components and thus to estimate the total ND-related  $\Delta k_{eff}$  component according to Eq. (4.3).

Next, to be on the conservative side, the total ND-related uncertainty will be composed from the  $\sigma_{SNF-Keff}^{(SHARK-X)}$  component corresponding to 50'000 years of cooling and the  $\sigma_{ND-Keff}^{(NUSS)}$  corresponding to zero cooling time (Tab. 4-13 and Tab. 4-14).

#### 4.5.4 Long-term nuclide evolution

The accuracy of the decay code employed and the nuclear data library was investigated and benchmarked and the results were illustrated in Chapter 2 of this report. Later, the impact of nuclear data uncertainty on the decay calculations performed with the code SERPENT2 was studied by perturbing the decay data with a modified version of the ENDF2C tool. The main outcome shows an impact of  $\sigma_{T1/2} \approx 15$  pcm on  $K_{eff}$  for the studied load.

#### 4.5.5 MCNP Monte Carlo uncertainty

The Monte Carlo method implemented in the MCNP6 code produces a  $K_{eff}$  value with an inherent statistical uncertainty,  $\sigma_{MC}$ . The number of cycles and histories per cycle were selected so as to yield  $\sigma_{MC} \approx \pm 25$  pcm, which is fairly low.

#### 4.5.6 Total sum of uncertainties components

The total uncertainty,  $\sigma_{tot}$ , which will be used in Eq. (4.1), is evaluated here in Tab. 4-15.

Tab. 4-15: Summary of all total uncertainty components.

Exposure (GWd/t)	$\sigma_{ND}$	$\sigma_{OP}$	$\sigma_{BU-eff}$	$\sigma_{TP}$	$\sigma_{T1/2}$	$\sigma_{MC}$	$1*\sigma_{tot}$	$2*\sigma_{tot}$
0	0.00367	0.00000	0.00000	0.00010	0.00015	0.00025	0.00368	<b>0.00737</b>
17.61	0.00560	0.00100	0.00200	0.00010	0.00015	0.00025	0.00604	<b>0.01208</b>
33.82	0.00700	0.00400	0.00200	0.00010	0.00015	0.00025	0.00831	<b>0.01662</b>
50.47	0.00834	0.00500	0.00700	0.00010	0.00015	0.00025	0.01199	<b>0.02397</b>
61.92	0.00930	0.00500	0.00700	0.00010	0.00015	0.00025	0.01267	<b>0.02534</b>
72.75	0.01026	0.00500	0.00700	0.00010	0.00015	0.00025	0.01339	<b>0.02679</b>

It is important to note that the total uncertainty is burnup-dependent due to the burnup dependency of the components  $\sigma_{ND}$ ,  $\sigma_{OP}$  and  $\sigma_{BU-eff}$ .

To better illustrate the impact of the burnup profile penalties considered and the uncertainty components, Fig. 4-4 shows the results obtained for the case of AC+FP, based on the data reported in Tab. 4-5, 4-9 and 4-15.

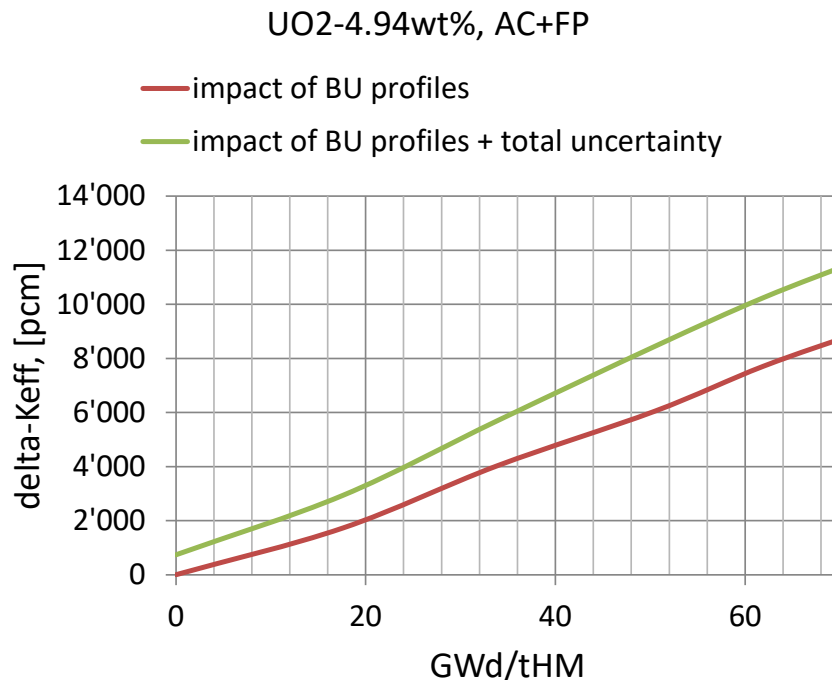


Fig. 4-4: Impact of the burnup profiles and the total uncertainty on the canister  $k_{eff}$  value.

## 4.6 Loading curve with combined uncertainty effects

### 4.6.1 Determination of the minimum BU required for fulfilment of the criticality safety criteria

The final target of the project is to develop a methodology for addressing a minimum average burnup for individual fuel assemblies required for full loading of the disposal canister without exceeding the defined upper subcritical limit. This goal is achieved by developing specific loading curves for discharged spent fuel, where the initial enrichment and final burnup of a fuel bundle will function as acceptance criteria for the loading of the disposal canister.

The development of the curve is done as follows: the left part of Eq. (4.1) is plotted as a curve depending on burnup (using the Excel smooth line interpolation option), while the right part of Eq. (4.1) can be shown as a constant line corresponding to the given USL value. If the burnup-dependent curve of (4.1),  $k_{eff}|_{Bounding\ FA\ pos}(BU) + \Delta k_{eff}^{Ax}(BU) + \Delta k_{eff}^{Rad}(BU) + 2\sigma_{tot}(BU)$ , and the burnup-independent USL line intersect, the burnup at the point of the intersection becomes the point on the loading curve corresponding to the given fuel enrichment. If the burnup-dependent curve of (4.1) is always below the USL value, then for the given enrichment the burnup equal to zero is shown on the loading curve. As presented in Chapter 2, for the PSI CSE methodology using MCNP in conjunction with ENDF/B-VII.1, and assuming the "administrative margin" equals 5'000 pcm, the USL value is defined according to (4.1) as  $0.99339 - 0.05000 = \mathbf{0.94339}$ .

To give an outlook on the general behaviour of the curve over the burnup, Fig. 4-5 shows the examples for the case of AC (Fig. 4-5a) and AC+FP (Fig. 4-5b) corresponding to the highest of all considered enrichments, 4.94 w/o. It can be seen again that the most conservative case for the credit of AC+FP is zero cooling time after discharge, while in the case of only AC the most conservative results generally correspond to the cooling time about 30'000 years, as expected.

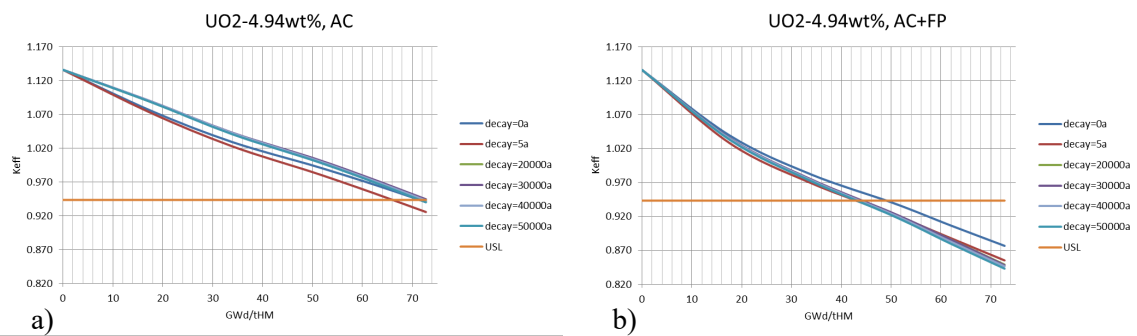


Fig. 4-5: Illustration of determination of the minimum burnup required for fuel to meet USL criticality safety criteria: a) AC, b) AC+FP.

In order to facilitate the understanding of the detection of the minimum required burnup for each particular enrichment, Fig. 4-6 to Fig. 4-11 are provided.

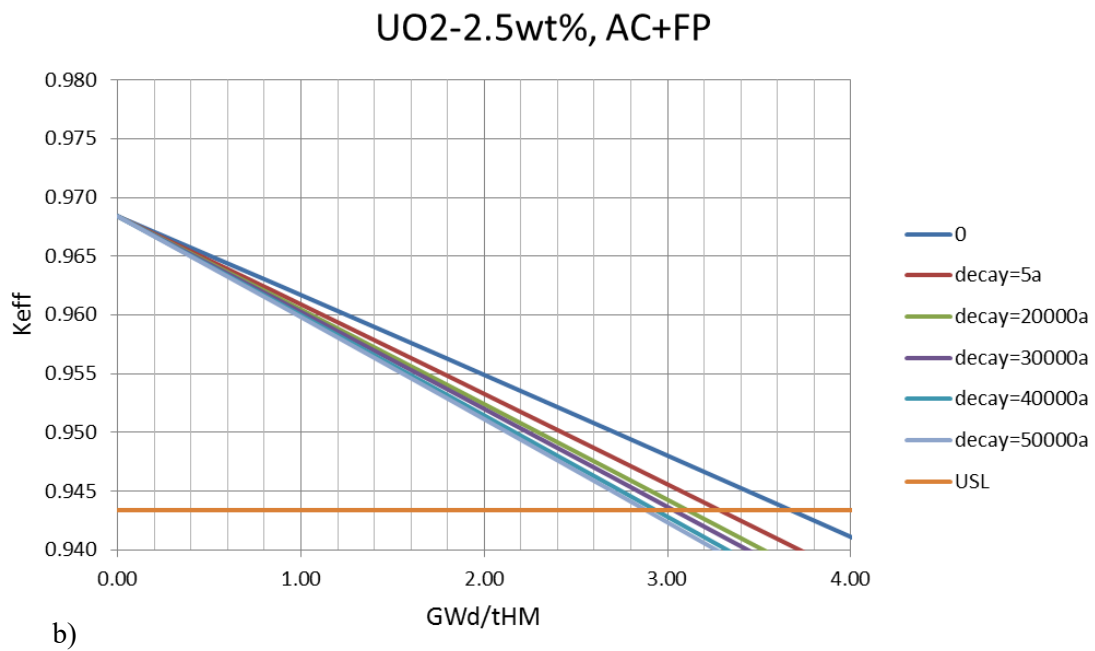
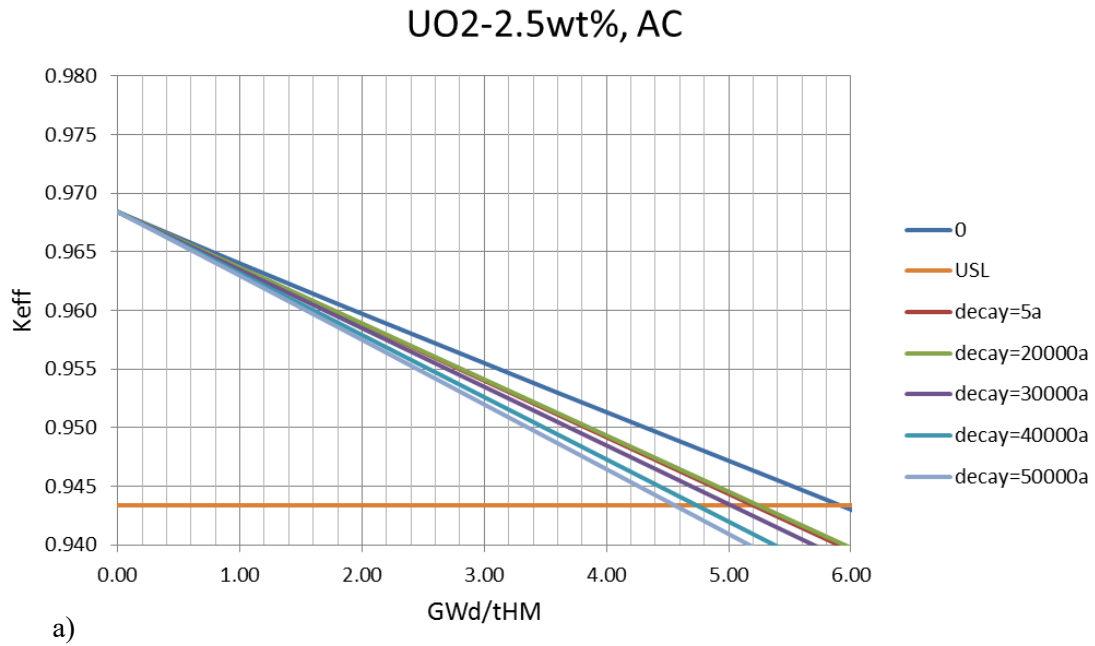


Fig. 4-6: Determination of the limiting BU for 2.5<sup>w</sup>/<sub>0</sub> PWR UO<sub>2</sub> fuel.  
a) AC, b) AC+FP.

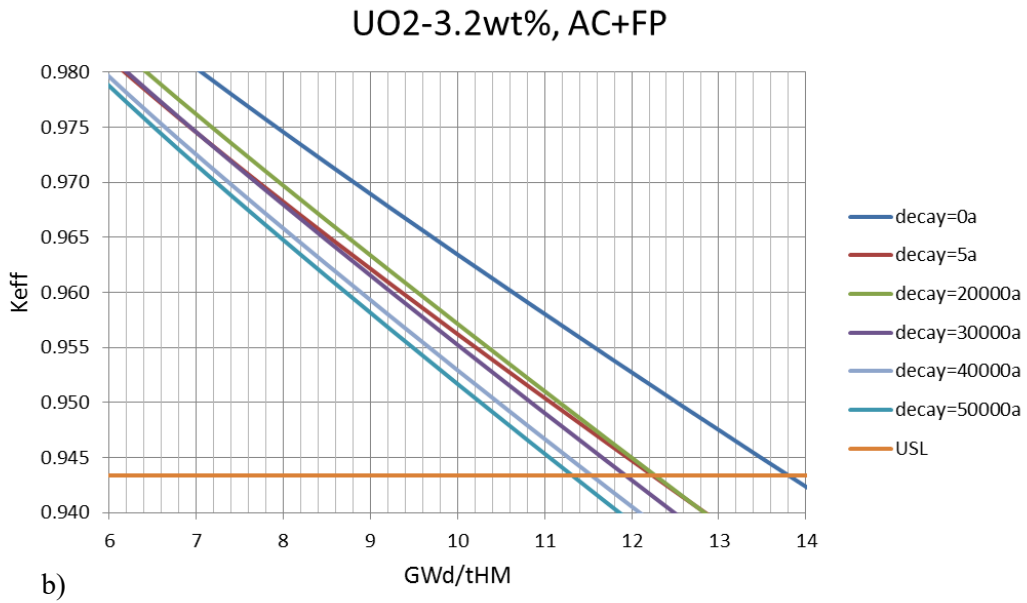
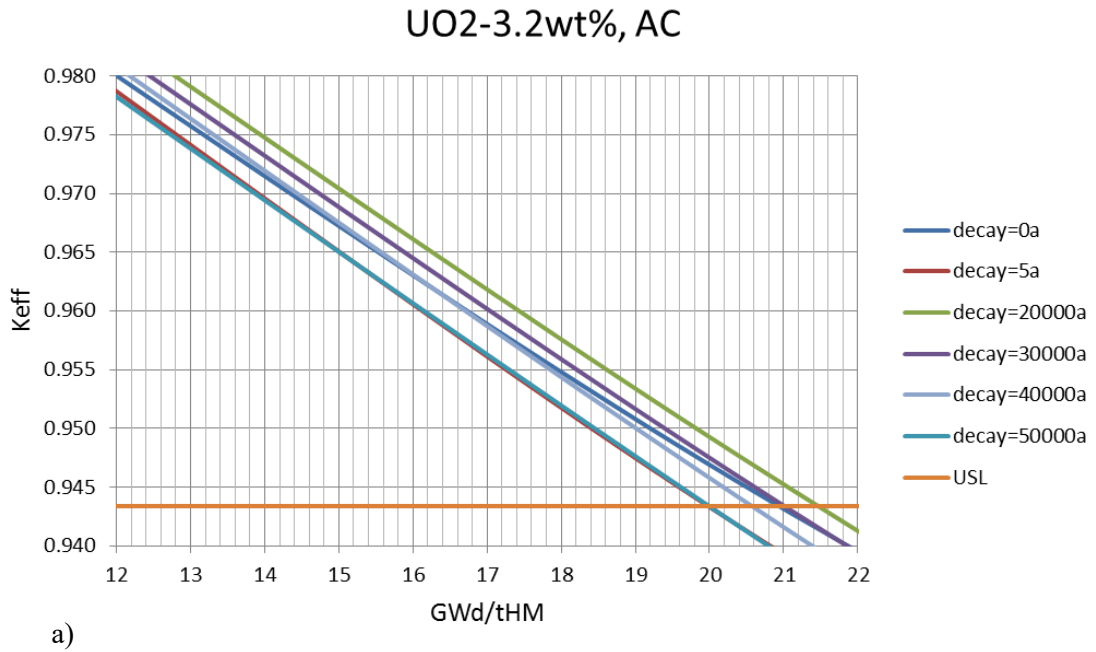


Fig. 4-7: Determination of the limiting BU for 3.2 % PWR UO<sub>2</sub> fuel.  
a) AC, b) AC+FP.

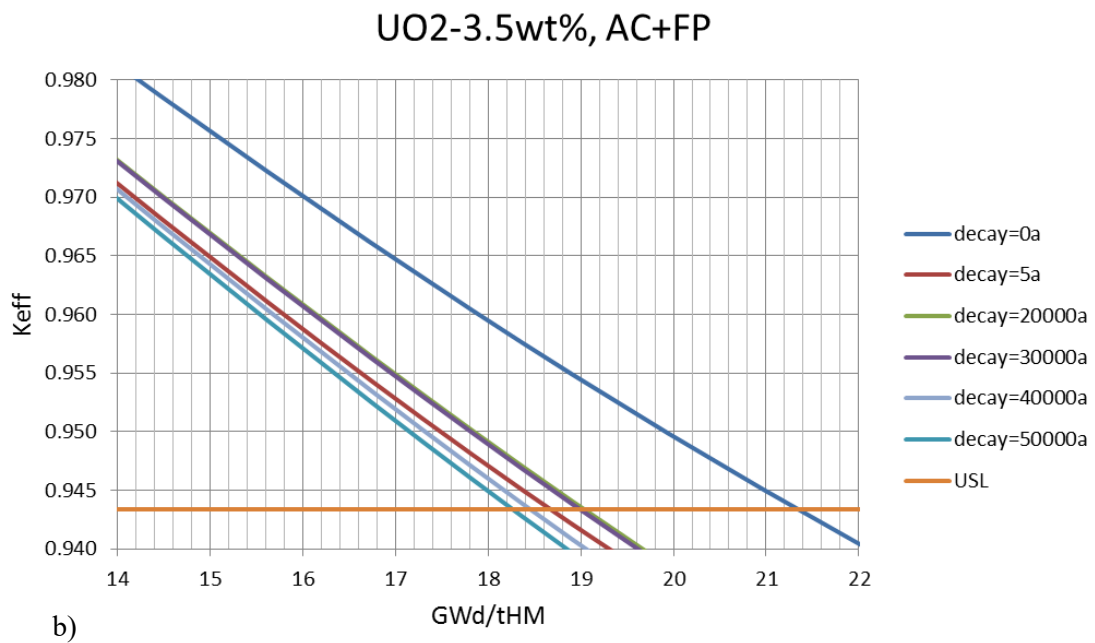
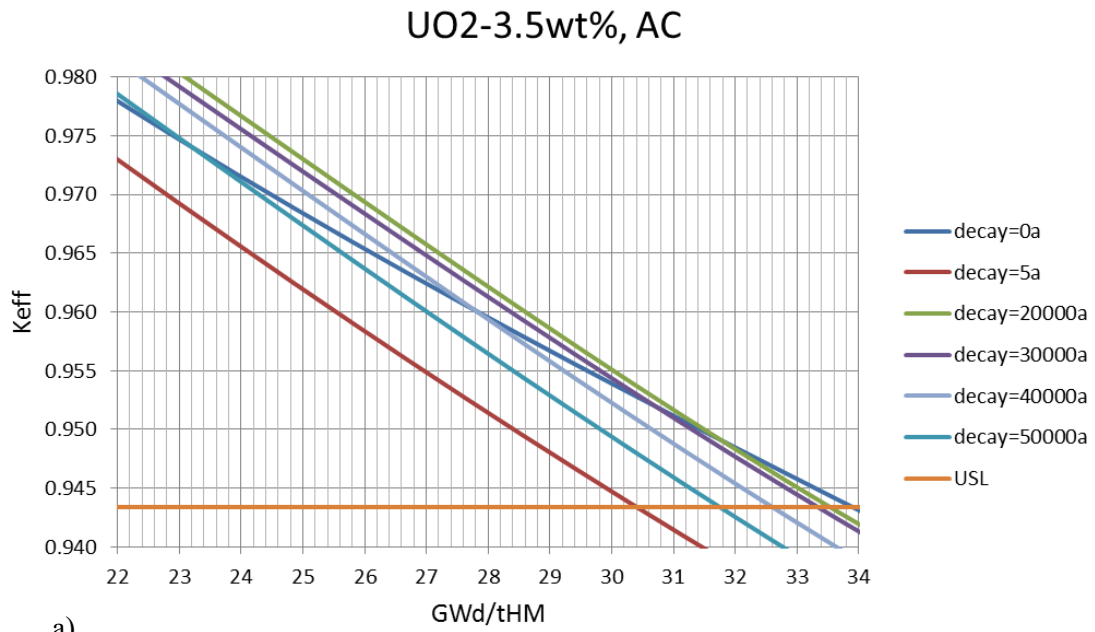


Fig. 4-8: Determination of the limiting BU for 3.5 % PWR UO<sub>2</sub> fuel.  
a) AC, b) AC+FP.

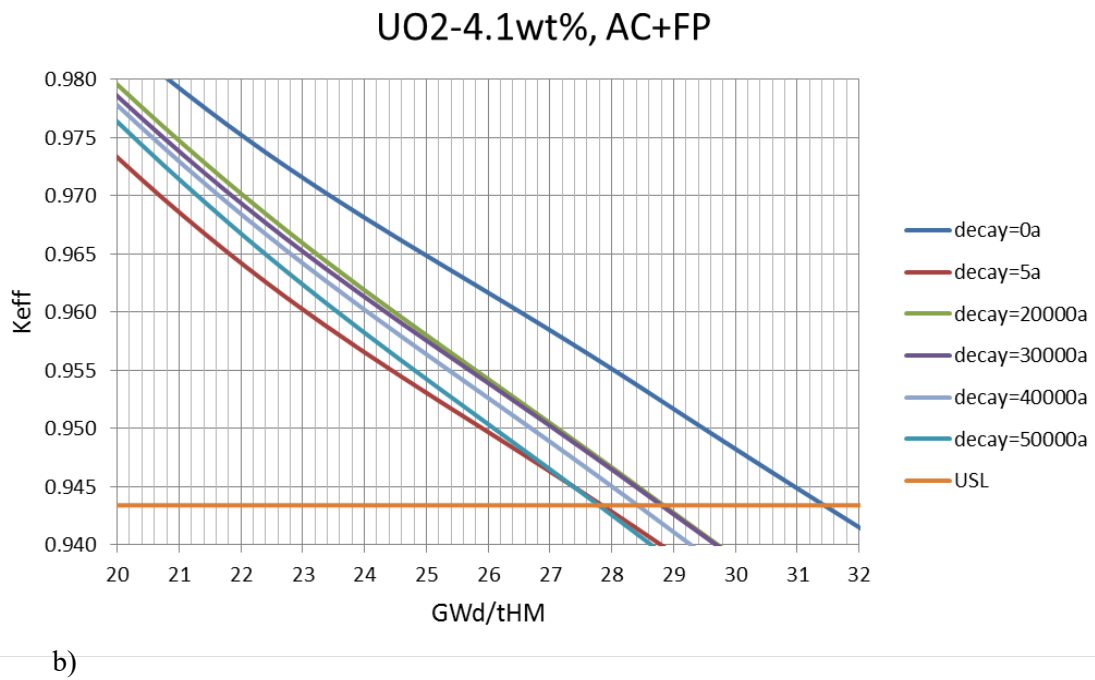
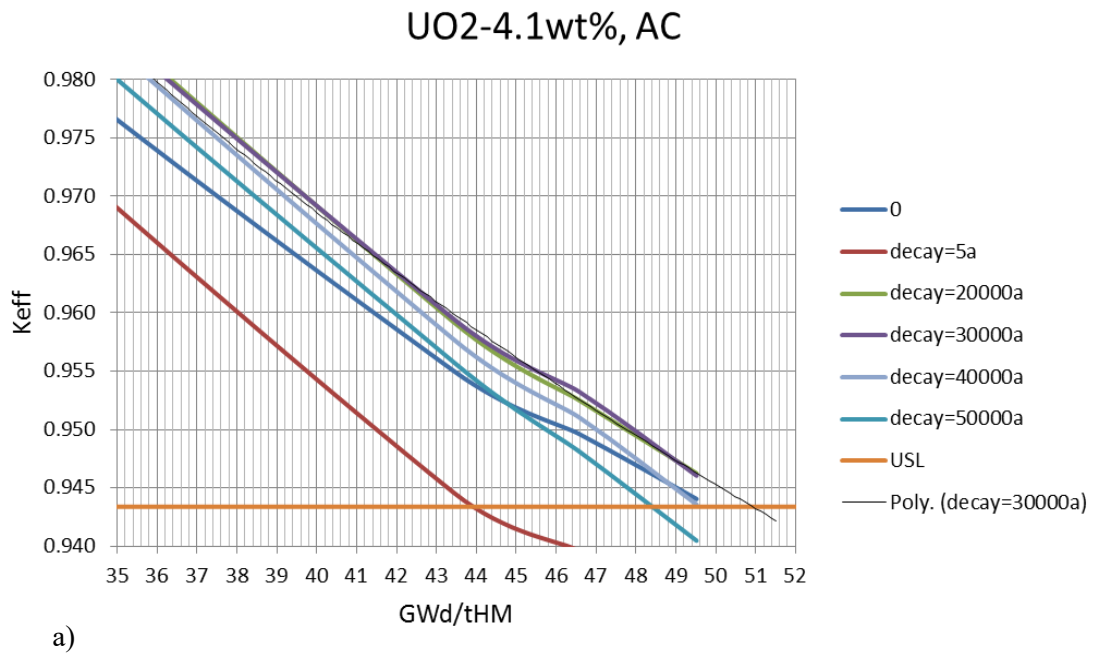


Fig. 4-9: Determination of the limiting BU for 4.1 % PWR UO<sub>2</sub> fuel.  
 a) AC, b) AC+FP.

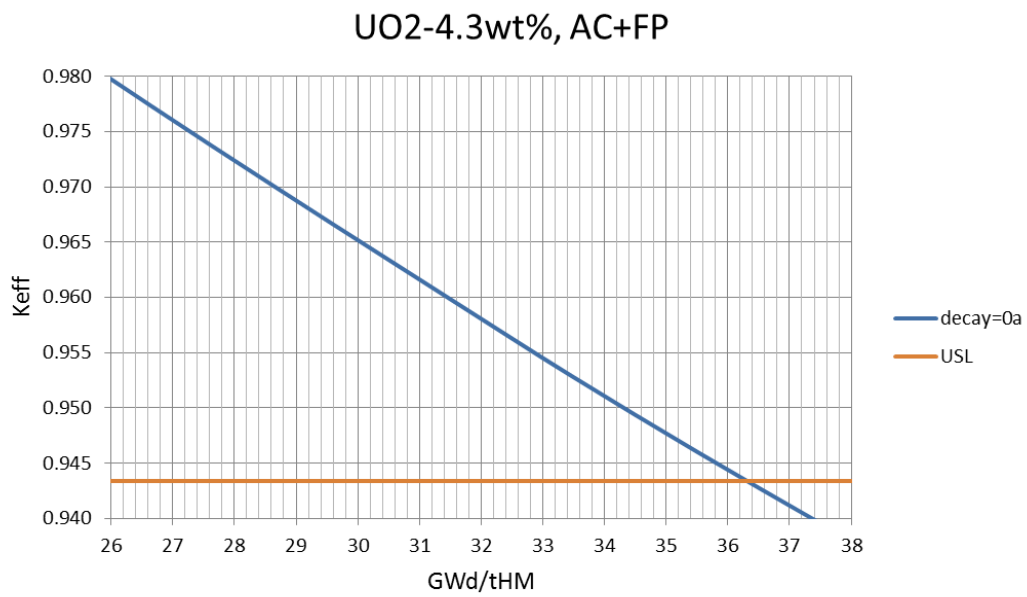
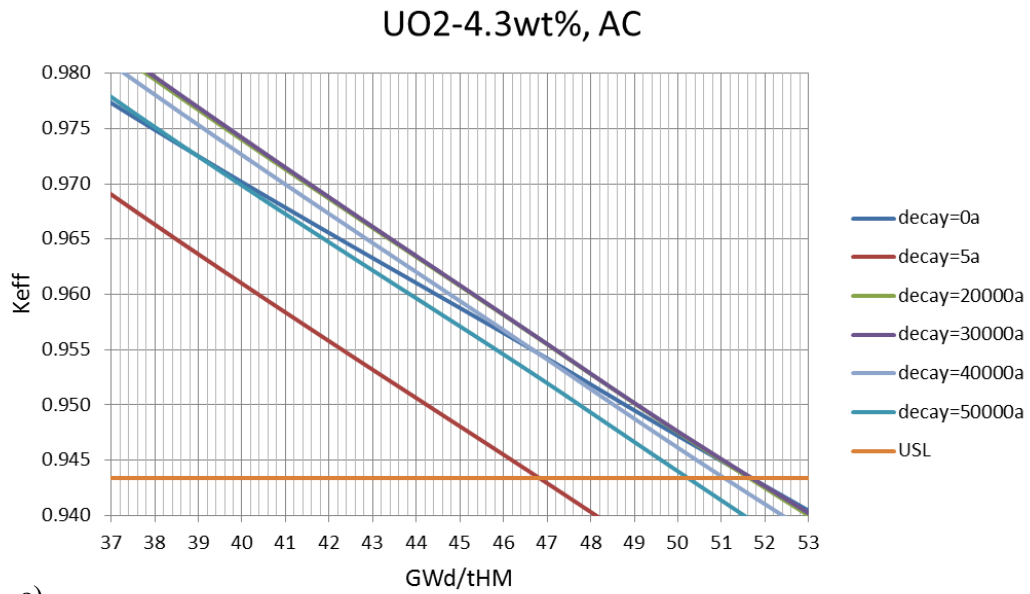


Fig. 4-10: Determination of the limiting BU for 4.3 % PWR UO<sub>2</sub> fuel.

a) AC, b) AC+FP.

(No results are available for the option AC+FP for cases other than decay time = 0 years.)

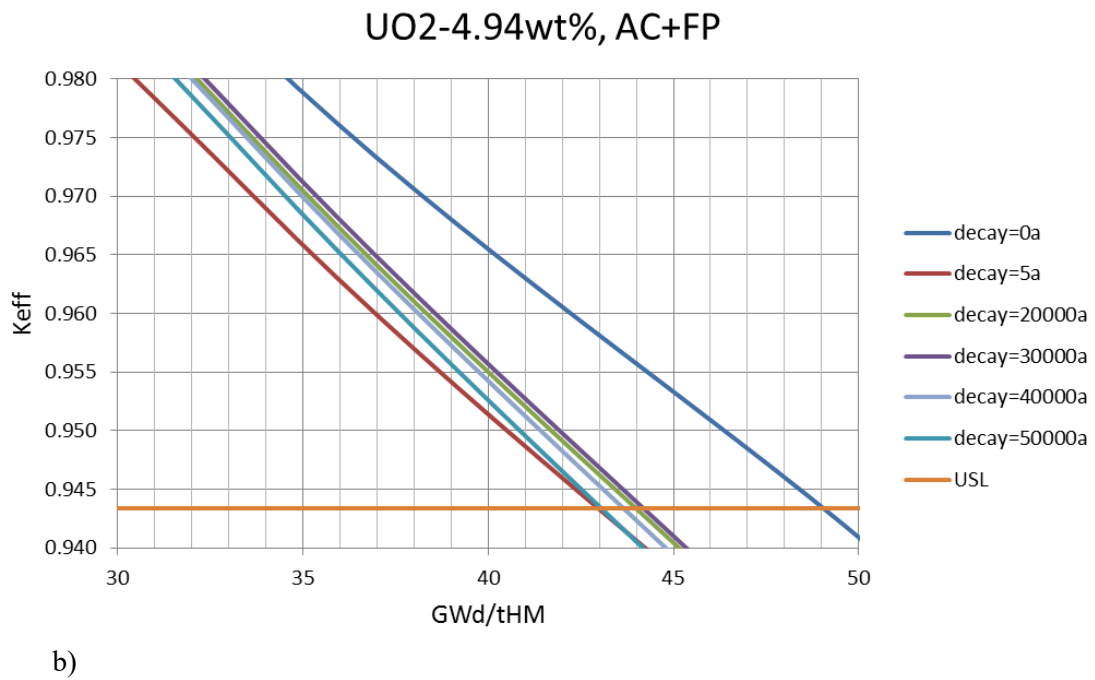
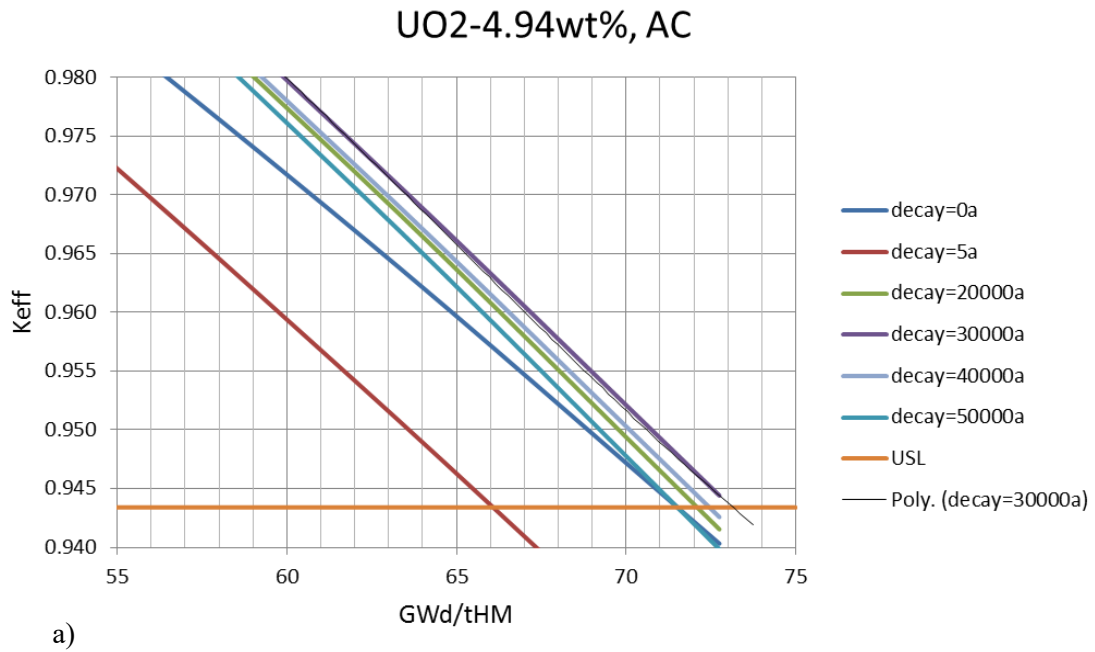


Fig. 4-11: Determination of the limiting BU for 4.94 % PWR UO<sub>2</sub> fuel.  
 a) AC, b) AC+FP.

### 4.6.2 Loading curve approximation

The results of the analysis of Fig. 4-6 to 4-11 with respect to the limiting burnup values satisfying Eq. (4.1) are summarised in Tab. 4-16.

Tab. 4-16: Minimum burnup required for meeting the criticality safety criteria.

Enrichment $w/o$	AC	AC+FP
1.90	0	0
2.50	~ 6.0*	3.7
3.20	21.5	13.8
3.50	33.9	21.4
4.10	~ 51.0*	31.5
4.30	51.7*	36.4*
4.94	~ 73.0*	49.1

\* These values are based on extrapolations or involve certain (minor) interpolations.

The loading curves are derived by applying the data of Tab. 4-16, as shown in Fig. 4-12.

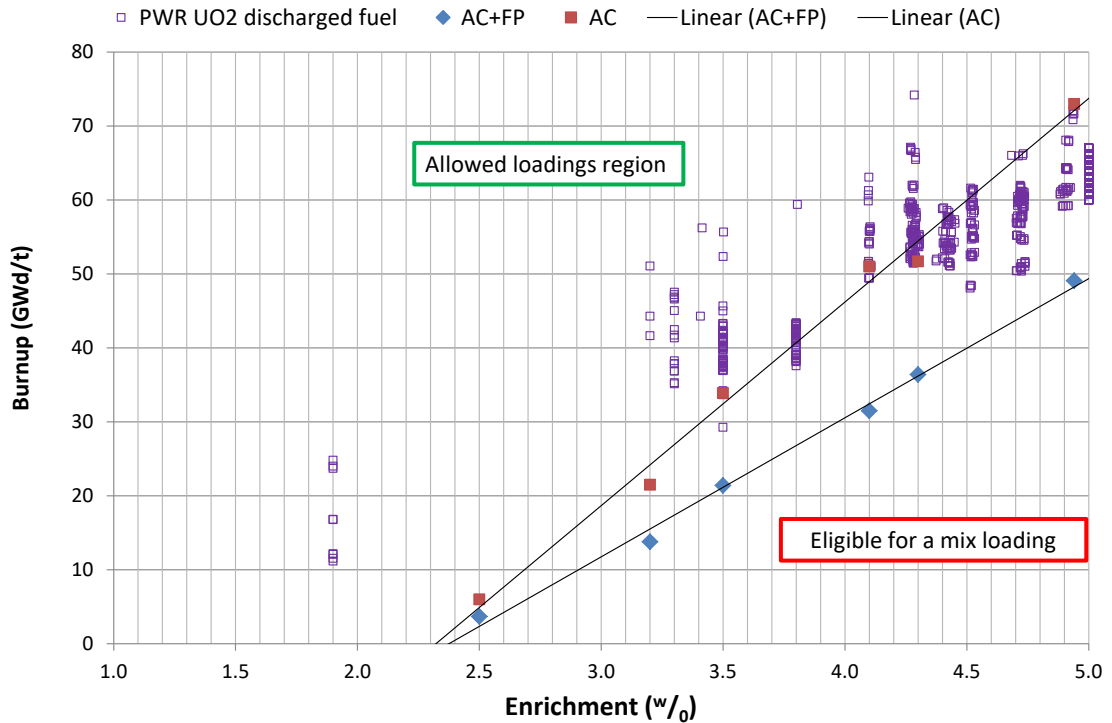


Fig. 4-12: Loading curve with all conservative effects for discharged spent fuel.

The data on the SNF burnups used in Fig. 4-12 are based on a Nagra assumption.

It becomes clear from these results that the given canister design meets the criticality safety criteria if the burnup credit is based on the actinides plus fission products (AC+FP) approach. In this case, most of the considered spent fuel assemblies, as plotted in Fig. 4-12, could achieve the criticality safety criteria.

### 4.7 Outlook on the obtained results

In order to provide a clearer illustration of the obtained results and to give an idea of what additional calculation effort could be suggested towards relaxation of the currently obtained burnup credit requirements, Fig. 4-13 is given below. This figure shows separately the different contributions to the derived burnup requirements for the single case of 4.94 wt% enrichment. Both AC (red lines) and AC+FP (blue lines) BUC options are demonstrated for three different cases:

1. "Nominal results" for the canister loaded with spent fuel with nominal BU profile; no uncertainties ( $\sigma_{tot}(BU)$ ) are taken into account (dashed lines).
2. The same as case #1, but the nominal burnup profiles are replaced by bounding ones (dotted lines).
3. The same as case #2, but the uncertainties are also taken into account (continuous lines).

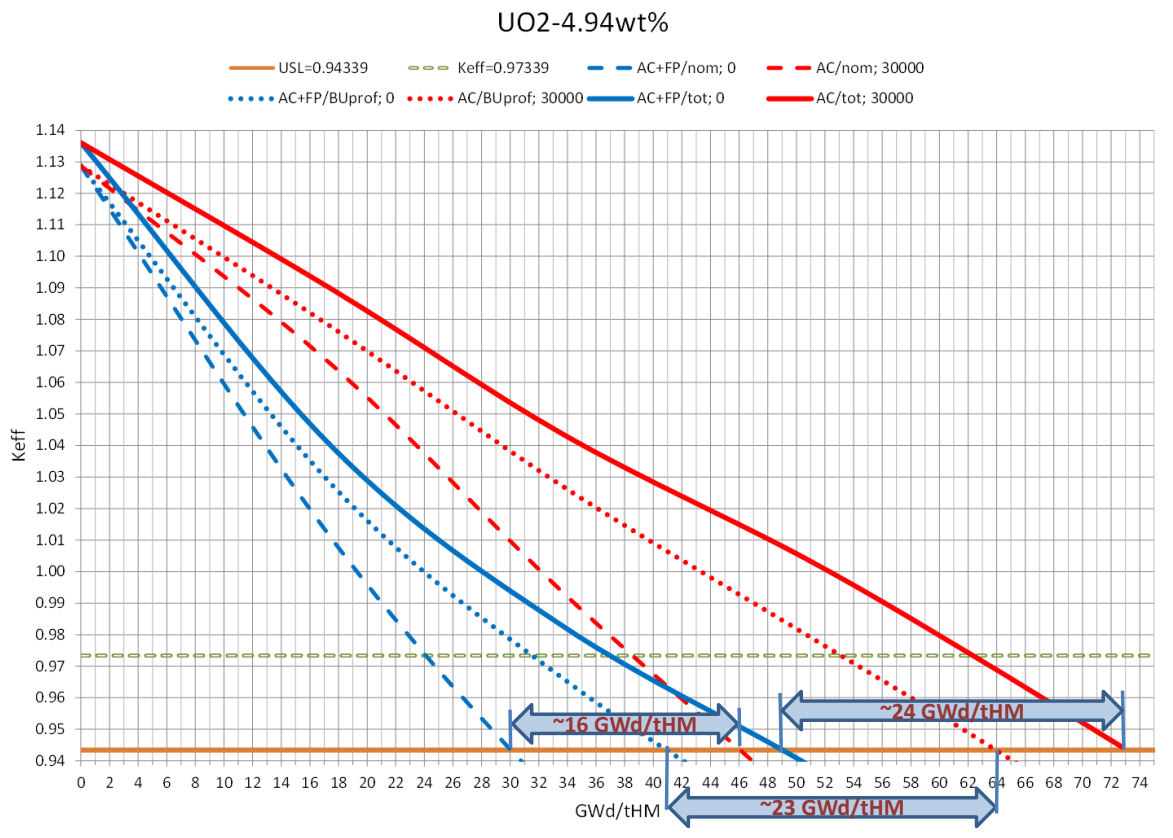


Fig. 4-13: Impact of different modelling components and options on the BU limits.

The figure also demonstrates how the burnup credit difference between the AC+FP and only AC options changes between the three cases considered. Note that, to be on the conservative side, for the AC case the decay time corresponds to 30'000 years, while for the AC+FP case the decay time is zero. It can be seen that the inclusion of the bounding burnup profiles significantly increases the difference between the AC and AC+FP cases. It also can be noted that the bounding burnup profiles bring most significant burnup penalties (consistent with Fig. 4-5), although the uncertainty component is also important. Thus, if the presently obtained loading curves are to be refined, it is recommended to start the in-depth analysis from a high-fidelity evaluation of the burnup profiles and then to focus on the most significant uncertainty components:

- Nuclear data (ND) combined impact ( $\sigma_{ND}$ )
- Operating conditions ( $\sigma_{OP}$ )
- Burnup-induced geometry changes ( $\sigma_{BU-eff}$ )

Finally, for general illustration purposes, Fig. 4-13 shows two  $USL/k_{eff}$  horizontal lines corresponding to the two values for the administrative margin: the conventional one of 5'000 pcm and, for comparison, a reduced one of 2'000 pcm<sup>6</sup>. This illustration allows prediction of how large a saving in the minimum burnup requirement could be achieved provided the administrative margin could be relaxed to 2'000 pcm by demonstrating the very unlikely accident scenario. According to Fig. 4-13, for example for the option of AC+FP, the saving would correspond to  $\sim 12$  GWd/t<sub>HM</sub>.

---

<sup>6</sup> The administrative margin to criticality is normally set to 5,000 pcm, i.e.  $K_{eff}$  of the system, plus the calculation bias and uncertainty in the bias should not exceed 0.95. More recently, an administrative margin of 0.98 (2,000 pcm) has been employed for the very unlikely accident conditions.



## 5 Conclusions

This technical report presents a preliminary criticality assessment obtained as part of the PSI/Nagra BUCSS-R research project conducted at PSI between 2014 and 2016. The report contains a brief description of the applied methodology for the loading curve derivation and, where appropriate, provides references on detailed descriptions of particular modelling aspects.

The loading curves presented were obtained for a reference disposal canister design provided by Nagra in the course of the project. However, Nagra is exploring various options for the selection of materials and design concepts for the disposal canister, which may require re-evaluation of the loading curves. The loading curves presented in this work show that only the AC credit approach (i.e. taking credit for the neutron absorption of non-fissile actinides, but not for the fission products) would not be sufficient to meet the USL criticality safety criteria for a non-mixed loading with fuel with an initial enrichment above  $\sim 3.5$  w/o, while the AC+FP approach (where the credit from neutron absorbers includes both non-fissile actinides and fission products) justifies the applicability of the considered canister design for safe disposal of spent nuclear fuel with all existing enrichments with required minimum burnups. A postulated case, consisting of FAs with 5 w/o initial enrichment and relatively low burnup, would be the only exception not fitting the loading criteria; however, this case belongs only to a theoretical last core discharge, where, in reality, a lower enriched fuel should be employed. The loading curves must be treated as preliminary since, as discussed in the report, there is still room for improvement in the assessment of different components of Eqs. (4.1 – 4.3). However, even if the confidence in every point on the loading curve assessed for the given enrichment may not be easily quantified, the fact that, overall, all the obtained points tend to lie on straight lines indicates that the loading curves obtained on the basis of the regression lines are reliable, since the uncertainties of the individual points should be compensated to a large extent.

It must also be underlined that the developed BUCSS-R standard execution sequence is now almost automatic and can thus be applied in the future for extended comprehensive studies in an efficient manner. Thus, it can be concluded that the goals of the BUCSS-R project were reached by the derivation of the preliminary loading curves with the developed BUCSS-R methodology, which is now in place at LRS/PSI for any future continuation or follow-up of the BUCSS-R project, noting that a need for further improvement was also identified during the stages of the project realisation.

Among the topics for further improvement of the BUCSS-R methodology (with respect to only the criticality safety and burnup credit assessments), other aspects can be proposed for consideration, such as the extension of the analysed FA sample to yield 95 %/95 % bounds for the loading curves, i.e. to safely cover the potential uncertainties from the operating condition variations, a refinement of the treatment of uncertainties with respect to the burnup axial and radial profile, allowing a consistent "Total Monte Carlo" assessment ("seamless" calculations of both depletion/decay and criticality models using the same Nuclear Data perturbation factors) and, of course, the assessment of long-term scenarios with canister and fuel evolution and degradation.



## 6 References

- ANS (1998): Nuclear criticality safety in operations with fissionable material outside reactors, ANSI, ANS-8.1-1998.
- ANS (2008): American Nuclear Society, Standards Committee Working Group ANS-8.27. American National Standard ANSI/ANS-8.27-2008. Burnup credit for LWR fuel" American Nuclear Society, 555 North Kensington Avenue, La Grange Park, Illinois 60526 USA.
- ANS (2012): Validation of neutron transport methods for nuclear criticality safety calculations, ANSI, ANS-8.24-2007 (R2012).
- Berglund, M. & Wieser, M.E. (2011): Isotopic compositions of the elements 2009 (IUPAC Technical Report), Pure Appl. Chem., vol. 83, no. 2, pp. 397 – 410.
- Broadhead, B.L., Rearden, B.T. & Hopper, C.M. (2004): Sensitivity- and uncertainty-based criticality safety validation techniques, Nucl. Sci. Eng., vol. 146, pp. 340 – 366.
- CASMO5 (2012): CASMO5 User's Manual, SSP-07/431 Rev 5.
- Dean, J.C. & Tayloe Jr., R.W. (2001): Guide for Validation of Nuclear Criticality Safety Calculational Methodology. NUREG/CR-6698. US Nuclear Regulatory Commission, Washington, DC.
- Diez, C.J., Buss, O., Hoefler, A., Porsch, D. & Cabellos, O. (2014): Comparison of nuclear data uncertainty propagation methodologies for PWR burn-up simulations, Ann. Nucl. Energy 77.
- DIN (1994): DEUTSCHE NORM DIN 25478. Application of Computer Codes for the Assesment of Criticality Safety, DIN-25478\_1994-07.
- DIN (2007): DEUTSCHE NORM DIN 25712. Kritikalitätssicherheit unter Anrechnung des Brennstoffabbrands bei Transport und Lagerung bestrahlter Leichtwasserreaktor-Brennelemente in Behältern. (Criticality safety taking into account the burnup of fuel for transport and storage of irradiated light water reactor fuel assemblies in casks). ICS 27.120.30. DIN Deutsches Institut für Normung e.V., Juli 2007.
- DIN (2009): DEUTSCHE NORM DIN 25471. Criticality safety taking into account the burnup of fuel elements when handling and storing nuclear fuel elements in fuel pools of nuclear power plants with lightwater reactors, DIN-25471:2009-05.
- DIN (2012): Kritikalitätssicherheit bei der Endlagerung ausgedienter Kernbrennstoffe, DIN-25472:2012-08 (D).
- DIN (2014): DEUTSCHE NORM DIN 25712:2014. Kritikalitätssicherheit unter Anrechnung des Brennstoffabbrands bei Transport und Lagerung bestrahlter Leichtwasserreaktor-Brennelemente in Behältern, 25712:2014-05 (D) -05.
- DOE (1999): Criticality Safety Good Practices Program. Guide for DOE Nonreactor Nuclear Facilities. DOE G 421.1-1, US Department of Energy, Washington, DC.

- ENDFB7 (2014): The ENDF/B-VII.1 ENDF and ACE files downloaded from National Nuclear Data Center (NNDC/BNL), Archive SB-BNL-DAT-001-14.
- Fensin, M.L., James, M.R., Hendricks, J.S. & Goorley, J.T. (2012): The new MCNP6 depletion capability, ICAPP, vol. 836.
- Ferroukhi, H., Hofer, K., Hollard, J.-M., Vasiliev, A. & Zimmermann M. (2008): Core Modelling and Analysis of the Swiss Nuclear Power Plants for Qualified R&D Applications, PHYSOR.
- Gutierrez, M., Caruso, S. & Diomidis, N. (2017): Criticality and shielding assessment of canister concepts for the disposal of spent nuclear fuel, International High-Level Radioactive Waste Management Conference, April 9 – 13, 2017, Charlotte, NC, Westin.
- Herrero, J.J., Pecchia, M., Ferroukhi, H., Canepa, S., Vasiliev, A. & Caruso, S. (2015): Computational Scheme for Burnup Credit applied to Long Term Waste Disposal. Proc. Int. Conf. Nuclear Criticality Safety, ICNC 2015, Charlotte, NC, USA, September 13 –17.
- Herrero, J.J., Vasiliev, A., Pecchia, M., Ferroukhi, H. & Caruso, S. (2016): Review calculations for the OECD/NEA Burn-up Credit Criticality Safety Benchmark, Ann. Nucl. Energy, vol. 87, pp. 48 – 57.
- Herrero, J.J., Rochman, D., Leray, O., Vasiliev, A., Pecchia, M. & Ferroukhi, H. (2016b): Caruso S., Impact of nuclear data uncertainty on safety calculations for spent nuclear fuel geological disposal, Nuclear Data 2016, Bruges, Belgium, September 11 – 16, 2016.
- Hunter, J.L. & Sutton, T.M. (2013): A Method for Reducing the Largest Relative Errors in Monte Carlo Iterated-Fission-Source Calculations, M&C 2013, 2013, pp. 2780 – 2791.
- IAEA (2001): Neuber, J.C., Evaluation of Axial and Horizontal Burnup Profiles. Proceedings of a Technical Committee meeting, Implementation of burnup credit in spent fuel management systems, IAEA-TECDOC-1241 (2000).
- IAEA (2005): Blatz, H. Regulations for the Safe Transport of Radioactive Material, IAEA, Safety Standards – TS-R-1.
- IAEA (2011): Geological Disposal Facilities for Radioactive Waste, IAEA, Safety Standards – SSG-14.
- IAEA (2014): Criticality Safety in the Handling of Fissile Material," IAEA, Safety Standards – SSG-27.
- ISO (2011): Nuclear criticality safety – Evaluation of systems containing PWR UOX fuels – Bounding burnup credit approach, ISO-27468:2011.
- Isotalo, A. (2013): Computational Methods for Burnup Calculations with Monte Carlo Neutronics, Aalto University.
- JEFF (2014a): The JEFF-3.1.2 Nuclear Data Library, SB-NEA-DAT-003-14.
- JEFF (2014b): JEFF32-ACE, Archive SB-NEA-DAT-004-14.

- Kellett, M.A., Bersillon, O. & Mills, R.W. (2009): The JEFF-3.1/-3.1.1 radioactive decay data and fission yields sub-libraries, No. 6287.
- Kelly, D.J., Sutton, T.M. & Wilson, S.C. (2012): MC21 Analysis of the Nuclear Energy Agency Monte Carlo Performance Benchmark Problem, PHYSOR 2012.
- Koning, A.J. & Rochman, D. (2012): Modern Nuclear Data Evaluation with the TALYS Code System, *Nucl. Data Sheets*, vol. 113, no. 12, pp. 2841 – 2934.
- Kühl, H., Johnson, L.H. & McGinnes, D.F. (2012b): Criticality and Canister Shielding Calculations for Spent Fuel Disposal in a Repository in Opalinus Clay. Nagra Technical Report NTB 12-41.
- Leppänen (2007): Development of a New Monte Carlo Reactor Physics Code, Helsinki University of Technology.
- Leppänen (2013): Serpent – a Continuous-energy Monte Carlo Reactor Physics Burnup Calculation Code. User's Manual, VTT.
- Leray, O., Grimm, P., Hursin, M., Ferroukhi, H. & Pautz, A. (2015): Uncertainty quantification of spent fuel nuclide compositions due to cross sections, decay constants and fission yields, PHYSOR 2014.
- Lichtenwalter, J.J., Bowman, S.M., DeHart, M.D. & Hopper, C.M. (1997): Criticality Benchmark Guide for Light-Water-Reactor Fuel in Transportation and Storage Packages, US-NRC, NUREG-CR-6361.
- Mennerdahl, D. (2012): Review of the Nuclear Criticality Safety of SKB's Licensing Application for a Spent Nuclear Fuel Repository in Sweden, Swedish Radiation Safety Authority, Technical Note-2012:65.
- Mueller, D.E., Elam, K.R. & Fox, P.B. (2008): Evaluation of the French Haut Taux de Combustion (HTC) Critical Experiment Data, US-NRC, NUREG-CR-6979.
- NEI (2014): Guidance for Performing Criticality Analyses of Fuel Storage at Light-Water Reactor Power Plants, NEI, 12-16 Rev. 1.
- Noguere, G., Bouland, O., Bernard, D., Leconte, P., Blaise, P., Penelieu, Y., Vidal, J.F., De Saint, J.C., Leal, L., Schillebeeckx, P., Kopecky, S. & Lampoudis, C. (2012): Improved MOX fuel calculations using new Pu-239, Am-241 and Pu-240 evaluations, WONDER-2012 - 3rd International Workshop On Nuclear Data Evaluation for Reactor applications, 2012, vol. 42, p. 05005.
- NUREG (2003): U.S. NRC. Recommendations for Addressing Axial Burnup in PWR Burnup Credit Analyses. NUREG/CR-6801.
- Patel, R., Punshon, C. & Nicholas, J. (2012): Canister Design Concepts for Disposal of Spent Fuel and High Level Waste. Nagra Technical Report NTB 12-06.
- Pecchia, M., Canepa, S., Ferroukhi, H., Herrero, J., Vasiliev, A. & Pautz, A. (2015b): COMPLINK: a versatile tool for automatizing the representation of fuel compositions in MCNP models, International Conference on Nuclear Criticality Safety (ICNC).

- Pecchia, M., Vasiliev, A., Ferroukhi, H. & Pautz, A. (2015c): Criticality Safety Evaluation of a Swiss wet storage pool using a global uncertainty analysis methodology, *Annals of Nuclear Energy*, Volume 83, pages 226 – 235.
- Pecchia, M., Vasiliev, A., Leray, O., Ferroukhi, H. & Pautz, A. (2015): Advanced calculation methodology for manufacturing and technological parameters uncertainties propagation at arbitrary level of lattice elements grouping, *J. Nucl. Sci. Technol.*, vol. 52, No. 7 – 8, pp. 1084 – 1092.
- Pelowitz, D.B. (2014): MCNP6 USER'S MANUAL. Code Version 6.1.1beta, Los Alamos, LA-CP-14-00745.
- Pusa (2013): Numerical methods for nuclear fuel burnup calculations, Aalto University.
- Radulescu, G. & Wagner, J.C. (2012): Burn-up Credit Criticality Safety Benchmark – Phase VII: UO<sub>2</sub> Fuel: Study of Spent Fuel Compositions for Long-term Disposal, ISBN 978-92-64-99172-9, OECD NEA.
- Radulescu, G., Gauld, I.C., Ilas, G. & Wagner, J.C. (2011): An Approach for Validating Actinide and Fission Product Burnup Credit Criticality Safety Analyses — Isotopic Composition Predictions, US-NRC, NUREG-CR-7108.
- Scaglione, J.M., Mueller, D.E., Wagner, J.C. & Marshall, W.J. (2012): An Approach for Validating Actinide and Fission Product Burnup Credit Criticality Safety Analyses—Criticality (keff) Predictions, US-NRC, NUREG-CR-7109.
- SCALE (2016): SCALE Code System. 2016. Version 6.2. ORNL/TM-2005/39.
- SERPENT (2015): Serpent – a Continuous-energy Monte Carlo Reactor Physics Burnup Calculation Code, VTT Technical Research Centre of Finland, June 18, 2015.
- SIMULATE (1995): SIMULATE-3. Advanced Three-Dimensional Two-Group Reactor Analysis Code, Studsvik Scandpower, SSP-95/15 – Rev 4.
- SKB (2010): Agrenius L., Criticality safety calculations of disposal canisters, SKB, Public Report – 1193244 4.0.
- Van Wijk, J., Van den Eynde, G. & Hoogenboom, J.E. (2011): An easy to implement global variance reduction procedure for MCNP, *Ann. Nucl. Energy*, vol. 38, no. 11, pp. 2496–2503, 2011.
- Vasiliev, A., Rochman, D., Zhu, T., Pecchia, M., Ferroukhi, H. & Pautz, A. (2015): Towards Application of Neutron Cross-Section Uncertainty Propagation Capability in the Criticality Safety Methodology. Proc. Int. Conf. Nuclear Criticality Safety, ICNC 2015, Charlotte, NC, USA, September 13 – 17, 2015.
- Wagner, J.C. & Parks, C.V. (2003b): Recommendations on the credit for cooling time in PWR burnup credit analysis, US-NRC, NUREG-CR-6781, 2003.
- Wagner, J.C., DeHart, M.D. & Parks, C.V. (2003): Recommendations for Addressing Axial Burnup in PWR Burnup Credit Analyses, US-NRC, NUREG-CR-6801, 2003.
- Wilson (2007): A Manual for CINDER'90 Version 07.4 Codes and Data, December 2007.

Zhu, T., Vasiliev, A., Ferroukhi, H., Pautz, A. & Tarantola, S. (2015): NUSS-RF: stochastic sampling-based tool for nuclear data sensitivity and uncertainty quantification, *J. Nucl. Sci. Technol.*, Vol. 52, No. 7 – 8, pp. 1000 – 1007.



## Appendix A: Effect of thermal scattering data on $K_{\text{eff}}$ for fresh fuel

In order to evaluate the impact of thermal scattering law data (TSL) on criticality calculations, a T/S cask loaded with  $\text{UO}_2$  PWR fresh fuel will be used as the reference for the calculations.

The thermal scattering data for H in  $\text{H}_2\text{O}$ , O in  $\text{UO}_2$ , U in  $\text{UO}_2$ , and Fe in the cask material are employed one at a time for the  $K_{\text{eff}}$  calculation to evaluate the impact of these data. The calculations are performed with SERPENT2 and the ENDF/B-VII.1 data distributed with MCNP6.

For the U in  $\text{UO}_2$ , three cases were considered, the first applying the thermal scattering data only to U-238 (standard), then only to U-235 (this is the case that failed with MCNP6 so we used SERPENT2) and, finally, using the thermal scattering data with both U-235 and U-238 which would correspond to the real physics of the problem. Other uranium isotopes have low concentrations here and will not have a noticeable impact. The TSL data used the discrete representation as continuous energy data cannot yet be used in SERPENT2.

Case	$K_{\text{eff}}$	Standard deviation	Difference with no TSL (pcm)
No TSL data	1.13663	0.00017	-
H in $\text{H}_2\text{O}$	1.14935	0.00017	1'272
Fe in cask	1.13641	0.00017	-22
O in $\text{UO}_2$	1.13668	0.00017	5
U-238 in $\text{UO}_2$	1.13604	0.00017	-59
U-235 in $\text{UO}_2$	1.13614	0.00017	-49
U-235 and U-238 in $\text{UO}_2$	1.13629	0.00016	-34
All of the above	1.14941	0.00017	1'278

The results show that only the inclusion of hydrogen in water has a considerable impact and the rest of the thermal scattering effects are not important. In any case, the results with TSL applied to both uranium isotopes should be treated with caution, as this use has not yet been verified in SERPENT2.



## **Appendix B: International Guidelines and Standards for BUC Implementation**

### **ISO 27468:2011**

The International Organization for Standardization has issued a guide for the application of a bounding burnup credit approach, but up to now it is only applicable to PWR-UOX fuel and does not cover BWR or MOX fuels (ISO 2011).

### **ANSI/ANS**

The ANS has developed updated guidelines for the consideration of the reactivity effect of fuel burnup in UO<sub>2</sub> LWRs for intact assemblies (ANS 2008).

The general expression to be used for the limit to the calculated multiplication factors of the loaded canisters is explained in detail in this standard. The limitation to the computed value includes the summation of the estimated biases and uncertainties in the result:

- Statistical or convergence uncertainties in the calculation
- Material and fabrication tolerances for the canister
- Uncertainties due to geometric or material representation limitations of the models used in the calculation
- Bias and uncertainty due to depletion uncertainty in the calculated nuclide compositions
- Allowance for uncertainty in the assigned burnup value
- The bias in the calculated value deduced from criticality benchmark experiments suitable for comparison which are again affected by:
  - Statistical or convergence uncertainty in the calculation
  - Uncertainty in the experiment itself
  - Uncertainties in the geometric or material representation in the models for calculation
- The possible uncertainty from extrapolation of the experimental bias to regions outside the applicability range of the experiment
- Bias and uncertainty from cross section data not covered by the benchmark experiments, but computed e.g. from individual isotope worth experiments
- An administrative margin to cover unknown uncertainties and ensure subcriticality

One key element of the above sequence is the validation phase of the codes to be employed in the calculation. Another standard deals with this concept (ANS 2012).

The design system, i.e. the canister, for which the level of subcriticality would be computed must fall within the area of applicability of the experiments chosen for validation. The ANS standards (ANS 1998) define the range of applicability as the limiting ranges of material compositions,

geometric arrangements, neutron energy spectra, and other relevant parameters within which the bias of a computational method is established. If the design system falls outside the area of applicability of the experiments, the standard allows for the use of trends in the bias to extend the range of the experimental conditions.

Apart from the traditional trending analyses (Dean et al. 2001), work from ORNL has been carried out to integrate the sensitivity and uncertainty analysis tools (Broadhead 2004) in the SCALE package (SCALE 2016) to define sensitivity-based and uncertainty-based integral indices suitable for evaluating first the applicability of the experiments to the system, and second the trending analysis.

The predicted biases for various systems were, in some cases, up to a factor of 5 difference between the various trending parameters. The main reason for these differences is that systems demonstrating similarity from the standpoint of certain parameters may be dissimilar with respect to other parameters. Nevertheless, the new definitions are more physically sound as trending parameters have been widely accepted; the weakness in the methodology is its dependence on high quality variance and covariance values for the cross section uncertainties and the experimental reactivities, but work is ongoing to tackle this problem.

Administrative and technical practices are also covered in the standard (ANS 1998), specifically the double contingency principle is included in the design of the processes. The criticality safety analysis is required to demonstrate that criticality cannot occur without at least two unlikely, independent and concurrent incidents or abnormal occurrences.

### **DIN – Deutsches Institut für Normung**

In Germany, burnup credit criticality safety analysis of spent nuclear fuel wet storage systems has to demonstrate compliance with the regulatory requirements laid down in the criticality safety standard DIN 25471 (DIN 2009). Application of burnup credit methods to the criticality safety analysis of transport and dry storage of spent nuclear fuel has to meet the requirements laid down in the criticality safety code DIN 25712 (DIN 2014).

Each of the safety standards consists of two parts. In the first part, the regulatory requirements are given, while the second part includes explanatory and advisory remarks which are non-compulsory. The regulatory requirements are addressed to:

- Implementation and validation of the depletion calculations and isotopic selection:
  - The depletion must follow plant-specific fuel designs, irradiation histories and operation strategies.
  - The depletion code must be validated.
  - The nuclides with a significant positive reactivity worth must be included.
  - Nuclides with a negative reactivity worth can be included only if their contribution to the isotopic bias of the  $K_{\text{eff}}$  can be validated.
  - Radionuclides with negative reactivity worth, but half-lives not significantly greater than the cooling time of the fuel, are allowed only if justified by the absorption of the daughter products or by analysis of  $K_{\text{eff}}$  with cooling time.
  - Nuclides forming volatile substances must not be included.

- Taking credit for cooling is allowed but it must be showed that  $K_{\text{eff}}$  does not become greater at a later time.
- Correction of calculated number densities to cover reactivity increases at a later time is allowed.
- Implementation and validation of the criticality calculations:
  - The criticality code shall be validated with adequate experiments.
  - The reactivity shall include uncertainties in  $K_{\text{eff}}$  from tolerances.
  - The impact of the burnup profiles shall be determined and no underestimation must be demonstrated.
- Determination of the reactivity effects of axial and horizontal burnup profiles.
- Determination of the criticality safety acceptance criterion and the loading criteria (loading curves). The margin is set to 0.95 including all calculational and mechanical uncertainties with a 95 % probability at a 95 % confidence level.
- Determination of zone-specific loading curves or loading criteria for transport or storage casks (DIN 25712). Optimisation is allowed:
  - Standard BUC: the loading curve applies to all the fuel positions of the cask.
  - Optimised BUC: the storage positions are grouped together in several zones with a separate loading curve, considering that all the loading curves are correlated.
  - Individualised BUC: for an individual loading of a cask, a BUC analysis is performed with a 99 %/99 % limit of the real burnups for the FA.
- Quantification and verification of the burnup of the fuel assemblies to be loaded in the spent fuel pool or the transport or dry storage casks:
  - Shall be based on the evaluation of the reactor records, and additionally on a consistency check by means of a measurement
  - Determination of burnup shall follow the German safety code KTA 1401
- The fuel handling procedures applied to the loading operations must avoid misloading events following the double contingency principle.

The second part of the safety standards includes guidance for performing:

- The depletion calculations (DIN 25471)
- Evaluation of axial and horizontal profiles (DIN 25712)
- Determination of 95 %/95 % tolerance limits (both standards)
- Determination of loading curves and evaluation of burnup verification data (DIN 25712)

There is also a norm on the validation of criticality safety codes (DIN 1994) and, more recently, a standard applied to waste disposal (DIN 2012).

### **Interim Staff Guidance 8 (NRC NUREG)**

This Interim Staff Guidance from the NRC is dedicated to the use of BUC in the criticality safety analyses of PWR spent fuel in transport and storage casks. This revision is based on two NUREGs (Scaglione et al. 2012, Radulescu et al. 2011) making use of available experimental data to support actinides plus fission products burnup credit, and it unifies the point of view of the regulator with respect to burnup credit application for pools and dry storage.

The guidance accepted the use of actinides plus fission products burnup credit and the use of administrative procedures to avoid misloading events instead of burnup measurements.

In the case of using the actinides only burnup credit approach, it points to documents where already selected experiments are listed (Mueller et al. 2008, Lichtenwaller et al. 1997). For the incorporation of fission products in the criticality analysis, a conservative value of 1.5 % of the worth of the minor actinides and fission products is allowed to cover the bias in the calculation, under some conditions. Additionally, a 3 % bias is allowed for well qualified codes different from the ones used in the validation; other values would need justification.

### **Nuclear Energy Institute 12-16**

The Nuclear Energy Institute has published guidance for criticality analysis applied to new and spent fuel from LWRs to be stored in pools or new fuel stored in fuel vaults (NEI 2014). This document is seeking NRC endorsement to substitute previous Regulatory Guides and, although related to applications other than fuel disposal, the points treated therein could be extrapolated to our problem.

The document supports the classical implementation for the criticality code validation based on bias and bias uncertainty estimation, together with a trending analysis, but it does not mention the ORNL methodology based on the c-index as trending parameter.

For the depletion uncertainty, it indicates the use of a 5 % in  $\Delta k$  as being acceptable when using ENDF/B-V through VII. The two approaches to validation, i.e. direct validation (plant measurements) or method components validation (chemical assays and cross section uncertainties), are included. However, it warns that bias and uncertainties derived from chemical assay data tend to be significantly conservative due to the large experimental uncertainties in the assays which propagate to the reactivity calculation.

The document states that analysis of MOX critical experiments is not needed for ENDF/B-V and VII as the bias for these is smaller than for UO<sub>2</sub> fresh experiments; of course, this observation is valid for the experiments considered.

For BWR, measured cold critical configurations performed at each start-up are proposed as a good validation source.

The use of an intermediary code validated against experiments is also proposed for the validation of the primary code in the methodology when this code is not capable of directly modelling the benchmark experiments.

## IAEA Safety Standards

An international safety standard on criticality safety in the handling of fissile material is provided by the IAEA (IAEA 2014), where general indications for the correct implementation of a criticality safety assessment are presented.

One important condition in the standard for the safe transport of radioactive material (IAEA 2005) states that the criticality safety condition should be computed with isotopic compositions either providing the maximum multiplication factor during the irradiation history (this is the fresh fuel assumption for PWR or the application of gadolinium burnup credit for BWR) or a conservative estimate of the neutron multiplication for the package assessment, after irradiation but prior to shipment; a measurement should confirm the conservatism of the isotopic composition employed.

Additionally, in the safety guide dedicated to geological disposal (IAEA 2011) it is stated that *"The geological disposal facility should be designed so that fissile material, when present, will remain in a subcritical configuration during the operational period. Assessment of the possible evolutions of the disposal system in the post-closure period should also address the criticality issue and should provide confidence that a subcritical condition will be maintained"*.

With respect to the long-term evolution of the waste package in the post-closure phase, *assessment of criticality safety presents particular challenges. Among these are the very long timescales that need to be considered. Following closure of a disposal facility, engineered barriers provided by the package design and the form of the waste will tend to degrade, allowing the possibility of separation, relocation and accumulation of fissile nuclides (as well as the possible removal of absorbers from fissile material). In addition, a previously dry environment may be replaced by a water saturated environment.*

*Consideration of the consequences of criticality after closure of a disposal facility will differ from that for, for example, fuel stores or reprocessing plants, where a criticality accident may have immediate recognizable effects. In the case of a disposal facility, disruption of protective barriers and effects on transport mechanisms of radionuclides are likely to be more significant than the immediate effects of direct radiation from a criticality event, because the radiation would be shielded by the surrounding host rock formation and/or backfill materials.*

*Over the very long timescales considered in post-closure criticality safety assessments, some reduction and change in the fissile inventory of the nuclear waste will occur owing to radioactive decay. However, such assessments should also take account of credible degradation of the engineered barriers of waste packages, with consequential relocation and accumulation of fissile and non-fissile components.*